Tissue Parameter Mapping in Children with Fetal Alcohol Spectrum Disorders

By Marilize Fourie
FRXMAR025

In fulfilment of the requirements for the degree of Master of Science in Biomedical Engineering.

Faculty of Health Sciences
UNIVERSITY OF CAPE TOWN

January, 2020

Supervisor: Dr. Marcin Jankiewicz
Co-supervisor: Prof. Ernesta Meintjes

DECLARATION

I, MARILIZE FOURIE, hereby declare that the work on which this thesis is based is my own original work (except where acknowledgements indicate otherwise) and that neither the whole, nor any part of it, has been, or is to be submitted for any other degree in this or any other University.

I empower the University to reproduce, for the purpose of research, either the whole or part of the contents of this thesis in any manner.

Signed by candidate

Signature

28 January 2020

Date

ACKNOWLEDGEMENTS

First of all I would like to thank Prof. Ernesta Meintjes and the MRI group at UCT without whom this dissertation opportunity would not have been possible. I would also like to thank the National Research Foundation (NRF) and National Institute of Health (NIH) for the financial support they have provided. Thank you to Sandra and Joseph Jacobson who recruited the cohort and initiated the FASD studies in the imaging group at UCT. I appreciatively thank Keri, who has spent hours helping and teaching me, as well as my co-supervisor Prof. Ernesta Meintjes, who has provided guidance and support every time it was needed. An enormous thank you to my supervisor, Dr. Marcin Jankiewicz, for guiding me throughout this dissertation. His patient understanding and support surpassed the expectation any student could have of their supervisor, I could never express enough gratitude for his belief in me even when I started doubting myself. Special thanks to all the researchers in the MRI group that made being a part of the group a very pleasant experience that will always occupy a special place in my heart. Last but not least, I would like to thank my parents, my sister, my best friend Heidi, and Shannon, for their unwavering support and belief in me right up until the end. I am eternally grateful for each and every one of you.

ABSTRACT

Background: Fetal alcohol spectrum disorders (FASD), which are caused by prenatal alcohol exposure (PAE), affects people around the world. Certain communities in South Africa have among the highest reported incidences of fetal alcohol syndrome (FAS) in the world. Although PAE-related brain alterations have been widely documented, the mechanisms whereby alcohol affects the brain are not clearly understood. MRI relaxation parameters T_1, T_2, T_2* and proton density (PD), are basic tissue properties that reflect the underlying biology. The present study aims to advance our understanding of how PAE alters the microstructural properties of tissue by examining PAE-related changes in these tissue parameters in adolescents with FASD.

Methods: The final sample used in this study consisted of 53 children from a previously studied longitudinal cohort (Jacobson et al., 2008) and 12 additionally recruited subjects. Of the 65 participants, 18 were diagnosed with FAS or partial FAS (PFAS) and made up the FAS/PFAS group, 18 were diagnosed as heavily exposed non-syndromal (HE) and 29 were age matched controls. Subjects were scanned at the Cape Universities Body Imaging Centre (CUBIC) located at Groote Schuur Hospital on a 3T Siemens Skyra MRI. Structural images were obtained using the MEMPRAGE sequence. From these images T_1, T_2, T_2* and PD parameter maps were constructed and segmented into 43 regions of interest (ROI) using Freesurfer, FSL and AFNI. Linear regression analyses were used to analyse group differences as well as correlations between parameter values and the amount of alcohol the mother consumed during pregnancy.

Results: Significant T_1 differences were found in the caudate, cerebellar cortex, hippocampus, accumbens, putamen, choroid plexus, ventral diencephalon (DC), right vessel and ventricles. Significant T_2 differences were found in the caudate, brain stem, corpus callosum (CC), amygdala, cerebral cortex, choroid plexus, vessels and ventricles. Significant T_2* differences were found in the cerebellar cortex, optic chiasm and ventricles. Significant PD differences were found in the hippocampus and left lateral ventricle. The exploratory nature of this study resulted in none of the results surviving FDR correction for multiple comparisons.

Conclusions: Overall, our findings point to regional PAE-related increases in water content and cellular and molecular changes in underlying tissue of the anatomical structure. Exceptions were the right cerebral cortex, brain stem, hippocampus, amygdala and ventral diencephalon where our findings point to less free water and increased cell density, and cerebellar cortex where simultaneous reductions in T_1 and T_2* suggest the possibility of increased iron content. In highly myelinated white matter structures, such as the CC and optic chiasm, our results point to PAE-related demyelination, and possibly increased iron. These findings extend previous knowledge of effects of PAE and demonstrate that tissues are affected at a microstructural level.

Key words: Parameter mapping, Fetal alcohol spectrum disorder (FASD), prenatal alcohol exposure (PAE), neurodevelopmental disorder, MRI

Table of Contents

LIST OF FIGURES

LIST OF TABLES

LIST OF ABBREVIATIONS

AA	Absolute alcohol
ARND	Alcohol-related neurodevelopmental disorder
BOLD	Blood oxygenation level dependant
CC	Corpus callosum
CUBIC	Cape Universities Body Imaging Centre
CV	Coefficient of variation
DTI	Diffusion tensor imaging
ETL	Echo train length
FA	Fractional anisotropy
FAE	Fetal Alcohol Effects
FAS	Fetal alcohol syndrome
FASD	Fetal alcohol spectrum disorders
FDR	False discovery rate
FID	Free induction decay
FoV	Field-of-view
FSE	Fast spin echo
GM	Gray matter
GRE	Gradient echo
HE	Heavily exposed
MRI	Magnetic resonance imaging
MS	Multiple sclerosis
MTR	Magnetization transfer ratio
NAA	N-acetyl aspartate
ND/AE	Neurobehavioral Disorder/Alcohol Exposed
PAE	Prenatal alcohol exposure
PET	Positron emission tomography
PD	Proton density
PFAS	Partial fetal alcohol syndrome
ROI	Regions of interest
RPI	Right posterior inferior
SE/AE	Static Encephalopathy/Alcohol Exposed
SE	Spin echo
SES	Socioeconomic status
TE	The echo
TLFB	Timeline follow-back
TR	The repetition
TSE	Turbo spin echo
VDC	Ventral diencephalon
WM	White matter

1. Introduction

Fetal alcohol spectrum disorders (FASD) is the overarching term used to describe the effects of prenatal alcohol exposure (PAE). To date, some of the highest incidence rates of FASD in the world have been reported in certain high-risk communities in South Africa. Although many studies have confirmed the negative effects of PAE on children and that these effects persist into adulthood, the mechanisms through which alcohol impacts the brain are not well understood.

In this study we examined PAE-related changes in tissue composition using magnetic resonance (MR) relaxometry. The tissue's cellular and molecular characteristics determine its relaxation times which in turn determine the contrast of the voxels in MRI image. These characteristics illustrate the structure of the tissue such as the proportion in which macromolecules are present, the density of the cells and the iron concentration. To our knowledge, this is the first study to directly measure and examine whether physical parameters of brain tissue differ between adolescents with FASD and healthy controls. We used Freesurfer to construct T_1, T_2, T_2* and proton density (PD) brain parameter maps for 65 children and examined group differences in 43 regions segmented by FreeSurfer. Averaged parameter estimates for each region were derived for each subject from the respective parameter maps.

Although none of the findings from this exploratory analysis survived after correction for multiple comparison, brain tissue parameter differences were evident in the corpus callosum, optic chiasm, hippocampus, cerebellum, putamen, brainstem, caudate, accumbens, ventral diencephalon and choroid plexus. Notably, most of these regions have been implicated in previous studies of FASD. This study suggests that PAE affects the microstructural properties of tissue in these regions. A combination of imaging modalities may become a useful tool in identifying subtle effects of FASD since facial dysmorphology diagnosis only applies to severe cases like fetal alcohol syndrome (FAS) and partial FAS, and alcohol consumption reporting is a biased measure with uncertain accuracy.

2. Background theory

2.1 Fetal Alcohol Syndrome

In the 1970's clinical reports on the effects of prenatal alcohol exposure were published by Jones *et al.* (1973) and the term fetal alcohol syndrome (FAS) was introduced (Jones and Smith, 1973). FAS falls under the larger umbrella term: fetal alcohol spectrum disorders, which encompasses the diversity of effects that may prevail in a person that has been prenatally exposed to alcohol. FAS represents the most severe case of these disorders (Gerberding and Cordero, 2004).

A diagnosis of FAS requires a dysfunctional central nervous system, growth defects that occur pre- and/ or postnatally, and distinctive craniofacial features as shown in Figure 1 below. Neurodevelopmental and neuropsychological features include difficulties with learning and memory, poorly modulated emotional responses, and problems with attention span (Thomas, Warren and Hewitt, 2010). Children with FASD also demonstrate deficits in gross motor functions like balance, coordination and ball skills (Lucas *et al.*, 2014) and sensory processing deficits that hinder the child's adaptive behaviour development (Carr, Agnihotri and Keightley, 2010). Jacobson et al. demonstrated a profound effect of PAE on eyeblink conditioning (EBC) (2008, 2011), a type of classical conditioning where a neutral or conditioned stimulus, like an auditory sound, is paired with one that is biologically potent or unconditioned, like a gentle puff of air to the eye, and a conditioned response is learned during the process, i.e. closing the eye after the auditory sound and before the puff of air. Children prenatally exposed to alcohol did not learn the conditioned response as quickly and effectively as their counterparts in the control group.

The changes in facial features reflect brain damage and are most prominent when alcohol is consumed during the tenth to twentieth week of pregnancy (Renwick and Asker, 1983). A person that only exhibits a couple of the craniofacial features and has a growth defect, a neurobehavioural deficit or a small head circumference, is diagnosed as having partial fetal alcohol syndrome (PFAS). A person that doesn't exhibit any of the craniofacial features, but has been exposed to alcohol prenatally and has a neurobehavioural deficit, is diagnosed with alcohol-related neurodevelopmental disorder (ARND). In our study there was another group of children with known alcohol exposure, but who did not meet diagnostic criteria for FAS, PFAS or ARND. We classified these children as heavily exposed (HE) non-syndromal.

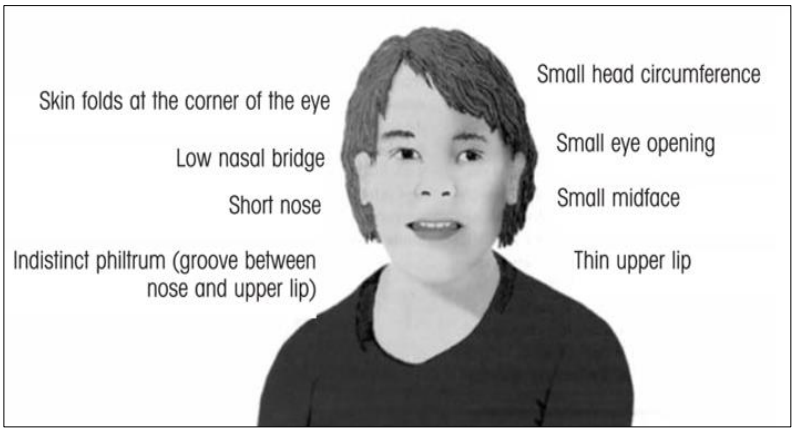

Figure 1: Craniofacial features resulting from FAS (Thomas, Warren and Hewitt, 2010).

FAS rates among children in the United States range between 0.3 (Abel and Sokol, 1991) to 2.2 (Abel and Sokol, 1987) children per every 1000 live births. In the high-risk American communities specifically, such as the American-Indian communities, the FAS rate was reported as high as 8 children per 1000 live births (May *et al.*, 2000). A study conducted in a high-risk community in the Western Cape province of South Africa, reported FAS rates of 38 to 42 children per 1000 live births. These numbers are an astonishing 18 to 141 times higher than those reported in the U.S. (May *et al.*, 2000). Reasons for these high rates include poor psychosocial circumstances as well as the traditional “dop” system, where the wine farm workers were partially compensated with wine for their labour (Croxford and Viljoen, 1999).

FAS is a worldwide concern as it occurs around the globe. Popova *et al.* (2017) estimated that 9.8% of mothers consume alcohol while pregnant, and the prevalence of FAS was determined as 14.6 per 10 000 people. It was further estimated that 1 in every 67 women who drink while expecting a child, deliver a baby with FAS, so that 119 000 children are born with FAS per year (Popova *et al.*, 2017). Figure 2 illustrates FAS prevalence around the globe. The five leading countries regarding FAS prevalence were Belarus (69.1 per 10 000 people), Italy (82.1 per 10 000 people), Ireland (89.7 per 10 000 people), Croatia (115.2 per 10 000 people) and South Africa (585.3 per 10 000 people). South Africa takes the lead with incidence rates more than five times that of Croatia, the second leading country in the world (Popova *et al.*, 2017). These statistics are based on incidences of FAS only, meaning that the full range of FASD will affect many more people.

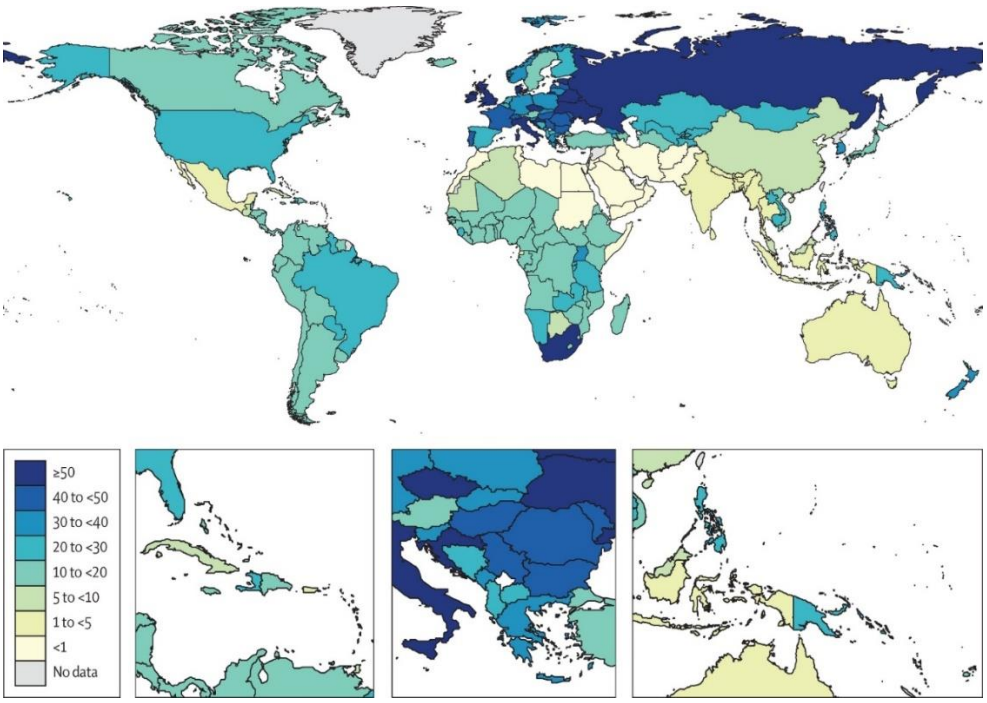

Figure 2: Global prevalence (per 10 000 people) of FAS among the general population in 2012 (Popova et al., 2017).

2.2 MRI principles

The human body consists of many molecules of which water makes up the most – approximately 68% in the adult human body and 73% in the adult human brain (Mitchell *et al.*, 1945). The hydrogen atoms in the water molecules contain a non-zero magnetic moment due to its charged, spinning nucleus (a single proton (spin)). The net magnetization vector refers to the resulting magnetic field from the combination of spins in the sample of the body. Since the spins are randomly orientated in the absence of an external magnetic field, the net magnetization sums to zero. The magnet of the MRI scanner creates a very strong uniform external magnetic field (B_0) causing spins to precess around it in either a parallel or anti-parallel direction. More spins align themselves in a parallel direction rather than anti-parallel to the magnetic field, causing a non-zero net magnetization.

The spins precess around the B_0 field at a certain frequency known as the Larmor frequency defined in equation 1 below, which is known as the Larmor equation. In this equation ω_0 represents the angular precessional frequency measured in radians per second (rad/s), B_0 is measured in Tesla (T) and γ represents the gyromagnetic ratio which is measured in radians per second Tesla (rad/s·T)

$$\omega_0 = \gamma B_0 \quad (1)$$

Each specific atomic nucleus has a constant gyromagnetic ratio associated with it. Hydrogen has a gyromagnetic ratio of 2.67 x 10^8 rad/s·T. From equation 1, one can see that the Larmor frequency is dependent on both the gyromagnetic ratio and the

magnetic field strength. The phenomenon where energy absorption occurs at the Larmor frequency is known as nuclear magnetic resonance. The energy needed for absorption by the proton is delivered in the form of a radiofrequency (RF) pulse that has a frequency (in our case) equal to hydrogen's Larmor frequency. The energy is transmitted by a transmitter RF coil inside the bore of the MRI scanner. This RF pulse causes the spins to change the orientation of their precession from the z-axis (aligned to the B_0 field's axis) to the transverse (xy) plane. A visualization of the coordinate system with the net magnetization vector (M) is illustrated in Figure 3.

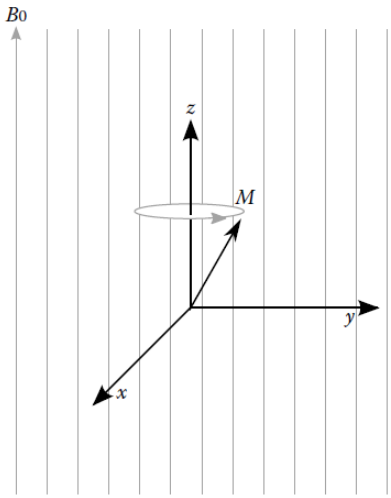

Figure 3: Typical coordinate system used to describe MRI concepts. The B_0 magnetic field is aligned with the z-axis and signal is measured in the xy plane. M represents the net magnetization vector that precesses around the z-axis (Berry and Bulpitt, 2009).

The magnetization vector has two components, a longitudinal component aligned with B_0 (M_z), and a transverse component oriented in the xy plane (M_{xy}). As an RF pulse is supplied to the system, the net magnetization vector which was originally aligned in the z-direction now has a non-zero transverse component M_{xy}. The magnetization vector and its two components are illustrated in Figure 4. The extent to which magnetization vector M deviates from B_0 is characterized by the flip angle (angle between z-axis and magnetization vector M). The flip angle defined as $\gamma \int_0^T |RF| dt$ is proportional to the integral under the envelope of the RF pulse of duration T, which in a case of a block excitation pulse is proportional to the amplitude of the RF pulse and the duration of the pulse T. An example of a 45° flip angle is shown in Figure 5.

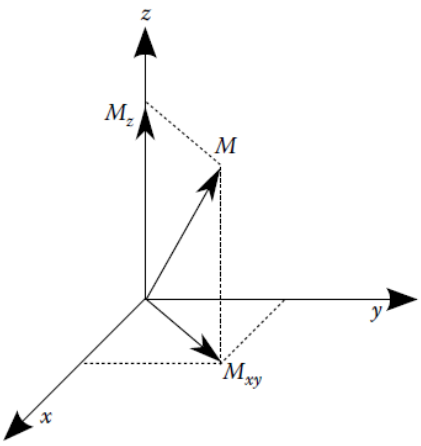

Figure 4: The longitudinal (M_z) and transverse (M_{xy}) components of the magnetization vector (M) (Berry and Bulpitt, 2009).

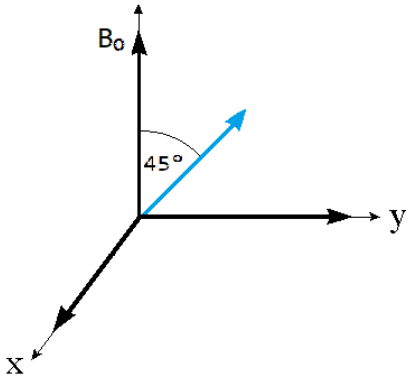

Figure 5: Example of a 45° flip angle.

Once the RF pulse is switched off, the spins move back to their equilibrium state that is aligned with the B_0 field. This happens as M spirals around the z-axis back to its original alignment causing the M_{xy} component to return to zero and the net magnetization to have a magnitude equal to M_z. The changing magnetic moment of M caused by the transmission of RF energy from the spins losing their energy, results in a free induction decay signal which produces an electrical signal that is picked up by the receiver RF coil. A computer receives the RF signal and performs an analogue to digital conversion. The digital signal represents the imaged body part and is stored in a Fourier space (k-space) representation. K-space stores digitized spatial frequencies acquired during data acquisition. From here the signals are sent to an image reconstructor where they are Fourier transformed into image space. In addition to RF transmitter and receiver coils, gradient coils (also in the bore of the main magnet), which create spatially dependent magnetic fields, are used to localize the signal in a slab, a slice, or a voxel.

2.3 Tissue parameters

After the RF pulse has been removed, the spins realign with the B_0 field, a process known as T_1 recovery. Recovery occurs longitudinally and transversely, corresponding

with the two components of the net magnetization vector, M_z and M_{xy}. The system is unsaturated when the net magnetization vector (M) is aligned with the B_0 field, i.e. when M_z is equal to M_0 and M_{xy} is equal to zero. The system becomes increasingly saturated as RF energy is continuously applied, and is fully saturated when there is no net magnetization in the B_0 field direction, i.e. when M_{xy} is equal to M and M_z is equal to zero. Equilibrium is achieved when the system is unsaturated, so that saturation recovery can be described as the process where the system changes from the saturated to the unsaturated state. The rate of saturation recovery is based on longitudinal and transverse relaxation mechanisms which depend on the type of tissue the spins are located in.

2.3.1 T_1 relaxation mechanism

Longitudinal relaxation is the process during which spins return to their equilibrium state along the z-axis. As this recovery continues, the M_z component becomes larger as the M_{xy} component becomes smaller. Viewing it from an energy balance perspective, the excited spins absorb RF energy during the RF excitation; immediately after the excitation this RF energy is transferred to the rest of the system (or lattice) and the spins return to their ground state. Longitudinal relaxation is also known as spin-lattice relaxation, or T_1 relaxation, where T_1 represents the time at which the spins have reached 63% of the net magnetization vector's recovery to equilibrium. A typical T_1 relaxation curve is shown in Figure 6. In this graph, time t = 0 indicates the time immediately after an RF pulse with a 90° flip angle, at this time the longitudinal component would have dissipated completely and M_z = 0. The M_z recovery function is stated in equation 2.

$$M_z = M_0 \left[1 - \exp\left(-\frac{t}{T_1}\right)\right] \tag{2}$$

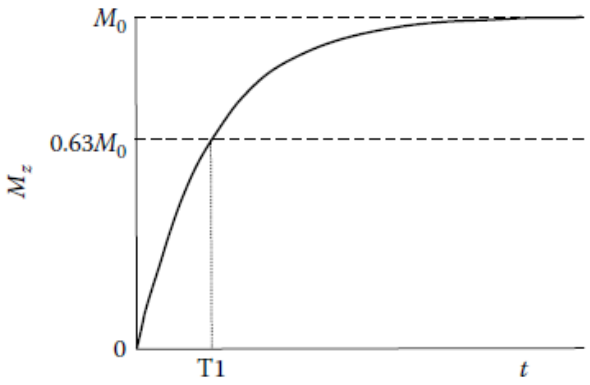

Figure 6: Longitudinal magnetization (M_z) recovery and its relation to T_1 (Berry and Bulpitt, 2009).

Near-complete recovery occurs at a time about five times T_1 when the system is once again almost completely unsaturated. By measuring the signal at different times, it is possible to calculate T_1 using equation 2. Different tissues have different T_1 relaxation

times. An example of the longitudinal relaxation of two different materials and their corresponding T_1 values are shown in Figure 7.

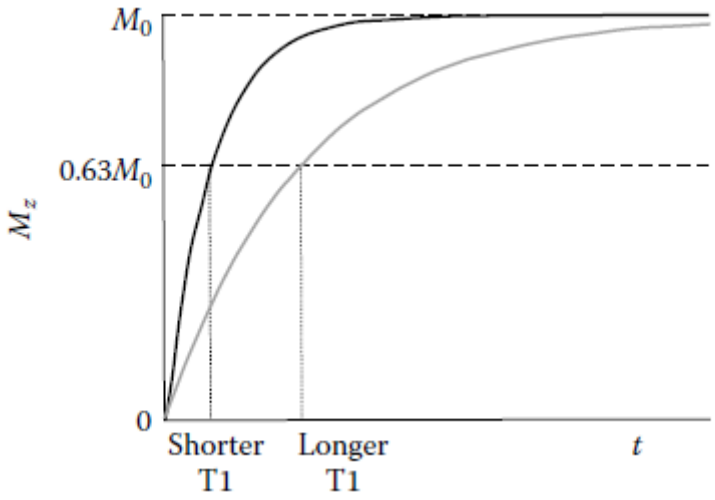

Figure 7: Longitudinal relaxation comparison of two different materials (Berry and Bulpitt, 2009).

A lot of what is understood about relaxation is based on the BPP theory of relaxation (Rao, 1965). This theory was formulated by Nicolaas Bloembergen, Edward Mills Purcell, and Robert Pound in 1948; and aimed to describe a pure substance's relaxation constant in relation to its state, whilst also regarding the effect of local disturbances in the magnetic field that is caused by the tumbling motion of the molecules (Bloembergen, Purcell and Pound, 1948). Atoms, and the molecules they form, are always in a state of vibration, rotation or translation and moving in arbitrary directions. Molecules change between these states of motion within a fraction of a second as they are continuously colliding with other molecules. The way in which the molecules are moving is termed molecular tumbling, and the time it takes a molecule to change from one state of motion to another is known as the correlation time (τ_c). The RF pulse excites the spins from a low energy state to a high energy state. The spins are stable in this high energy state so that they do not spontaneously return to the low energy state after the RF pulse has been removed, but rather return to the low energy state due to the interaction with magnetic moments of neighbouring spins. The closest neighbouring spin for a hydrogen proton in a water molecule is the other hydrogen atom in that molecule, so that relaxation in mainly a result of the magnetic moment the spin experiences from that atom as it is tumbling relative to its moment (Rao, 1965).

The spectral density function, J(ω), describes the range of motional frequencies a group of molecules with an average τ_c will have (McRobbie *et al.*, 2006). The function indicates how many nuclei tumble over a range of frequencies. An example of three spectral density functions is shown in Figure 8 with long, medium and short τ_cs. Molecules with a long τ_c have mostly very low motional frequencies as they spend a longer time in one motional state before colliding with another molecule. Molecules with shorter τ_cs experience collisions more frequently and accordingly their motional states change with an increased frequency. The molecules have to resonate at the

Larmor frequency for T_1 relaxation to occur. Since the molecules experience a range of motional frequencies, their molecular moments have a frequency distribution as well. It follows that the higher the number of protons tumbling near the Larmor frequency, the more efficiently T_1 relaxation occurs. Protons in free fluids like CSF or blood have very short τ_cs, while larger molecules like proteins have longer τ_cs because the water is bound to the molecule in the form of a hydration layer. Molecules with τ_cs between those of free fluid and bound water will have more protons tumbling at the Larmor frequency, meaning these molecules have shorter T_1 values than in the other two cases (McRobbie *et al.*, 2006).

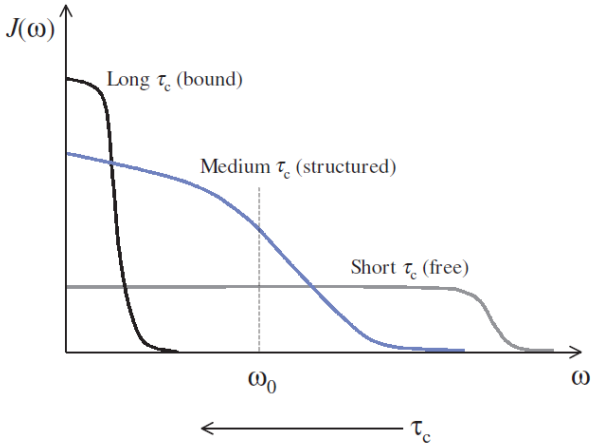

Figure 8: The spectral density functions J(ω) of three substances with long, medium and short correlation times (τ_c) respectively (McRobbie *et al.*, 2006).

2.3.2 T_2 relaxation mechanism

Transverse relaxation, also known as T_2 relaxation or spin-spin relaxation refers to the decay of the net magnetization's transverse component. The driving force behind the decay is the interaction between neighbouring proton's magnetic moments, so that energy is transferred within the spin-spin system, as opposed to longitudinal relaxation where energy transfer from the spins to the surrounding environment is the driving force behind T_1 recovery. The nuclei start spinning out of phase with each other in the xy plane due to slight differences between their spinning frequencies. This difference is caused by the very small differences in the magnetic fields the protons experience, which is caused by the slight difference in chemical environment around each proton. The vector of the transverse component, M_{xy}, is equal to the sum of all the individual contributions of the protons, so that the vector decreases as the spins go out of phase.

The process of growth and decay of transverse magnetization is shown in Figure 9. Figure 9(a) illustrates the spins out phase at a time before the RF pulse was applied and M_{xy} is equal to zero. Immediately after the RF pulse (b), the spins are in phase with one another and M_{xy} is at a maximum. Once the RF pulse is removed (c), spins start going out of phase again and M_{xy} starts decreasing. As time passes the spins become completely out of phase (d), this happens at a time smaller than the tissue's T_1 value and M_{xy} is again zero. When considering T_2 it is assumed that the variations

in magnetic fields are only caused by differing chemical environments and the B_0 field is perfectly homogenous. The decay curve of transverse magnetization is illustrated in Figure 10. T_2 is the time at which transverse magnetization has decayed to a value of 37% of the net magnetization as shown in Figure 10. The time t = 0 on the decay curve represents the time immediately after the RF pulse has been removed. Equation 3 shows the transverse magnetization decay component.

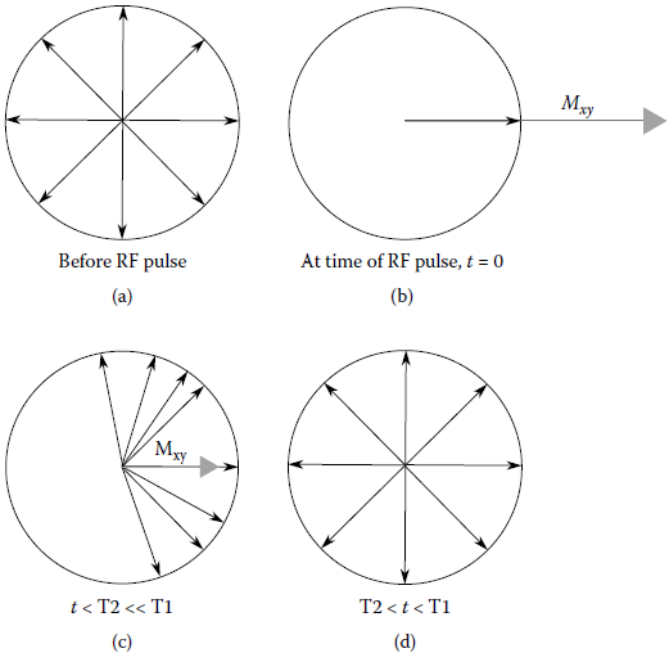

Figure 9: The changing behaviour of the spins that cause growth and decay of transverse magnetization (Berry and Bulpitt, 2009).

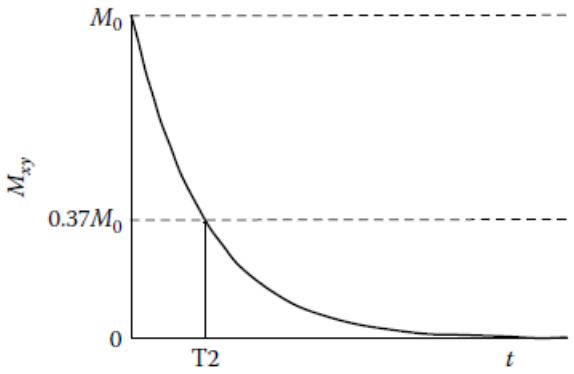

Figure 10: Transverse magnetization (M_{xy}) decay and its relation to T_2 (Berry and Bulpitt, 2009).

$$M_{xy} = M_0 \left[\exp\left(-\frac{t}{T_2}\right)\right] \quad (3)$$

Transverse magnetization decay can also be described using molecular dynamics. Protons with short τ_cs tumble at high frequencies and will 'see' the magnetic moment of the other hydrogen proton in the molecule fluctuate very quickly, so that the average effect of the magnetic field is zero. Correspondingly, the local field is practically

homogenous and minimal dephasing occurs, causing T_2 times to be long. On the other hand, protons tumbling at low frequencies will dephase efficiently, as the effect of the magnetic moment of its neighbouring spins are large and changes in the magnetic field are very slow. This causes T_2 values to be short. Bound hydrogen protons have the shortest T_2 values, while free protons have the longest T_2's and protons with intermediate binding have T_2 values between those of bound and free protons (Rao, 1965).

As previously stated, a homogenous B_0 magnetic field is assumed when considering T_2, but there are inhomogeneities present in the B_0 field which cause additional dephasing of the spins. T_2* is the time constant related to decay that occurs from both intrinsic dephasing and inhomogeneities in the magnetic field that cause dephasing. Since additional dephasing occurs, decay is faster, which means T_2* is always shorter than T_2 as is shown in Figure 11. The B_0 field inhomogeneities can be a result of inherent magnet defects or susceptibility induced field distortions originating from the tissues themselves present in the field.

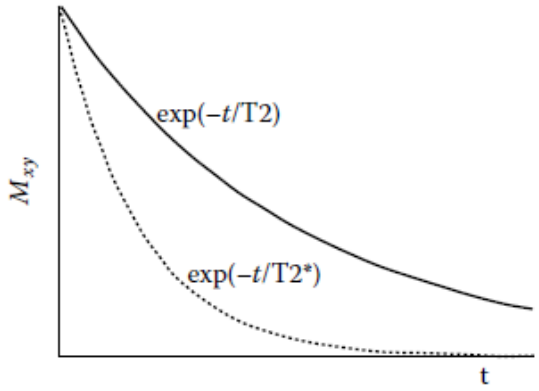

Figure 11: The T_2* decay curve and how it compares to the slower T_2 decay curve (Berry and Bulpitt, 2009).

As T_1, T_2 and T_2* are tissue dependant they can be used to generate contrast in images. These relaxation times can also be expressed as relaxation rates, where the rate is equal to the inverse of the respective relaxation time, e.g. the T_1 relaxation rate $R_1 = 1/T_1$ and has the units [1/ms].

2.3.3 Proton density

There is another tissue characteristic that can be used to generate image contrast known as tissue proton density (PD). In this case, scanning parameters are chosen in such a way that the effects of T_1 and T_2 are minimised, resulting in PD being the primary determinant of contrast in the scan (Tofts, 2004). This means TR is chosen to be larger than T_1 and TE is chosen to be smaller than T_2. Thus the signal received by the RF coils results from the number of protons present in the tissue, rather than on the relaxation times of the tissue. For tissues with very short T_2 (e.g., bone and cartilage), achieving TE<T_2 may not be possible with conventional scanners, making

the corresponding proton density invisible. PD contrast can be seen as a quantitative measurement of the number of protons per unit of tissue (Tofts, 2004). The number of protons in a unit of tissue impacts the transverse magnetization of that unit, where a higher number of protons increase transverse magnetization resulting in a brighter signal contrast, and vice versa.

Even though scanning parameters can be set up to minimize the effects of T1 and T2, PD weighting is intrinsic in all images. PD is directly proportional to signal, e.g. if PD in a voxel is halved, the signal will be halved as well (Tofts, 2004). This means PD can be calculated as a by-product from for instance a T_1-weighted image, as is the case in this study.

2.4 Signal equation

Equation 4 gives the MRI signal equation, where S_0 represents a scaling constant, which is related to proton density (k*PD), TR and TE are the repetition and echo times, respectively, α represents the flip angle, and T_1 and T_2 are the longitudinal and transverse relaxation rates. Depending on the type of sequence used, T_2 can be replaced with T_2*, where the latter includes transverse relaxation processes arising from field inhomogeneities in addition to spin-spin interactions. While PD, T_1 and T_2 are intrinsic tissue parameters, TR, TE and α are operator selected machine parameters.

$$S = S_0 \frac{(1-e^{-\frac{TR}{T_1}})\sin\alpha}{1-e^{-\frac{TR}{T_1}}\cos\alpha} e^{-\frac{TE}{T_2}} \quad (4)$$

By choosing appropriate extrinsic parameters, the intrinsic parameters can be measured. For small TE, the term $e^{-\frac{TE}{T_2}}$ approaches unity, leaving T_1 and S_0 as the only unknowns in the equation. T_1 and S_0 can be solved using simultaneous equations generated from measuring the signal (S) for two different flip angles (α). S_0 can then be used to calculate PD. Alternatively, when TR is chosen to be very large, the term $e^{-\frac{TR}{T_1}}$ approaches 0 and the T_1 effect is eliminated. Selecting multiple TE values will then generate simultaneous equations that can be used to solve for T_2 (or T_2*) and S_0. Note that the effect of T_1 is minimized for small flip angles due to the sinα and cosα terms, while flip angles approaching 90° maximise T_1 effects.

2.5 Scanning sequences

2.5.1 Spin echo and turbo spin echo

Pulse sequences are the software programmes that control the hardware during acquisition of an MR image. The spin echo (SE) pulse sequence is one of the most widely used sequences and was first demonstrated by Erwin Hahn in a paper

published in 1950 (Hahn, 1950). This sequence consists of a 90°- 180° RF pulse pair that generates a spin echo. The 90° pulse flips the longitudinal magnetization into the transverse plane. As soon as the pulse is removed the spins start dephasing, this is known as free induction decay (FID). The 180° pulse is then applied, which rotates the spins around the x-axis so that instead of dephasing, the spins will rephase again as they continue to precess. The spin echo forms when the spins are once again in phase with one another. The reversing of the spins will cause any dephasing that resulted from field inhomogeneities, tissue susceptibility differences and chemical shifts to be rephased, so that any remaining signal loss of the echo is due to spin-spin interactions only, i.e. effects of T_2 relaxation. The sequence needs to be repeated several times in order to acquire the entire image. The time at which the sequence is repeated is known as the repetition time (TR). The repetition time allows the longitudinal magnetization to recover so that the transverse magnetization can be generated with the next pulse sequence repetition.

Slice select gradients are turned on during all excitation pulses (90°- and 180° RF pulses) as they determine which protons get excited. Phase encoding gradients generate phase shifts so that a pulse repetition occurs for each phase-encoding gradient strength. These gradients are turned on temporarily before readout. Frequency-encoding gradients are turned on throughout readout as the precession frequencies need to be altered while they are being measured. The spin echo pulse sequence is shown in Figure 12 and illustrates the RF pulse pair, the spatial localization gradients, the FID, the spin echo and the time between the middle of the first RF pulse and the peak of the spin echo known as the echo time (TE).

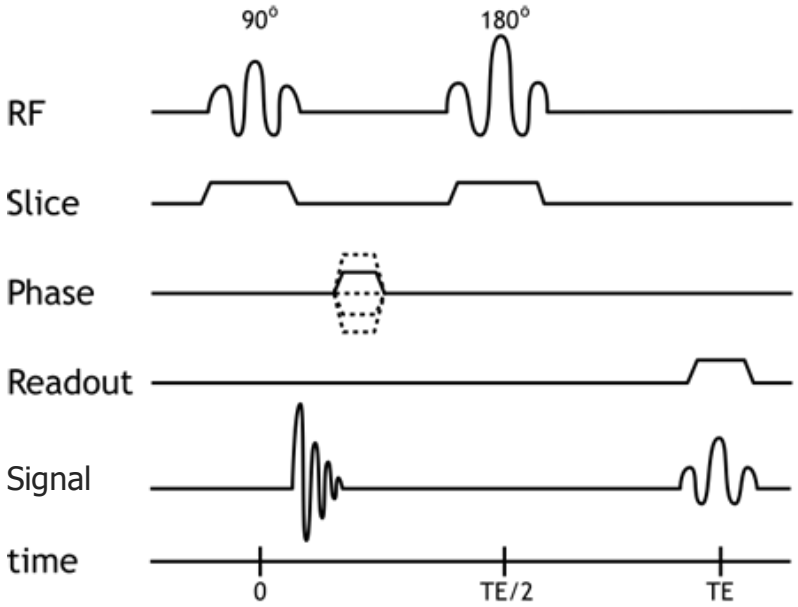

Figure 12: Simplified spin echo sequence illustrating the 90°- and 180° RF pulses followed by the FID and formation of the spin echo at the echo time (TE) (for simplicity, slice rephase and readout dephase gradient lobes are not shown) (adapted from Hammer, 2014).

The system can be stimulated with extra180° RF pulses after the first 180° pulse to rephase the spins multiple times without having to wait for time TR. This is known as

a turbo spin echo or fast spin echo (TSE or FSE) sequence. With every 180° pulse the MR signal becomes increasingly diminished, as spin-spin interactions cause each successive echo to be smaller than the previous one. The echo train length (ETL) defines the number of echoes obtained after a single 90 pulse; the ETL of a typical TSE sequence is 8 to 16 echoes. When TR and TE are both short, T_1-weighted images are obtained, long TR and short TE yield proton density weighted images, and when TR and TE are both long, images are T_2-weighted. Figure 13 shows a TSE sequence with an ETL of 3.

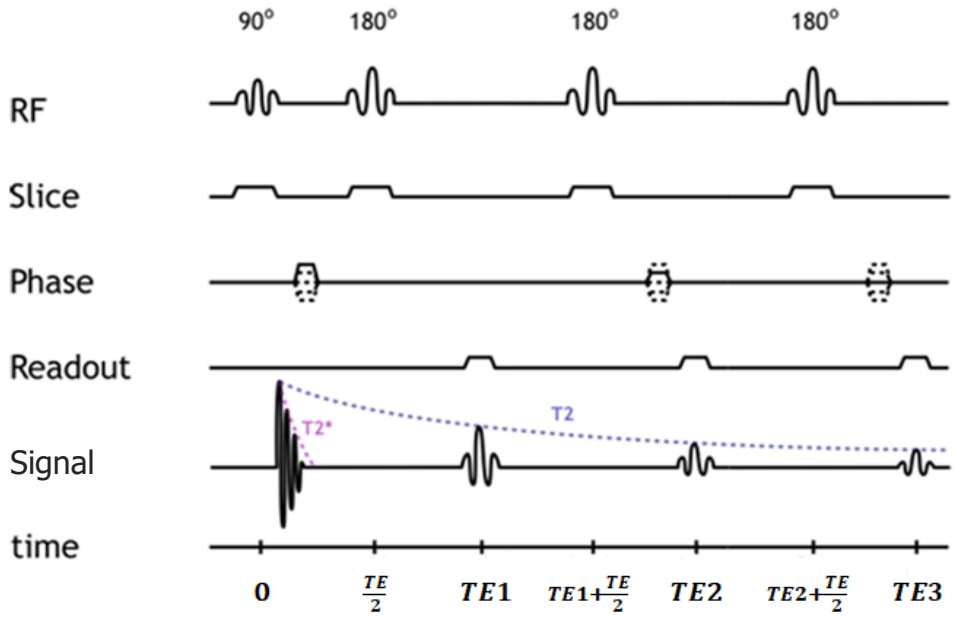

Figure 13: Turbo spin echo (TSE) sequence diagram illustrating the multiple 180° pulses and echoes following the 90° pulse (for simplicity, slice rephase and readout dephase gradient lobes are not shown) (Adapted from Hammer, 2014).

2.5.2 Gradient echo

While a spin echo is generated by pairs of radiofrequency pulses, a gradient echo (GRE) sequence comprises a single RF pulse and uses a gradient reversal to produce the echo. The RF pulse is followed by phase dispersion of the precessing spins. This phase dispersion is accelerated by applying a gradient that spatially varies the static magnetic field. When the direction of the gradient is reversed, the spin dephasing is inverted and the spins refocus to form an echo, called a gradient (recalled) echo. It is important to note that although the refocused spins are dephased and rephased by the gradient, the T_2 and T_2* process are not affected (Elster, 1993).

The rephasing gradient only rephases spin dephasing that was caused by the dephasing gradient. It follows that unlike SE sequences, GRE sequences do not rephase dephasing that occurs as a result of B_0 field inhomogeneities, chemical shifts or static tissue susceptibility gradients. As such, image contrast is determined by T_2* rather than T_2 (Elster, 1993). Typically, GRE sequences use an initial flip angle of less

than 90 degrees. The flip angle defines the amount of longitudinal magnetization that is rotated into the transverse plane. A smaller flip angle preserves a larger amount of longitudinal magnetization that can be used for the next repetition of the sequence. A typical GRE sequence is illustrated in Figure 14.

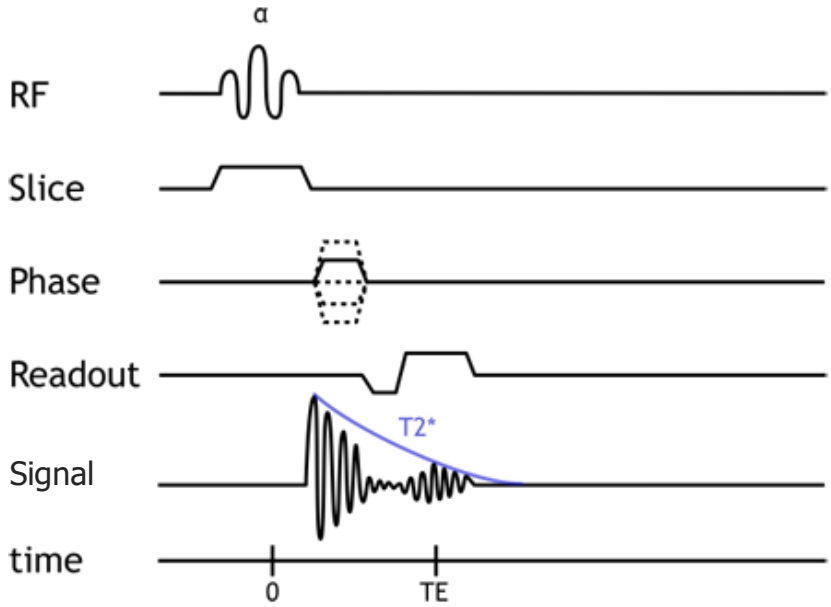

Figure 14: A typical GRE sequence illustrating how the gradient initially dephases the spins and then another gradient rephases them to form the gradient echo (for simplicity, slice rephase and readout dephase gradient lobes are not shown) (Hammer, 2014).

2.6 Literature review

2.6.1 Brain alterations observed on neuroimaging in individuals with FASD

Numerous neuroimaging articles have reported atypical brain development in various regions in children, adolescents and young adults with FASD. These articles discuss alterations in regions such as the corpus callosum (CC), caudate, hippocampus, cerebellum, amygdala, pallidum, putamen, thalamus and various cortical regions as observed on structural MRI, functional MRI (fMRI), diffusion tensor imaging (DTI), spectroscopy and positron emission tomography. These articles and their key findings are summarised in Table 1. In the table FA refers to fractional anisotropy.

Table 1: Summary of articles reporting brain alterations in children, adolescents and young adults with FASD.

Paper	**Subject age in years (mean ± SD)**	**Sample size**	**Mother alcohol consumption**	**Key finding(s)**
Structural MRI				
(Archibald *et al.*, 2001)	FAS: 11.4 ± 3.3 PAE: 14.8 ± 4.4 Controls: 12.8 ± 4.8	FAS: 14 PAE: 12 Controls: 41	Not available	Alcohol exposed subjects had: * lower wholebrain volume, wholebrain grey matter volume and wholebrain white matter volume * lower **cerebrum** and **caudate** volumes * lower **cerebellar** white matter * a relatively spared **hippocampus** volume
(Suttie *et al.*, 2018)	FAS: 12.6 ± 3.2 HE: 12.2 ± 2.0 Controls: 12.6 ± 2.3	FAS: 22 HE: 50 Controls: 47	Quantities not reported	* **CC** and **caudate nucleus** morphology were able to differentiate between the three groups as accurately as facial dysmorphology * **Caudate nucleus** left-right dense surface model asymmetry observed in control subjects are curtailed in the HE group and much less prominent in the FAS group
(Zhou *et al.*, 2018)	PAE: 12.8 ± 3.3 Controls: 12.1 ± 3.3	PAE: 78 Controls: 79	Not reported	* The PAE group illustrated a decrease in volume of the **amygdala, caudate, cerebrum, cerebellum, pallidum, putamen and thalamus** * Decreased cortical thickness in PAE group both globally and regionally, while the pattern and extent of cortical thickness asymmetry remained comparable between the groups
(Hendrickson *et al.*, 2017)	PAE: 13.09 ± 2.07 Controls: 13.99 ± 1.96	PAE: 92 Controls: 83	PAE: > 13 drinks/week or > 4 drinks per occasion at least once per week during pregnancy Controls: < 1 drink/week and never > 2 drinks on any one occasion or no drinking at all	* PAE group illustrated significantly less cortical gyrification over large areas of the **cerebral cortex** as compared to controls

(Biffen *et al.*, 2018)	FAS: 10.4 ± 0.9 PFAS: 10.5 ± 0.4 HE: 11.0 ± 0.7 Controls: 10.6 ± 0.5	FAS: 9 PFAS: 19 HE: 24 Controls: 19	FAS: 0.8 ± 1.8 oz/day 4.9 ± 1.8 oz/occasion PFAS: 1.0 ± 0.6 oz/day 3.8 ± 1.7 oz/occasion HE: 0.2 ± 0.7 oz/day 3.4 ± 2.4 oz/occasion Controls: 0.0 ± 0.0 oz/day 0.06 ± 0.3 oz/occasion	* Increased alcohol exposure levels are associated with volume reductions of the **CC, caudate nucleus and hippocampus**
(Nardelli *et al.*, 2011)	FASD: 11.3 ± 3.1 Controls: 11.3 ± 3.0	FASD: 28 Controls: 56	FASD: 1-2 drinks per occasion at least once a week during the first trimester of pregnancy Controls: No drinking	* Children with FASD were found to have smaller intracranial, total white matter and cortical grey matter volumes, as well as smaller deep grey matter volumes in the following structures: **hippocampus, amygdala, thalamus, caudate, putamen and globus pallidus**
(Joseph *et al.*, 2014)	FAS/PFAS: 11.8 ± 1.2 Controls: 11.5 ± 1.1	FAS/PFAS: 12 Controls: 19	FAS: 2.8 ± 2.4 oz/day 6.7 ± 3.4 oz/occasion Controls: 0.0002 ± 0.001 oz/day 0.1 ± 0.3 oz/occasion	* Significant variations in the shape of the **caudate nucleus** and **hippocampus** were found between controls and alcohol exposed subjects * Higher amounts of alcohol exposure was associated with contractions of localized regions in both the **caudate nucleus** and **hippocampus.**
(Roussotte *et al.*, 2012)	FASD: 12.97 ± 1.81 Controls: 12.82 ± 1.83	FASD: 55 Controls: 37	FASD: Data was only available for 17 subjects but was not reported in the article Controls: <= 1 drink/week on avg and <= 2 drinks on any single occasion	* Lower wholebrain volume and wholebrain white matter volume in FASD children * Lower cortical grey matter cerebrum volume in FASD children * Lower **caudate**, globus pallidus, **putamen**, thalamus, **hippocampus** and **ventral DC** volumes in children with FASD
(Treit *et al.*, 2013)	First scan: FASD: 8.2. ± 1.8 Controls: 11.4 ± 2.1 Last scan: FASD: 8.5 ± 1.6 Controls: 12.0 ± 1.8	FASD: 17 Controls: 27	FASD: Not reported Controls: at most an avg of 2 drinks across pregnancy	* Exposed children had smaller wholebrain volume and wholebrain white matter volumes * Exposed children had smaller cortical grey matter cerebrum volume * Exposed children had smaller **caudate,** globus pallidus, **putamen**, thalamus, **hippocampus and amygdala** volumes

(Astley *et al.*, 2009)	FAS/PFAS: 12.7 ± 2.4 Static Encephalopathy/ Alcohol Exposed (SE/AE): 12.2 ± 2.0 Neurobehavioral Disorder/Alcohol Exposed (ND/AE): 12.4 ± 2.3 Controls: 12.4 ± 2.7	FAS/PFAS: 20 SE/AE: 24 ND/AE: 21 Controls: 16	FAS/PFAS: 5.5 ± 1.7 days/week 11.6 ± 7.1 drinks/occasion SE/AE: 3.9 ± 2.1 days/week 14.1 ± 8.9 drinks/occasion ND/AE: 5.3 ± 2.1 days/week 11.7 ± 7.3 drinks/occasion Controls: 0 ± 0 days/week 0 ± 0 drinks/occasion	* Alcohol exposed subjects have lower wholebrain volume * Alcohol exposed subjects have lower **caudate, putamen** and **hippocampus** volumes
(Sowell *et al.*, 2001)	FAS/PAE: 13.0 ± 4.0 Controls: 13.5 ±5.2	FAS/PAE: 20 Controls: 21	Not available	* PAE children have smaller wholebrain volumes, smaller wholebrain white matter volumes and smaller wholebrain grey matter volumes * **CC** has a smaller surface area and is displaced in PAE children compared to controls
(De Guio *et al.*, 2014)	FAS: 9.3 ± 0.3 HE: 9.6 ± 0.6 Controls: 9.3 ± 0.4	FAS: 9 HE: 15 Controls: 16	FAS: 1.8 ± 2.2 oz/day 4.8 ± 1.8 oz/occasion HE: 0.5 ± 0.5 oz/day 3.0 ± 1.4 oz/occasion Controls: 0.0 ± 0.0 oz/day 0.1 ± 0.3 oz/occasion	* Subjects exposed to alcohol have smaller wholebrain volumes, smaller wholebrain white matter volumes and smaller wholebrain grey matter volumes
(Mattson *et al.*, 1996)	FAS: 13.0 (Range: 8-19) Controls: 12.3 (Range: 8-18)	FAS: 6 Controls: 7	Not reported	* Smaller **cerebrum, cerebellar** vault, **caudate** and **diencephalon** volumes were found in children with FAS
(Zhou *et al.*, 2011)	PAE: 12.8 ± 3.3 Controls: 12.1 ± 3.3	PAE: 33 Controls: 33	Not reported	* The PAE group illustrated lower wholebrain volume and wholebrain grey matter volume * Thinner **cortical** thickness was observed in the PAE group
(Rajaprakash *et al.*, 2014)	ARND: 11.4 ± 1.9 Controls: 11.0 ± 1.5	ARND: 36 Controls: 52	Not available	* The ARND children had smaller **cortical** surface area
(O'Hare *et al.*, 2005)	FAS: 12.6 ± 4.3 PAE: 13.1 ± 3.8 Controls: 13.5 ± 5.2	FAS: 14 PAE: 7 Controls: 21	Not reported	* Children prenatally exposed had lower **cerebrum** volumes * Exposed children had a displaced and smaller **cerebellar** vermis

(Willoughby *et al.*, 2008)	FASD: 12.21 (Range: 9.3-15.4) Controls: 12.39 (Range: 9.7-14.8)	FASD: 19 Controls: 18	Not available	* Participants with FASD displayed smaller wholebrain and **hippocampus** volumes
(Coles *et al.*, 2011)	Dysmorphic: 23.1 ± 2.2 ARND: 23.1 ± 1.6 Controls: 22.7 ± 1.7	Dysmorphic: 30 ARND: 36 Controls: 26	Dysmorphic: 13.5 ± 13.6 oz/week ARND: 7.7 ± 13.1 oz/week Controls: 0 ± 0 oz/week	* Smaller wholebrain and **hippocampus** volumes were found in PAE participants
Yang 2012 (Yang, Phillips, *et al.*, 2012)	FASD: 12.8 ± 2.3 Controls: 12.3 ± 2.4	FASD: 82 Controls: 71	FASD: > 4 drinks/occasion or > 13 drinks/week Controls: <= 2 drinks/occasion <= 1 drink/week	* Lower wholebrain white matter volume were found in exposed children * **CC** displayed a smaller surface area and thinner splenium and anterior regions in exposed children
(Yang, Roussotte, *et al.*, 2012)	FASD: 13.4 ± 1.9 Controls: 13.0 ± 2.0	FASD: 69 Controls: 58	FASD: Not reported Controls: <= 1 drink/week on avg or <= 2 drinks on any one occasion	* Thicker **cerebral** cortices were found in FASD participants
(Sowell *et al.*, 1996)	FAS/PAE: 15.1 (Range: 8-22) Controls: 14.3 (Range: 8-24)	FAS/PAE: 9 Controls: 24	Not available	Subjects that have been exposed had: * Lower **cerebral** volumes * Less **cerebellar** white matter
(Riley *et al.*, 1995)	FAS/PAE: 13 (Range: 8-18) Controls: 14 (Range: 8-19)	FAS/PAE: 13 Controls: 12	Not reported	* Exposed participants had lower **CC** volumes and smaller midsagittal CC surface areas
Functional MRI				
(Fan *et al.*, 2017)	FAS/PFAS: 11.0 ± 1.0 HE: 11.4 ± 0.7 Controls: 11.6 ± 1.0	FAS/PFAS: 19 HE: 19 Controls: 19	FAS/PFAS: 0.9 ± 0.8 oz/day 4.0 ± 2.0 oz/occasion HE: 0.8 ± 0.9 oz/day 3.9 ± 3.2 oz/occasion Controls: 0.0 ± 0.0 oz/day 0.1 ± 0.3 oz/occasion	* Compared to controls the FAS/PFAS and HE groups displayed less resting state functional connectivity in: -right postcentral gyrus in anterior default mode network -right middle frontal gyrus in salience network and -right precentral gyrus in the ventral attention network The FAS/PFAS group also showed less connectivity in: -left precentral gyrus in dorsal attention network and -left crus II in right executive control network

(Diwadkar *et al.*, 2013)	FAS/PFAS: 9.3 ± 0.2 HE: 9.7 ± 0.6 Controls: 9.3 ± 0.4	FAS/PFAS: 17 HE: 13 Controls: 17	FAS/PFAS: 0.9 ± 0.8 oz/day 4.0 ± 2.0 oz/occasion HE: 0.8 ± 0.9 oz/day 3.9 ± 3.2 oz/occasion Controls: 0.0 ± 0.0 oz/day 0.1 ± 0.3 oz/occasion	* Different sub-network recruitment patterns were observed between groups during verbal working memory tasks: -Controls: left inferior frontal **gyrus** (Broca's area) -HE: fronto-striatal regions (left dorsal prefrontal **cortex** and left **caudate)** -FAS/PFAS: **cerebellar** subregions and parietal **cortex**
(Meintjes *et al.*, 2010)	FAS/PFAS: 10.1 ± 1.2 Controls: 10.4 ± 1.2	FAS/PFAS: 15 Controls: 18	FAS/PFAS: 2.7 ± 2.1 oz/day 6.6 ± 6.0 oz/occasion Controls: 0.0 ± 0.0 oz/day 0.1 ± 0.7 oz/occasion	* During math/number processing tasks exposed participants showed a change in activity compared to controls in: - more activity in the **cerebellum** cortex bilaterally, right vermis of the cerebellum and bilateral red nuclei of the **midbrain** - more activity in the occipital **gyri** bilaterally, left superior temporal gyrus and right posterior cingulate and left angular gyrus in the parietal lobes - less activity in the right posterior horizontal intraparietal sulcus and right superior frontal and precentral sulcus - higher number of parietal regions recruited during tasks
(Malisza *et al.*, 2012)	ARND: 12.21 ± 1.63 Controls: 11.60 ± 1.29	ARND: 22 Controls: 21	Not reported	* Spatial working memory tasks revealed that compared to controls the ARND group had: - less activation in the left thalamus, right **amygdala, brainstem** and left red nucleus - more activation in the right red nucleus - different amounts of activity in various **cortical** areas
(Fryer *et al.*, 2007)	PAE: 14.45 ± 3.28 Controls: 14.53 ± 2.74	PAE: 13 Controls: 9	Not reported	* Response inhibition tasks showed alcohol exposed participants had: - less activity in the right **caudate** - different amounts of activity in various **cortical** areas
DTI				
(Ma *et al.*, 2005)	PAE: 20 ± 2 Controls: 21 ± 1	PAE: 9 Controls: 7	PAE: >= 2 drinks/week during pregnancy Controls: No drinking	* Children prenatally exposed to alcohol had lower fractional anisotropy and higher MD values in the genu and splenium of the **CC**
(Lebel *et al.*, 2008)	FASD: 9.1 ± 2.2 Controls: 9.8 ± 2.2	FASD: 24 Controls: 95	Not available	* The right **putamen** and right **thalamus** of children with FASD have a higher MD values compared to controls * The MD of the genu of the **CC** was lower in children with FASD * The splenium of the **CC** and the left **thalamus** of children with FASD had lower FA values

(Fryer *et al.*, 2009)	PAE: 13.85 ± 3.11 Controls: 13.18 ± 2.94	PAE: 15 Controls: 12	PAE: >= 4 drinks/occasion (at least once/week) or >= 14 drinks/week during pregnancy Controls: No drinking	* Exposed subjects had lower FA values in the body of the **CC**
(Wozniak *et al.*, 2009)	FASD: 12.6 ± 2.2 Controls: 12.6 ± 2.2	FASD: 33 Controls: 19	FASD: Rank 4 - Daily chronic drinking or heavy weekly binge drinking Rank 3 - Heavy maternal drinking occurred, but less frequent than rank 4 Controls: No drinking	* Participants with FASD had lower FA values in the posterior mid-body of the **CC**
(Sowell *et al.*, 2008)	FASD: 10.53 ± 2.71 Controls: 11.24 ± 2.81	FASD: 17 Controls: 19	FASD: Not available Controls: <= 1 drink/week on avg and <= 2 drinks on any single occasion	* Lower FA values were found bilaterally in the lateral splenium of the **CC** as well as the **brainstem** of children with FASD
(Lebel *et al.*, 2010)	FASD: 9.2 ± 2.2	FASD: 21	Not available	* Significant correlations were found between FA values and mathematical test scores in clusters located in the left **cerebellum** and bilateral **brainstem**
(Spottiswoode *et al.*, 2011)	PAE: 11.8 ± 1.2 Controls: 11.8 ± 1.2	PAE: 13 Controls: 12	PAE: 2.7 ± 2.3 oz/day 6.5 ± 3.3 oz/occasion Controls: 0.004 ± 0.01 oz/day 0.17 ± 0.4 oz/occasion	* Exposed children displayed lower FA values in the left middle **cerebellar** peduncle
(Green *et al.*, 2013)	FASD: 10.0 ± 1.6	FASD: 14	Not available	* Significant positive and negative correlations were found between FA values and saccade reaction times in clusters located in the right **CC,** genu of the **CC** and left **cerebellum**
Spectroscopy				
(Cortese *et al.*, 2006)	FAS: 11.23 ± 1.1 Fetal Alcohol Effects (FAE): 11.6 ± 0.7 Controls: 11.7 ± 0.5	FAS: 7 FAE: 4 Controls: 4	Not reported	* Subjects exposed to alcohol had a higher NAA/Creatine ratio in the left and right **caudate** nucleus compared to controls * Higher levels of NAA (N-acetylaspartate) were found in the left **caudate** of the FAS group compared to controls

(Fagerlund *et al.*, 2006)	FASD: 18.3 (Range: 14-21) Controls: 18.8 (Range: 14-21)	FASD: 10 Controls: 10	Not reported	* FASD participants had: - Lower NAA/Creatine ratios in the right parietal **cortex** and **CC** - Lower NAA/Choline ratios in the right parietal **cortex** and left **thalamus** - Higher absolute signal intensity for creatine in the bilateral parietal **cortex,** left **thalamus** and **CC** - Higher absolute signal intensity for Choline in the bilateral parietal **cortex,** left **thalamus** and right frontal **cortex** - Higher absolute signal intensity for NAA in the right frontal **cortex** and bilateral **thalami**
(Gonçalves *et al.*, 2009)	FASD: 13.6 ± 3.8 Controls: 12.1 ± 3.4	FASD: 8 Controls: 8	Not reported	* Exposed subjects had a higher myo-inositol/creatine ratio in the left **cerebellum**
PET (Positron emission tomography)				
(Clark *et al.*, 2000)	FASD: 20.6 ± 4.4 Controls: 22.8	FASD: 19 Controls: 15	Not reported	* Children with FASD had lower metabolic rates in the **thalamus, caudate** and right **putamen**

2.6.2 Relaxometry of grey and white matter

Table 2 provides a summary of grey and white matter tissue parameter values previously reported. Unless stated otherwise, these are mean ± standard deviation (SD). 'NR' indicates data that were not reported. The IT'IS Database for thermal and electromagnetic parameters of biological tissues reports an average T_2 value from 9 studies (5 that studied grey matter and 4 that studied white matter) (Hasgall PA *et al.*, 2018). References to these studies are not provided by the database.

As evident from Table 2, white matter typically has shorter T_1 values than grey matter. This is due to the presence in white matter of myelin sheaths that insulate nerve axons to increase electrical impulse speed. Myelin is rich in lipids, proteins, cholesterol and iron, and has less free water content. Shorter T_1's in white matter therefore point to a higher volume fraction of myelin, and specifically higher concentrations of myelin-bound cholesterol (Koenig, 1991).

Table 2: Tissue parameter values previously reported for grey and white matter.

Scanning technique/ Method	**Field Strength**	**Sample size**	**Subject age**	**Grey matter value (ms)**	**White matter value (ms)**	**Reference**
T1						
Rapid slice profile corrected 2D variable flip angles (VFA)	3T	6	28 ± 2 (mean ± SD)	1433 ± 80	969 ± 85	(Dieringer *et al.,* 2014)
Variable TR spin-echo	3T	19	29-47	1331 ± 13 (mean ± std error)	832 ± 10 (mean ± std error)	(Wansapura *et al.*, 1999)
Magnetization prepared rapid gradient echo (MPRAGE)	3T	4	24,39,40,43	1607 ± 76	838 ± 50	(Wright *et al.*, 2008)
T2						
Multiple spin-echo method	3T	19	29-47	79.6 ± 0.6 (mean ± std error)	110 ± 2 (mean ± std error)	(Wansapura *et al.*, 1999)
Gradient echo-spin echo (GESE)	3T	4	24-44	Frontal: 76 ± 2 Occipital: 68 ± 6	71 ± 2	(Cox and Gowland, 2008)
Average from various studies reported by the IT'IS Database	3T	NR	NR	92.6 ± 16.9	60.8 ± 13.1	(Hasgall PA *et al.*, 2018)
T2*						
Fast low-angle shot (FLASH)	3T	7	28-51	Frontal: 51.8 ± 3.3 (mean ± std error) Occipital: 41.6 ± 2.0 (mean ± std error)	Frontal: 44.7 ± 1.2 (mean ± std error) Occipital: 48.4 ± 4.5 (mean ± std error)	(Wansapura *et al.*, 1999)
Multi-slice, multi-echo GRE	3T	6	37 ± 10.9 (mean ± SD)	59.7	54.6	(Peters *et al.*, 2006)
PD						
Inversion recovery	1.4T	4	NR	86 ± 11	77 ± 11	(Wehrli *et al.*, 1985)
32-echo single slice	1.5T	12	24-46	83	71	(Whittall *et al.*, 1997)

Unless stated otherwise, values are mean ± standard deviation

2.6.3 Clinical interpretation of tissue parameter differences

Although many studies have shown that relaxation times differ between healthy and diseased tissues (for example, Damadian, 1971; Damadian *et al.*, 1973, 1974; Miller, Thompson and Filippi, 2003), the mechanisms underlying these changes are not well understood as the factors that influence tissue parameter values are many and complex. Eickhoff *et al.* (2005), for example, reported that lower cell density (and less structure) in the outer cortical layers correspond to longer T_1 relaxation times, and Ogg and Steen (1998) that increasing iron content in the cortex, caudate, putamen and frontal white matter is associated with decreasing T_1 values. Higher iron content in the globus pallidus and putamen has been linked to shorter T_2 decay, and higher free water content and fewer macromolecules to longer T_2 (Schenker *et al.*, 1993). In 2008, Akber (Akber, 2008) compiled a summary of T_1 and T_2 relaxation times measured between 1987 and 2007 in pathological human and animal brain, heart, liver, spleen, lung, breast, kidney, muscle and miscellaneous tissues. Pathologies in the brain included infarction, tumour, abscess, glioblastoma, meningioma, metastasis, neurinoma, schizophrenia, adenoma, cyst, glioma, hemangioblastoma, multiple sclerosis (MS), encephalomyelitis, astrocytoma, angiomatous, craniopharyngioma, edema, edenoma, endothelioma, ependymoma, hematoma, oligoastrocytoma, psammoma, neuroma, Tourette's syndrome, systemic lupus erythematosus, demyelination, schwannoma, cold injury and bilateral common carotid artery occlusion.

Findings linking relaxation times with water content have been inconsistent, with some studies showing associations (Bakay *et al.*, 1975; Go and Edzes, 1975; Naruse *et al.*, 1982, 1986; Yoshiharu Horikawa *et al.*, 1986; Kamman *et al.*, 1988; Schad *et al.*, 1989; Kotwica, Thuomas and Persson, 1989; Boisvert, Handa and Allen, 1990; Shioya *et al.*, 1990; Fu, Tanaka and Nishimura, 1990; Kamman, Go and Berendsen, 1990; Iwama *et al.*, 1992; Boxt *et al.*, 1993; Knight *et al.*, 1994; Lin *et al.*, 1997; Manfredonia *et al.*, 2007), and others not (Iwama *et al.*, 1992). Akber (1992b) suggests that T_1 differences between tumour, edema and healthy tissues may instead be due to differences in oxygen concentration (Akber, 1987, 1988, 1989b, 1989a, 1990), since there is low oxygen tension at the centre of tumours that increases outwards and towards normal tissue (Gatenby *et al.*, 1985, 1988). Healthy tissue in close proximity to tumours have been shown to have higher T_1 values than distant healthy tissue (Beall and Hazlewood, 1983; Boesiger *et al.*, 1990) .

Despite being the topic of numerous studies (Cope, 1969; Blicharska *et al.*, 1970; Hollis *et al.*, 1973; Block and Maxwell, 1974; Civan and Shporer, 1975; Lewa and Zbytniewski, 1977; Hazlewood, 1979; Shah *et al.*, 1982a; Ling, 1983; Cameron, Ord and Fullerton, 1984; Schuhmacher *et al.*, 1985; Ling, 1989; Ling, Kolebic and Damadian, 1990; Fahlvik *et al.*, 1990; Fahlvik, Holtz and Klaveness, 1990; Negendank *et al.*, 1991; Akber, 1992; Niemi, Komu and Koskinen, 1992; Ranade and Shingatgeri, 1992; Akber, 1993; Li *et al.*, 1996), paramagnetic ions do not appear to affect relaxation times. Shah *et al.* (1982b) reported lower amounts of paramagnetic ions in tumour-bearing spleen and higher amounts of paramagnetic ions in tumour-bearing

liver of mice, but no significant differences in T_1 values. Similarly, Negendank *et al.* (1991) found no significant differences in T_1 and T_2 between healthy and leukemia affected spleen tissue, but lower amounts of paramagnetic ions in the cancer affected tissue.

Various studies have hypothesised that the presence or absence of protein in a cell may influence relaxation parameters since the protein surface is bound to a portion of the cell water (Odeblad and Lindstrom, 1955; Huggert and Odeblad, 1959; Bratton, Hopkins and Weinberg, 1965; Hazlewood, Nichols and Chamberlain, 1969; Civan and Shporer, 1975; Escanye, Canet and Robert, 1982; Cameron, Ord and Fullerton, 1984; Koenig and Brown, 1985; Brown *et al.*, 1986; Rorschach and Hazlewood, 1986). A study by Ranade, Partain and Price (1988), however, reported no correlation between longer T_1 and levels of protein content in healthy tissue versus diseased tissue.

In multiple sclerosis (MS), hypointense lesions had lower fractional anisotropy (FA) and higher apparent diffusion coefficients on DTI (Droogan *et al.*, 1999; Nusbaum, Lu, *et al.*, 2000; Nusbaum, Tang, *et al.*, 2000; Castriota-Scanderbeg *et al.*, 2003), higher levels of choline and lower levels of NAA (Van Walderveen *et al.*, 1999; Li *et al.*, 2003), and higher water content, T_1 and T_2 (Vavasour *et al.*, 2007). Two studies demonstrated correlation between T_1 hypointensity and axonal loss (Van Waesberghe *et al.*, 1999; Bitsch *et al.*, 2001), with one showing increasing T_1 hypointensity during demyelination that decreased again when remyelination occurred (Bitsch *et al.*, 2001).

In MS patients, lesions with longer T_2 values had lower myelin water fractions (MWF), higher water content, longer T_1 values and lower magnetization transfer ratios (Laule *et al.* 2007; MacKay *et al.*, 2009). Laule *et al.* (2007) suggest that the long T_2 signals are attributable to higher levels of extracellular water content. Lower signal intensities on T_2-weighted images have also been associated with increasing iron content (Drayer *et al.,* 1986).

Iron directly influences T_2* in both healthy and diseased tissue (Gelman *et al.*, 1999; Bartzokis and Tishler, 2000; Brass *et al.*, 2006; Duyn *et al.*, 2007; Fukunaga *et al.*, 2010; Langkammer *et al.*, 2010; Pitt *et al.*, 2010; Bagnato *et al.*, 2011; Bagnato, Hametner and Welch, 2013; Mehta *et al.*, 2013). Iron induces microscopic field gradients and has a paramagnetic effect on susceptibility that causes the T_2* signal to decay faster (Langkammer *et al.*, 2010; Bagnato, Hametner and Welch, 2013). The effect of iron on the T_2* signal increases with an increase in magnetic field strength (Bizzi *et al.*, 1990; Schenck, 1995; Yao *et al.*, 2009).

Iron is not the only factor that influences T_2* measurements – boundaries such as tissue-tissue, tissue-bone, and tissue-air, as well as increasing heterogeneity, also result in faster T_2* signal decay (Bagnato, Hametner and Welch, 2013). Other factors that impact signal decay include calcium (Wu *et al.*, 2009; Baheza *et al.*, 2015), macroscopic geometry (Chu *et al.*, 1990; Shmueli *et al.*, 2009), white matter (WM) fibre bundle orientation in relation to the magnetic field (He and Yablonskiy, 2009;

Bender and Klose, 2010; Lee *et al.*, 2010, 2011), and deviations in myelin content (Ogg *et al.*, 1999; Li *et al.*, 2009; Zhong *et al.*, 2011). Myelin is diamagnetic and contains high water content that enhances the T_2* signal, this is best observed in WM regions that contain low iron concentrations and high levels of myelin such as the optic radiations (Li *et al.*, 2012). Miniscule fibre direction dependent field deviations are caused by diamagnetic myelin fibres with an anisotropic structure (Li *et al.*, 2012). These field deviations can increase the T_2* *in vivo* by up to 60% (Lee *et al.*, 2012; Sati *et al.*, 2012). A study by Fukunaga *et al.* (2010) extracted the iron in both white and grey matter and still observed diamagnetic frequency contrast in WM relative to grey matter (GM). The authors suggest diamagnetism is higher in myelinated WM with no iron content than in GM with no iron content. An experimental demyelination study in animals found a significantly higher T_2* in WM and an insignificantly higher T_2* in GM when compared to that of healthy animals, validating myelin as an essential source of T_2* contrast (Lee *et al.*, 2012).

PD strongly correlates with water content in brain tissue as the majority of MRI visible protons are in water (Tofts, 2004). Therefore PD is higher in regions that are inflamed or where there is edema (Gracien *et al.* 2016; Just and Thelen, 1988; Gideon et al, 1999). Tofts (2004) gives two reasons for differences between PD values and actual water content – firstly, bound water that is 'MRI invisible' can form part of the total water content but will not reflect in the PD value; and secondly, non-water environments like macromolecules or proteins can house a significant amount of MRI invisible protons. Although PD will likely correlate strongly with T_1 values, its biological interpretation is simpler as it is approximately equal to the mobile water content of the tissue.

Since no single biological mechanism can fully explain tissue parameter changes, information from other imaging modalities may prove useful. For example, functional MRI exploits blood oxygenation level dependent (BOLD) signals, where more activity results in higher blood oxygenation levels and ultimately longer T_2^* relaxation times. In spectroscopy studies, lower NAA levels in normally appearing WM point toward axonal loss or dysfunction (Miller, Thompson and Filippi, 2003), and in DTI higher FA values indicate well-structured and organized WM tracts. Damaged tracts will have longer T_1 values as there will be less structure and more free water content.

In summary, T_1 is related to water and iron content, as well as the degree of myelination, gliosis and axonal damage. T_2 is primarily a marker of myelin content, but is also affected by iron and water proportions, and T_2* provides the most direct information about iron content. PD mainly reflects water content. Although the mechanisms of tissue parameter value changes are not well understood, differences in these values between healthy and pathological tissues are well established. These differences have the potential to become clinical markers able to detect subtle disease-related differences, possibly before other changes are evident. To our knowledge, no studies have examined effects of PAE on brain tissue parameters.

3. Methodology

3.1 Cohort information and sample demographics

The sample consisted of 53 Cape Coloured children from a longitudinal cohort (Jacobson *et al.*, 2008) who have been followed into adolescence. The children were born to pregnant women recruited prospectively between July 1999 and January 2002 at an antenatal clinic (ANC) in Cape Town. Women were screened by a research nurse at the mother's initial visit to the clinic. Mothers who drank >14 beverages a week and/or participated in binge drinking (i.e., consumed at least 5 standard drinks per occasion) were invited to participate in the study, as well as the next mother presenting at the ANC with a similar gestational age who abstained or drank only minimally. Detailed alcohol consumption data were collected at 3 time points using the timeline follow-back interview (TLFB; Jacobson *et al.*, 2002) – once at enrolment, once at mid-pregnancy, and within 1 month after delivery. The latter interviews aimed to determine the mother's alcohol consumption in the 2nd and 3rd trimesters. An additional 12 subjects were recruited during adolescence for whom usable neuroimaging data were available. Their mothers were administered the TLFB retrospectively to determine their alcohol use in a typical 2-week period during pregnancy.

The study excluded women with major medical problems (e.g., diabetes, cardiac problems requiring treatment, epilepsy), multiple births, and those younger than 18 years, as well as infants with neural tube defects, seizures and significant chromosomal anomalies. Mothers who reported using cocaine or pot during pregnancy were also excluded to ensure drug use wasn't driving any observed differences.

Alcohol intake volume and type of beverage consumed were converted to ounces (oz) of absolute alcohol (AA; 1 oz ≈ 2 standard drinks), where each ounce approximates to 30 mL of absolute alcohol, and three intake measures were constructed: average oz of AA consumed per day (AA/day), oz AA consumed per occasion (dose/occasion) and frequency of consumption (days/week; Jacobson *et al.*, 2008). Natural logarithm values of AA/day were used for analysis due to non-normal distribution of these data.

In 2005 a diagnostic clinic was organized in which the children from the longitudinal cohort were assessed by two expert FASD dysmorphologists and diagnosed as either FAS, PFAS, heavily exposed (HE) non-syndromal, or controls (non-syndromal with no or light exposure; Jacobson *et al.*, 2008). The dysmorphology clinics were repeated in 2009, 2013, and 2016, at which time the additional 12 adolescents were examined. Since the FAS and PFAS groups were very small (N=8 and10, respectively), these children were combined into one group (FAS/PFAS, N=18) in our analyses.

Following initial pre-processing of neuroimaging data, parameter mapping data from 2 subjects (one from the longitudinal cohort and one from the additional recruited adolescents) were affected by an aliasing artefact (i.e. the field-of-view (FoV) was too

small in the readout direction) and were not included in our analysis. The mean age of the 65 adolescents was 16.4±1.0 years (mean ± standard deviation) at the time of scanning. The sample characteristics of the participants are summarised in Table 3.

To account for variability between the children, their age, sex and whole brain parameter values were included as confounders in all analyses. Additional confounders included were the number of cigarettes the mother smoked per day during pregnancy, and her socioeconomic status (SES). SES was measured using the Hollingshead's four factor index, which includes the mother's marital status, retired/employed status, educational attainment and occupational prestige (Hollingshead, 2011). The chosen confounders overlap with the confounders used in previous studies (Jacobson *et al.*, 2008; Lindinger *et al.*, 2016).

Table 3: Sample demographics

Sample characteristics (N = 65)			
	FAS/PFAS (N=18) [mean (SD)]	Heavily exposed (N=18) [mean (SD)]	Controls (N=29) [mean (SD)]
Prenatal alcohol exposure			
Absolute alcohol/day across pregnancy (oz)	1.09 (0.82)	0.90 (1.13)	0.00 (0.00)
Absolute alcohol/occasion across pregnancy (oz)	4.00 (1.48)	3.62 (1.86)	0.04 (0.22)
Drinking frequency across pregnancy (days/week)	1.73 (0.94)	1.32 (1.17)	0.00 (0.01)
Potential confounders			
Child			
Sex (% male)	61	72	66
Age at assessment	16.74 (0.78)	16.24 (1.29)	16.21 (0.94)
Mother			
Smoking during pregnancy (cig/day)	5.69 (5.06)	8.06 (7.38)	3.45 (5.45)
Socio-economic status	18.67 (9.09)	19.13 (5.58)	22.30 (6.75)

3.2 Image acquisition

Imaging took place at the Cape Universities Body Imaging Centre (CUBIC) located at Groote Schuur Hospital using a 3T Siemens Skyra MRI scanner. The structural images used for tissue segmentation in Freesurfer, were obtained using the MEMPRAGE sequence: $TR/TE_1/TE_2/TE_3/TE_4$ = 2530/1.69/3.54/5.39/7.24 ms; field-of-view (FoV) 224 mm, with 176 slices, 1.0x1.0x1.0 mm^3. T_1, T_2* and PD were measured from images acquired with a multi-echo gradient echo (GRE) sequence for three different flip angles – 5°, 15° and 30°. The eight echo times (TE) at which the signal was sampled were 2.68, 4.64, 6.64, 8.64, 10.64, 12.64, 14.64 and 16.64 ms and the repetition time (TR) was set to 20 ms. There were 144 slices acquired at each flip angle with FoV 224x224x144 mm^3, slice thickness 1 mm and in-plane resolution 1.0x1.0 mm^2. The scanning protocol to measure T_2 consisted of a turbo spin echo (TSE) sequence with multiple echoes. The signal was sampled at TE's 10.5, 21.0 31.5 42.0 52.5, 63.0 73.5, 84.0, 94.5, 105.0, 115.5, 126.0, 136.5, 147.0, 157.5, 168.0, 178.5, 189.0, 199.5 and 210.0 ms, covering a wide range of values for model fitting that includes both short, medium and long T_2 tissue constituents. Other parameters were TR 5410 ms, 25 slices, thickness 5.0 mm, slice gap 1.5 mm, in-plane resolution 1.0 x 1.0 mm^2, and FoV 250 mm. Due to odd echo dephasing (Brown *et al.*, 2014) effects that resulted due to the second (even) echo time (i.e. 21 ms) being exactly double that of the first (i.e. 10.5 ms), we were forced to exclude the images from the first echo in the analysis.

3.3 Image processing and parameter map construction

3.3.1 Segmentation

A combination of FreeSurfer (v6.0.1), FSL (v5.0.9) and AFNI (v17.2.07) were used for image processing and parameter mapping. FreeSurfer's recon-all command was used for image reconstruction. Full details of what recon-all includes can be found at https://surfer.nmr.mgh.harvard.edu/fswiki/recon-all. The root-mean-square (RMS) T1-weighted images constructed from the four echoes acquired during the MEMPRAGE acquisition are used as input. Recon-all segments the brain volume into cortical and subcortical regions. The automatic segmentation of the subcortical regions is done by assigning each voxel a neuroanatomical label (Fischl *et al.*, 2002). The label is determined by probabilistic information obtained from a manually labelled training set. A typical segmentation output is shown in Figure 15. Freeview (v2.0) was used to visually inspect the recon-all output.

The following are outputs of recon-all:

- The intensity normalized anatomical T_1 volume (T1.mgz)
- The automatically segmented volume (which contains segmented grey matter, white matter and subcortical structures) (aseg.mgz)
- The white matter mask (wm.mgz)

- The skull stripped T_1 volume of the brain (brain.mgz)

All outputs were overlaid and examined for proper alignment and image quality.

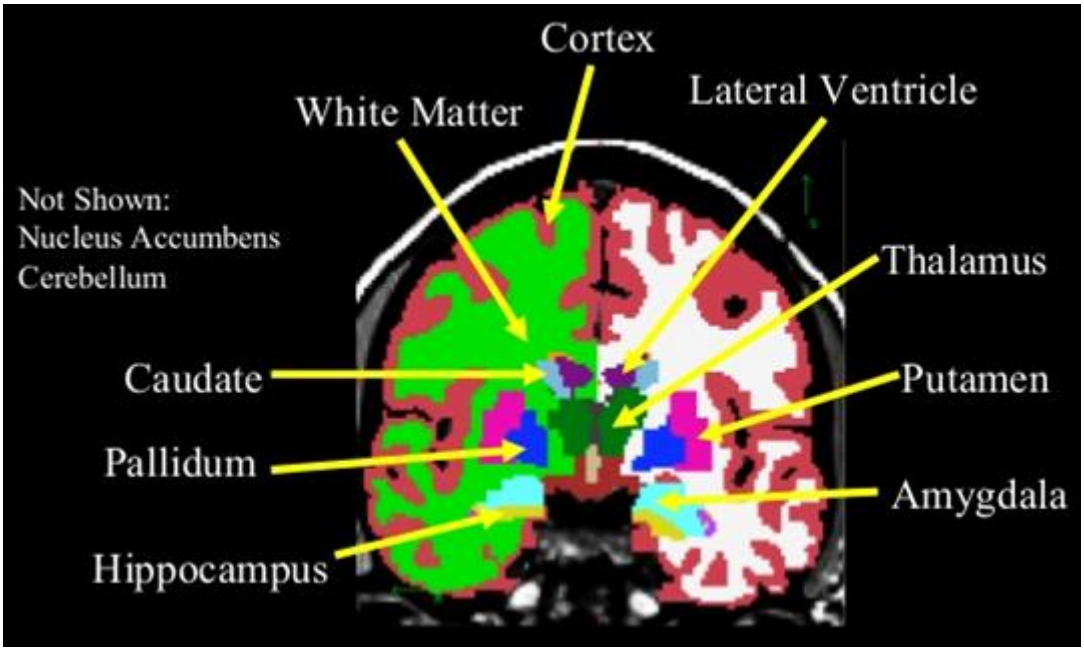

Figure 15: Typical volumetric segmentation (aseg.mgz) output by Freesurfer (Fischl *et al.*, 2002).

In the present study, we examined 43 regions-of-interest (ROIs). These regions (Table 4) include white and grey matter structures, CSF (all the CSF in the brain that is not in the ventricles), ventricles, vessels, the ventral diencephalon (VDC; which consists of a group of structures that cannot be distinguished from one another) and the choroid plexus (a group of cells producing CSF). It is important to note that the left and right vessels do not refer to blood vessels. According to Freesurfer expert Bruce Fischl in an email communication on the 21st of August 2014 at 10:23 am (Freesurfer archives, 2014), it refers to inferior sections of the pallidum/putamen that have much darker intensity values than grey matter. Therefore, it makes more sense to label it separately as it aids in more accurate labelling. He also mentions that the vessels might be lacunae rather than part of a structure. The colour assigned by FreeSurfer to each region is also illustrated in the table.

3.3.2 Parameter mapping – data preparation

The FreeSurfer mri_convert command was used to convert raw dicom images to mgz and nii format in order for the respective programs to identify and use the files when necessary. AFNI's 3dresample command was used to ensure that all images were oriented right posterior inferior (RPI). The T_1, T_2* and PD parameter maps were constructed from multi-echo GRE volumes collected at 3 different flip angles, while the T_2 parameter maps were constructed from multi-echo TSE volumes. FreeSurfer's function mri_ms_fitparms (Fischl et al., 2004; Deoni, Peters, & Rutt, 2005) uses the

standard signal equation shown in Section 2.4 to estimate the T_1, T_2,T_2* and PD parameters. The method described in Fischl *et al.* (2004) estimates the parameters by minimizing the standard deviation between the measured signals and signal model (given by equation 4).

To ensure proper alignment of parameter maps with segmented subcortical structures, it was necessary to align (using AFNI's 3dAllineate command) the skull stripped PD map with the skull stripped brain volume that was output by recon-all (brain.mgz). The PD parameter map was skull stripped using FSL's brain extraction tool (bet2). For each subject a brain mask was created from the skull stripped PD map, which was used to mask the T_1, T_2* and T_2 maps. The resulting maps were aligned with the structural T_1-weighted (brain.mgz) file to ensure accurate segmentation.

FreeSurfer's mri_binarize command was used to construct subject-specific binary masks of each ROI from the segmented volumes (aseg file). Using fslmaths, each ROI mask was multiplied by the subject's T_1, T_2*, PD and T_2 maps to calculate the average parameter value for that ROI. The outputs were stored in a text file using FSL's fslstats. In addition to the ROIs mentioned above, the average parameter values across all white matter were also calculated. The output data were initially exported to Microsoft Excel where the PD values were normalized to CSF by dividing, for each subject, the PD value of every region by the PD value of CSF for that subject.

Table 4: Regions segmented by FreeSurfer for which parameter values were calculated. The segmented volume (aseg.mgz) output by Freesurfer assigns each region a different colour as indicated in the table.

Grey matter	Brain stem	
	Left accumbens area	
	Right accumbens area	
	Left amygdala	
	Right amygdala	
	Left caudate	
	Right caudate	
	Left cerebellum cortex	
	Right cerebellum cortex	
	Left hippocampus	
	Right hippocampus	
	Left pallidum	
	Right pallidum	
	Left putamen	
	Right putamen	
	Left thalamus	
	Right thalamus	
White matter	Left cerebellum white matter	
	Right cerebellum white matter	

	Anterior corpus callosum	
	Mid-anterior corpus callosum	
	Central corpus callosum	
	Mid-posterior corpus callosum	
	Posterior corpus callosum	
	Optic chiasm	
Total GM	Left cerebral cortex	
	Right cerebral cortex	
Total WM	Left cerebral white matter	
	Right cerebral white matter	
	Subcortical white matter	
Ventricles and Vessels	Third ventricle	
	Fourth ventricle	
	Left lateral ventricle	
	Right lateral ventricle	
	Left inferior lateral ventricle	
	Right inferior lateral ventricle	
	Left vessel	
	Right vessel	
Miscellaneous	Left ventral diencephalon	
	Right ventral diencephalon	
	Left choroid plexus	
	Right choroid plexus	
	Cerebrospinal-fluid (CSF)	

3.3.3 Parameter mapping – data analysis

Statistical analyses were performed in R (v3.4.1). The compiled Excel spreadsheets were loaded into R and combined with the demographic data. Outliers were identified for each ROI by checking for parameter values removed more than 3 standard deviations (SD's) from the mean. The largest value in the ROI within the 3 SD limitation was assigned as the upper bound, and the smallest value as the lower bound. To ensure outliers weren't driving results they were winsorized in a scale manner as illustrated in Figure 16.

T-tests were carried out for each ROI between the original data and the data that contained winsorized values to ensure there weren't significant differences between the two datasets. Since none of the t-tests were significant, the winsorized datasets were used in all analyses. Winsorizing the data additionally reduced the skewness so that parametric tests could be used. Data for absolute alcohol per day across pregnancy (aadxp) were log transformed due to skewness.

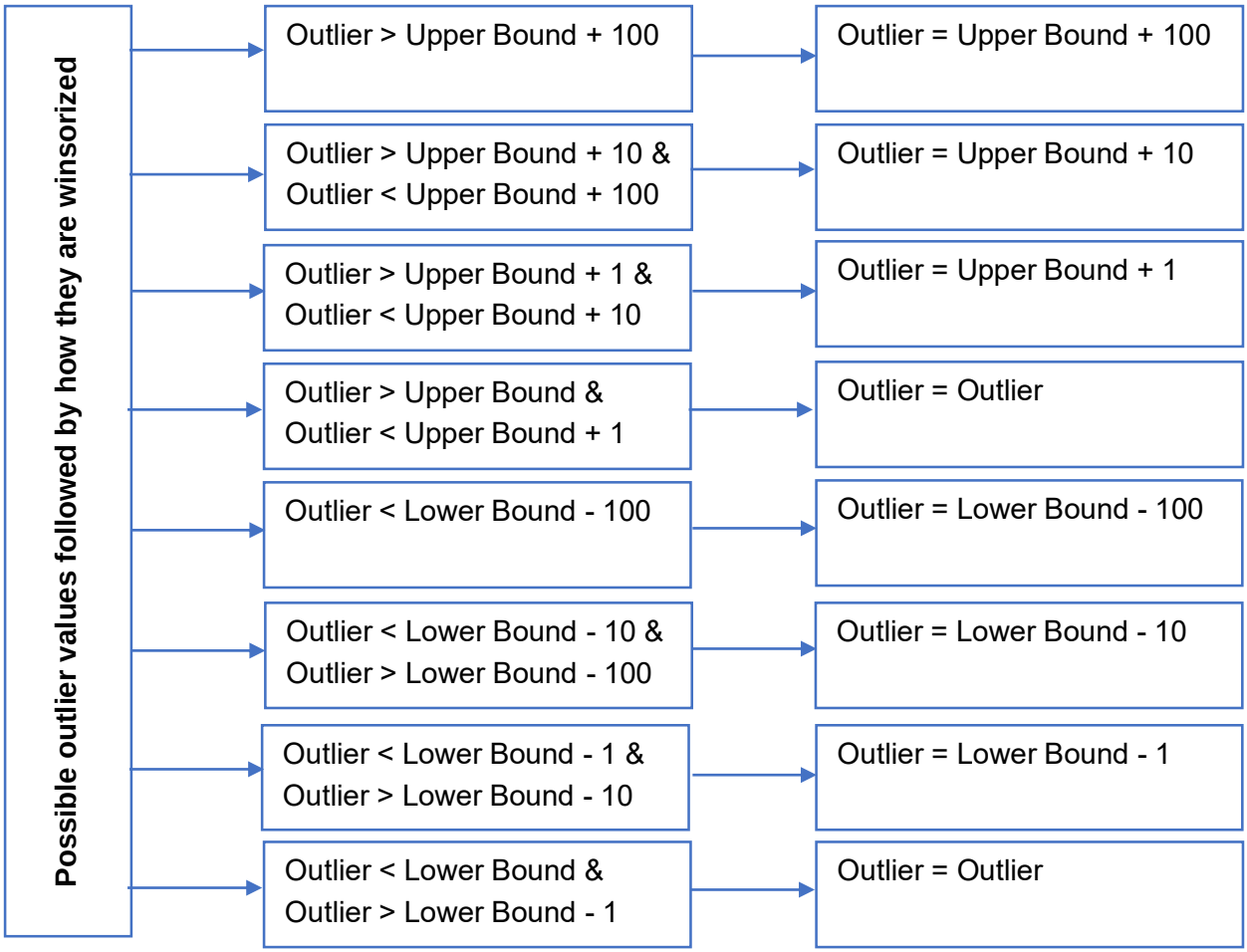

Figure 16: Illustration indicating how outliers were winsorized.

After data preparation, subjects were grouped according to their diagnosis, i.e. FAS, PFAS, HE and controls. FAS is the most severe diagnosis followed by PFAS; HE denotes children with confirmed alcohol exposure, but lacking the facial phenotype, and controls are those who weren't exposed to alcohol, or were only minimally exposed. As mentioned before, the FAS and PFAS groups were combined into one group (FAS/PFAS) for group analyses to increase statistical power. In each region, the average value and standard deviation of each tissue parameter were calculated for each diagnostic group. To elucidate the distribution of the data, the coefficient of variation (CV) was calculated by dividing the standard deviation by the mean, and multiplying the answer by 100 to express it as a percentage. This standard deviation to mean ratio gives an indication of the relative variability of tissue parameter values in the region.

In R, analyses of covariance (ANCOVA) are done using multiple linear regression models with diagnosis as a categorical variable. The multiple linear regression equation is shown in Equation 5, where y represents the tissue parameter value (dependent variable), x_1 is diagnosis, x_2 to x_n are the confounding variables, b_0 represents the intercept, and b_1 to b_n represents the coefficients or beta values that indicate how much the value of y (the tissue parameter value) changes for every one unit change in a parameter (x_1 to x_n).

$$y = b_0 + b_1 x_1 + b_2 x_2 + \ldots + b_n x_n \quad (5)$$

In every region, multiple regression analysis was used to determine whether tissue parameter values differed between the three groups. As mentioned previously, age, sex, number of cigarettes smoked by the mother per day during pregnancy, socioeconomic status (SES), and whole brain parameter values were included as confounders in all analyses. The linear model (lm) and summary functions in R were used to calculate and view results. For each region showing a significant difference between at least two groups, box-and-whisker plots overlaid with scatterplots of the parameter values were constructed. The whiskers extend to 3 SD's beyond the mean.

Since little is known about the mechanisms through which PAE affects the brain, this project was exploratory in nature and no specific hypotheses were tested. Due to the small effect sizes expected, adjustment for multiple comparisons (i.e. in 43 ROIs) would likely yield all results insignificant. Therefore, corrected p-values were not viewed as critically important in this exploratory analysis, although the FDR (false discovery rate) correction method was used to calculate corrected p-values (Benjamini and Hochberg, 1995). This method was chosen as it is less stringent than controlling the family-wise error rate or Bonferroni adjustment.

Additional analyses included investigating the relationship between the amount of alcohol the mother consumed during pregnancy and tissue parameter values in the child. Three alcohol measures were considered: aadxp, which gives the ounces absolute alcohol consumed per day by the mother across pregnancy; aaddxp, which gives the ounces absolute alcohol consumed by the mother on the days that she drank; and freqxp, which describes how frequently the mother drank (days/week) across pregnancy. One ounce absolute alcohol (AA) is equivalent to two standard drinks. All confounders were included in the multiple regression models. We report beta values and standard errors of the alcohol measures for all regions where the association with at least one of the three alcohol measures was significant. Standardised beta values were computed using the lm.beta function in the "QuantPsyc" package to facilitate comparison of the strength of the associations in the different regions. Standardised beta values give an indication of the amount of variance in the dependent variable (y) that is explained by each independent variable.

Using the ggplot2 package designed for R, linear regression plots were made of all regions showing significant association of tissue parameter values with level of alcohol exposure. The alcohol measure that rendered the most results was used to draw plots for the respective tissue parameter. When constructing the plots, the regression models did not include confounders. The R^2 values for these models are reported at the top of the plots, together with the p-value from the regression model including all confounders. Regression plots were also constructed excluding the control group to determine if associations would be stronger, but the majority of R^2 values did not increase and therefore these plots were not included.

4. Results

Table 5 gives tissue parameter values averaged across all subjects for total grey (left and right combined) and white (left and right cerebral and subcortical combined) matter.

Table 5: Total grey matter and white matter tissue parameter values averaged across all subjects.

	T_1 (ms)	T_2 (ms)	T_2* (ms)	PD
Total Grey Matter	1421 ± 30	136 ± 2	67 ± 1	1918 ± 44
Total White Matter	1106 ± 19	101 ± 2	48 ± 2	1537 ± 84

4.1 T_1 results

Examples of the T_1 maps and their corresponding segmentation overlays are shown for axial, coronal and sagittal slices in Figure 17. The scalebar demonstrates the range of T_1 values measured. The colour legend of the neuroanatomical regions as segmented by Freesurfer are as in Table 4. Average T_1 parameter values showed differences (at $p<0.1$) between any two diagnostic groups in 12 of 43 regions (Table 6 and Figure 18). In 7 regions, namely bilateral accumbens, left caudate, right putamen, third and left lateral ventricles, and right vessel, increasing levels of alcohol exposure were associated with higher T_1 values, while increasing alcohol exposure was related to decreasing T_1 values in right cerebellar cortex (Table 7 and Figure 19). Regression plots were not included if $R<0.1$. None of these findings survived after FDR correction.

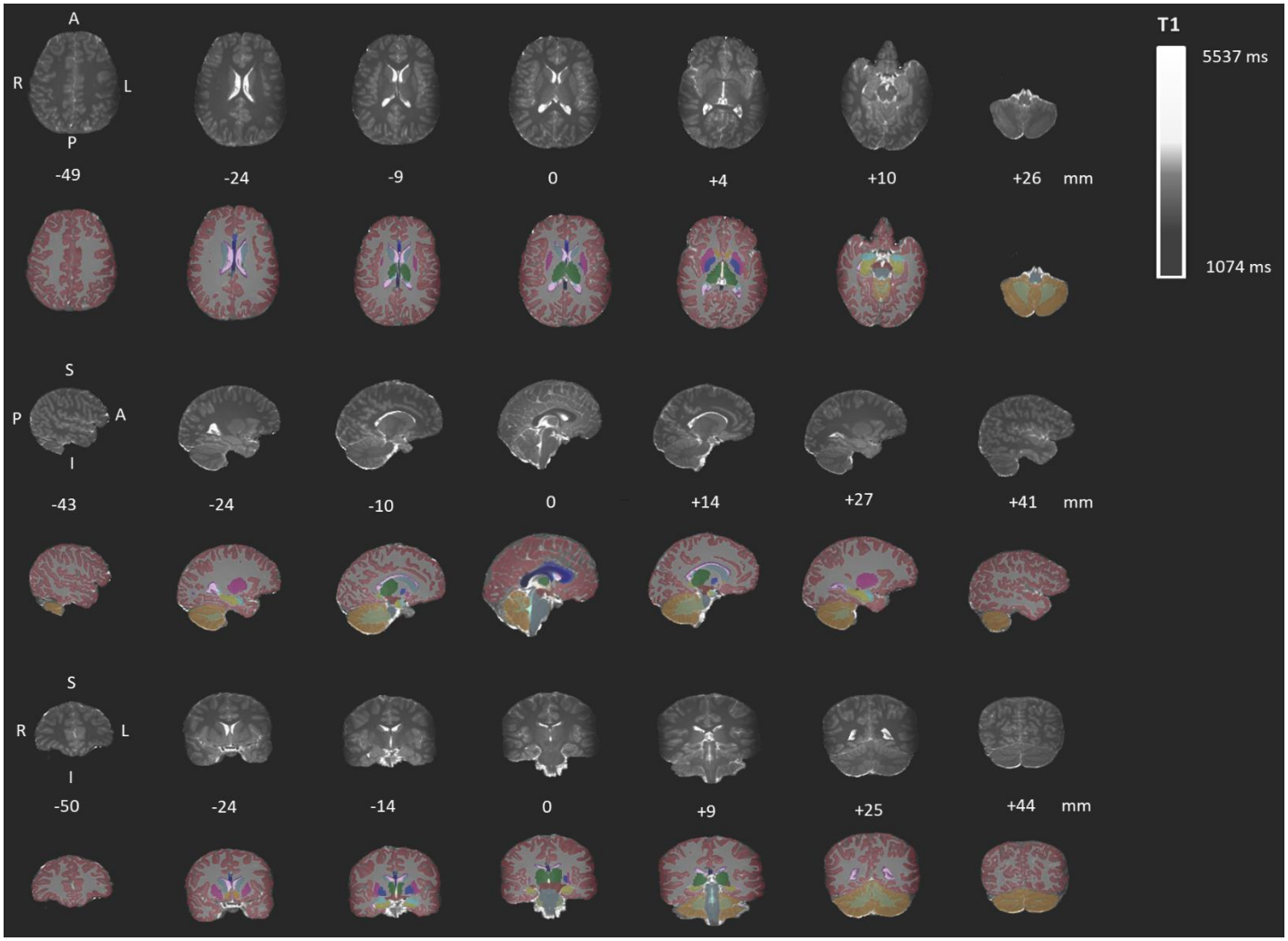

Figure 17: Example of T_1 maps in the axial (top), sagittal (middle) and coronal (bottom) orientations. Seven slices of each orientation is illustrated in grayscale. The Freesurfer segmentation map (aseg.mgz) overlaid on the slice is illustrated below each respective slice. The middle (fourth) slice represents the approximate middle of the brain and is referenced as 0 mm. The number below each slice indicates its position (in mm) from the reference slice. For the axial view, slices start with the most superior view on the left, and end with the most inferior view on the right. For the sagittal view, slices start in the right side of the brain and progress toward the left side of the brain. For the coronal orientation, slices start in frontal cortex on the left, and move towards the back of the brain to the right. The first image for each orientation indicates the right (R), left (L), superior (S) and inferior (I) positions of the brain. Colours corresponding to different Freesurfer segmented regions are as listed in Table 4.

Table 6: Regions showing T_1 differences (at $p<0.1$) between any two diagnostic groups.

T_1 measures (ms)				Pairwise p-values		
Region	**Controls**	**HE**	**FAS/PFAS**	**Controls vs FAS/PFAS**	**Controls vs HE**	**FAS/PFAS vs HE**
Right amygdala	2383 ± 128 (5)	2374 ± 103 (4)	2350 ± 118 (5)	**0.063**	0.582	0.213
Right cerebellar cortex	1909 ± 174 (9)	1841 ± 131 (7)	1883 ± 110 (6)	**0.008**	**0.033**	0.544
Left hippocampus	2290 ± 156 (7)	2294 ± 116 (5)	2286 ± 175 (8)	**0.095**	0.611	0.27
Right hippocampus	2355 ± 141 (6)	2332 ± 109 (5)	2302 ± 156 (7)	**0.016**	0.453	0.108
Right thalamus	1956 ± 148 (8)	1978 ± 83 (4)	1937 ± 142 (7)	**0.08**	0.77	**0.061**
Right cerebellar white matter	1635 ± 100 (6)	1616 ± 124 (8)	1609 ± 76 (5)	**0.099**	0.695	0.234
Central corpus callosum	1641 ± 160 (10)	1580 ± 140 (9)	1609 ± 201 (13)	**0.062**	0.223	0.512
Left lateral ventricle	4300 ± 627 (15)	4659 ± 457 (10)	4698 ± 692 (15)	0.107	**0.028**	0.619
Right inferior lateral ventricle	3227 ± 545 (17)	3480 ± 429 (12)	3179 ± 572 (18)	0.744	0.119	**0.09**
Right vessel	2339 ± 339 (14)	2567 ± 285 (11)	2393 ± 349 (15)	0.844	**0.025**	**0.028**
Right ventral DC	1937 ± 122 (6)	1927 ± 88 (5)	1909 ± 111 (6)	**0.041**	0.311	0.311
Left choroid plexus	3068 ± 392 (13)	3198 ± 376 (12)	3020 ± 405 (13)	0.501	**0.096**	**0.036**

Values are mean ± standard deviation (Coefficient of Variation, %); Green shading denotes $p<0.05$; Gray shading denotes $0.05<p<0.1$.

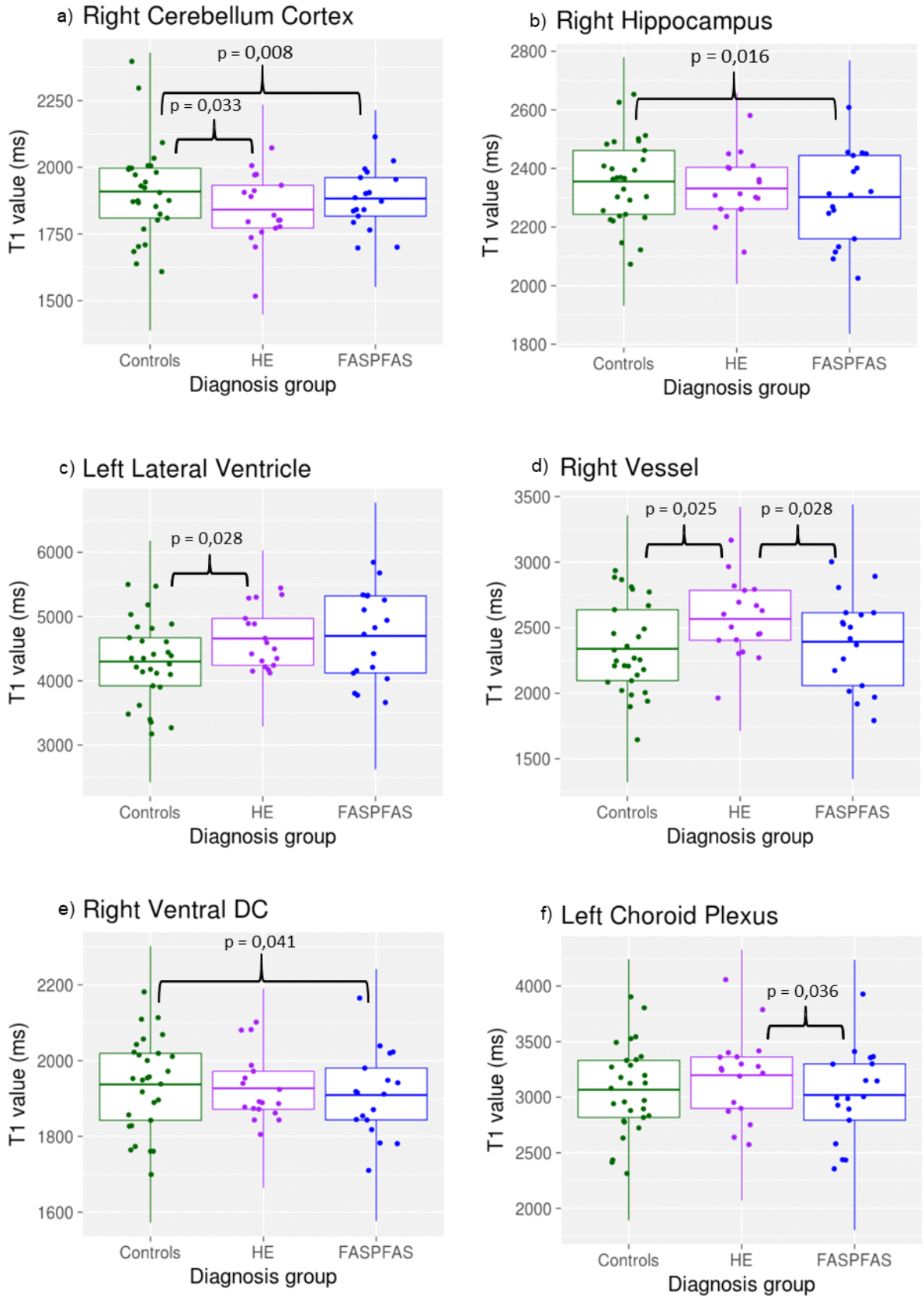

Figure 18: Box-and-whisker plots of T_1 in regions showing significant differences between any two diagnostic groups, namely the a) right cerebellar cortex, b) right hippocampus, c) left lateral ventricle, d) right vessel, e) right ventral diencephalon (DC), and f) left choroid plexus. HE, Heavily Exposed non-syndromal; FASPFAS, group comprising children with either FAS or PFAS.

Table 7: Regions where average T_1 parameter values are at least weakly associated (at $p<0.1$) with one or more of the measures describing the amount of alcohol the mother consumed across pregnancy.

	Absolute alcohol (AA) consumed per day across pregnancy (oz AA/day)		**Absolute alcohol (AA) consumed per occasion across pregnancy (oz AA/ drinking day)**		**Frequency of drinking across pregnancy (days/week)**	
Regions	**β ± Std Error (Standardised β)**	**p-value**	**β ± Std Error (Standardised β)**	**p-value**	**β ± Std Error (Standardised β)**	**p-value**
Left accumbens area	102 ± 56 (0,24)	**0.075**	8 ± 11 (0,11)	0.442	287 ± 147 (0,26)	**0.057**
Right accumbens area	125 ± 57 (0,3)	**0.032**	12 ± 11 (0,16)	0.262	347 ± 149 (0,32)	**0.023**
Left caudate	129 ± 66 (0,27)	**0.056**	15 ± 13 (0,17)	0.238	367 ± 173 (0,29)	**0.038**
Right cerebellar cortex	-89 ± 43 (-0,25)	**0.040**	-20 ± 8 (-0,31)	**0.012**	-228 ± 112 (-0,24)	**0.047**
Right putamen	66 ± 31 (0,26)	**0.04**	4 ± 6 (0,09)	0.482	179 ± 82 (0,26)	**0.034**
Third ventricle	356 ± 224 (0,22)	0.117	21 ± 42 (0,07)	0.625	1371 ± 574 (0,32)	**0.02**
Left lateral ventricle	524 ± 193 (0,35)	**0.009**	79 ± 36 (0,29)	**0.034**	1397 ± 505 (0,35)	**0.008**
Right vessel	171 ± 101 (0,21)	**0.096**	22 ± 19 (0,15)	0.26	495 ± 264 (0,23)	**0.066**

Green shading denotes significance at $p<0.05$; gray shading denotes significance at $p<0.1$.

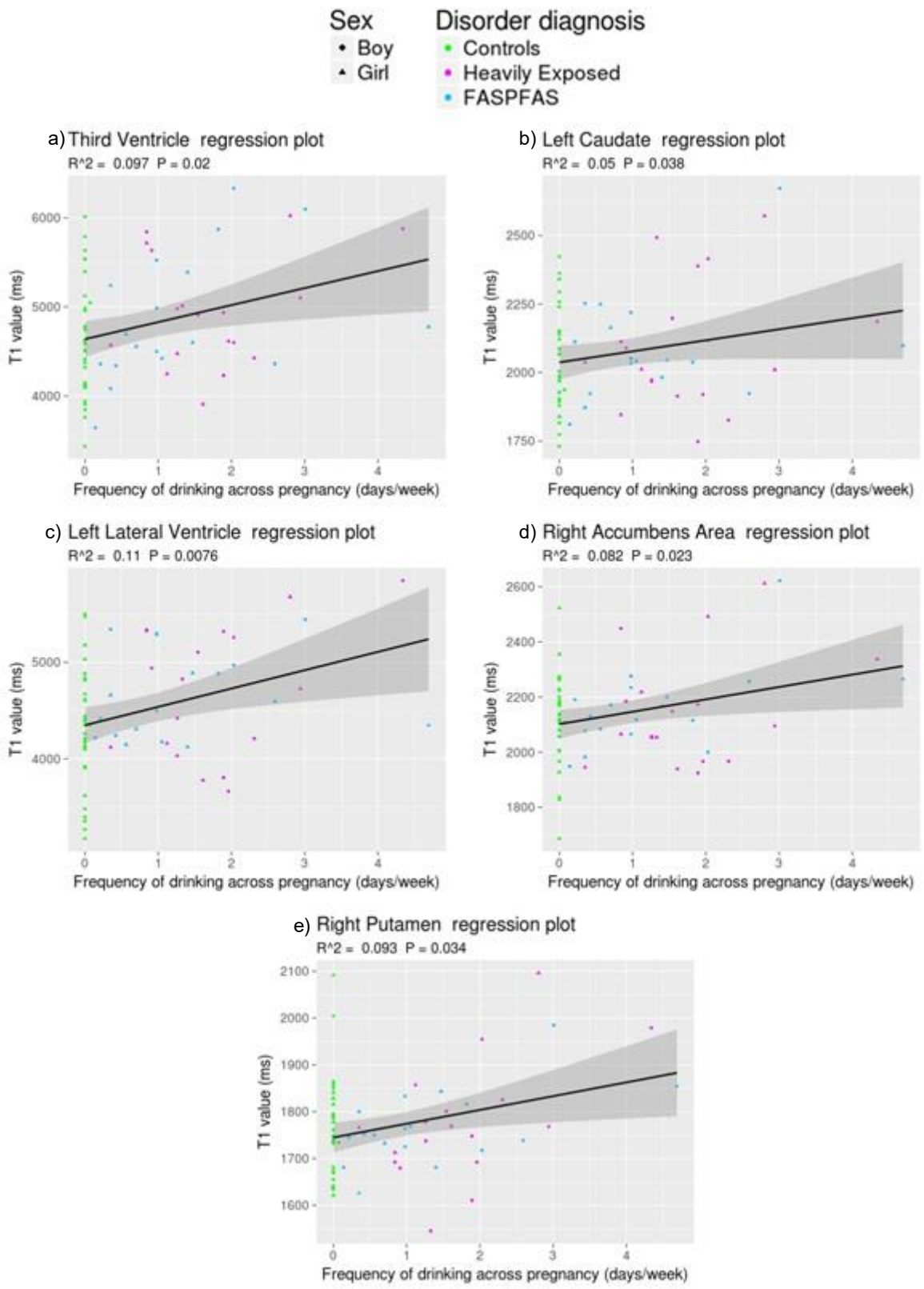

Figure 19: Plots showing regional T_1 parameter values as a function of how often the mother drank during pregnancy in the a) third ventricle, b) left caudate, c) left lateral ventricle, d) right accumbens and e) right putamen. Heavily exposed are children with confirmed high levels of alcohol exposure who are non-syndromal; FASPFAS denotes children with a diagnosis of either FAS or PFAS.

4.2 T_2 results

Examples of the T_2 maps and their corresponding segmentation overlays are shown for axial, coronal and sagittal slices in Figure 20. The scalebar demonstrates the range of T_2 values measured. The colour legend of the neuroanatomical regions as segmented by Freesurfer are as in Table 4. Average T_2 parameter values showed differences (at $p<0.1$) between any two diagnostic groups in 19 regions (Table 8 and Figure 21). In 5 regions (bilateral caudate, mid-posterior corpus callosum, left lateral ventricle, right vessel), increasing levels of alcohol exposure were associated with higher T_2 values, while increasing alcohol exposure was related to decreasing T_2 values in three regions (left amygdala, left cerebellar cortex, central corpus callosum) (Table 9 and Figure 22). Regression plots were not included if $R<0.1$. None of these findings survived after FDR correction.

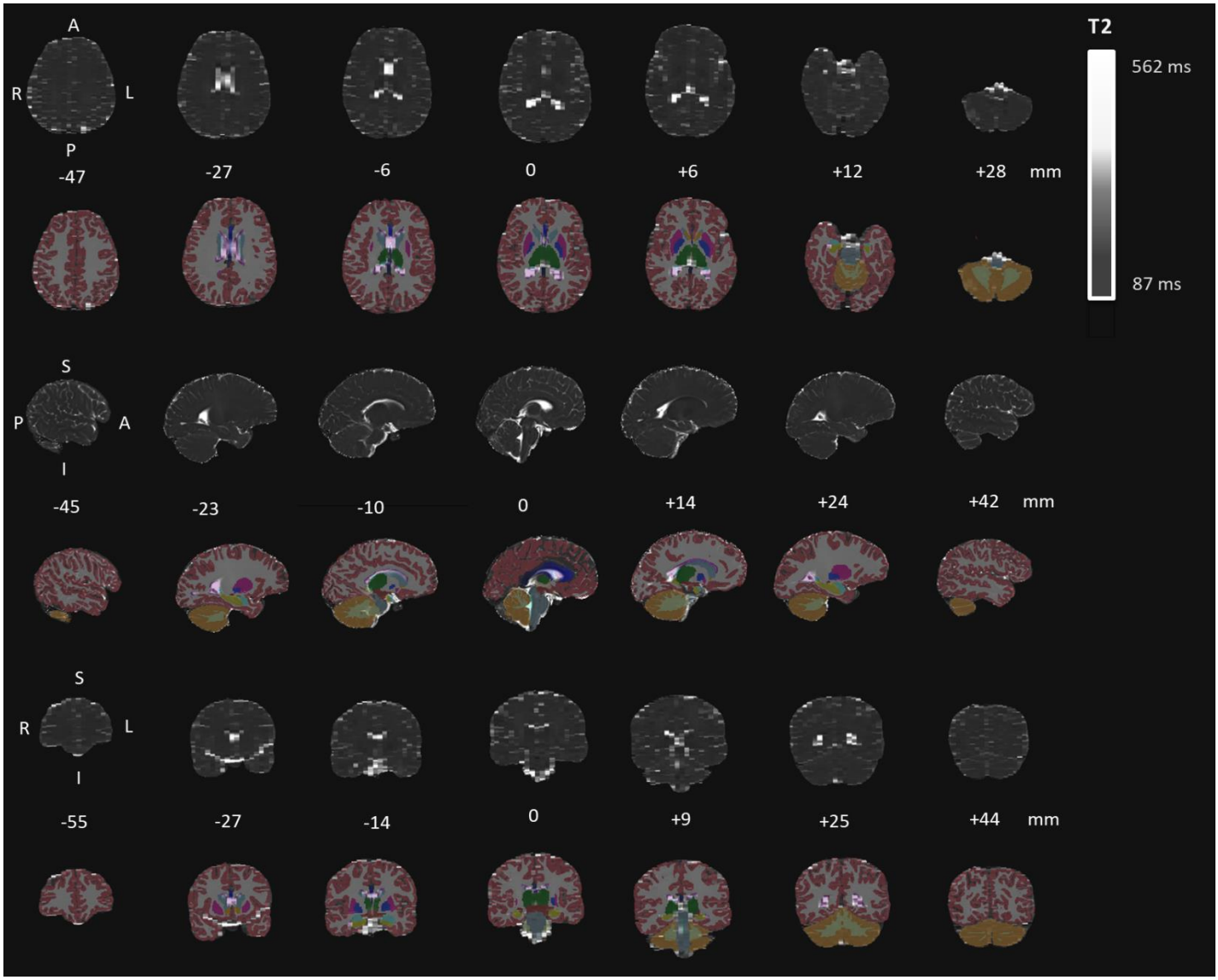

Figure 20: Example of the T_2 maps in the axial (top), sagittal (middle) and coronal (bottom) orientations. Seven slices of each orientation is illustrated in grayscale. The Freesurfer segmentation map (aseg.mgz) overlaid on the slice is illustrated below each respective slice. The middle (fourth) slice represents the approximate middle of the brain and is referenced as 0 mm. The number below each slices indicates its position (in mm) from the reference slice. For the axial view, slices start with the most superior view on the left, and end with the most inferior view on the right. For the sagittal view, slices start in the right side of the brain and progress toward the left side of the brain. For the coronal orientation, slices start in frontal cortex on the left, and move towards the back of the brain to the right. The first image for each orientation indicates the right (R), left (L), superior (S) and inferior (I) positions of the brain. Colours corresponding to different Freesurfer segmented regions are listed in Table 4.

Table 8: Regions showing T_2 differences (at $p<0.1$) between any two diagnostic groups.

T_2 measures (ms)				Pairwise p-values		
Region	**Controls**	**HE**	**FAS/PFAS**	**Controls vs FAS/PFAS**	**Controls vs HE**	**FAS/PFAS vs HE**
Brain stem	163 ± 13 (8)	157 ± 12 (8)	166 ± 8 (5)	0.922	**0.037**	**0.044**
Left amygdala	123 ± 8 (6)	120 ± 5 (4)	119 ± 8 (7)	**0.046**	0.165	0.574
Left caudate	159 ± 21 (13)	183 ± 41 (22)	170 ± 39 (23)	0.176	**0.004**	0.132
Right caudate	150 ± 26 (17)	163 ± 31 (19)	172 ± 27 (16)	**0.016**	**0.078**	0.544
Left hippocampus	137 ± 11 (8)	140 ± 15 (11)	144 ± 12 (8)	**0.095**	0.445	0.402
Mid-anterior corpus callosum	164 ± 41 (25)	148 ± 41 (28)	143 ± 31 (21)	**0.095**	0.167	0.794
Central corpus callosum	178 ± 36 (20)	164 ± 34 (21)	157 ± 37 (24)	**0.084**	0.173	0.741
Mid-posterior corpus callosum	153 ± 32 (21)	175 ± 41 (23)	167 ± 37 (22)	0.23	**0.022**	0.29
Optic chiasm	315 ± 92 (29)	311 ± 85 (27)	368 ± 91 (25)	0.119	0.623	**0.062**
Right cerebral cortex	137 ± 8 (6)	133 ± 8 (6)	138 ± 10 (7)	0.334	**0.032**	0.258
Left cerebral white matter	102 ± 2 (2)	102 ± 3 (3)	103 ± 3 (2)	**0.078**	0.794	**0.064**
Right cerebral white matter	101 ± 2 (2)	101 ± 3 (3)	102 ± 3 (3)	0.554	**0.089**	**0.036**
Subcortical white matter	99 ± 2 (2)	98 ± 2 (2)	99 ± 2 (2)	0.799	**0.087**	**0.071**
Third ventricle	288 ± 95 (33)	339 ± 96 (28)	320 ± 109 (34)	0.427	**0.035**	0.211
Left lateral ventricle	460 ± 77 (17)	530 ± 114 (22)	499 ± 132 (26)	0.198	**0.004**	0.12
Left vessel	150 ± 32 (21)	174 ± 42 (24)	153 ± 39 (26)	0.888	**0.015**	**0.032**
Right vessel	149 ± 33 (22)	181 ± 42 (23)	168 ± 51 (31)	0.287	**0.007**	0.113
Left choroid plexus	331 ± 68 (21)	384 ± 98 (26)	333 ± 72 (22)	0.809	**0.006**	**0.019**
Right choroid plexus	347 ± 74 (21)	380 ± 101 (27)	348 ± 50 (14)	0.983	**0.096**	0.128

Values are mean ± standard deviation (Coefficient of Variation, %); green shading denotes significance at $p<0.05$; gray shading denotes significance at $p<0.1$.

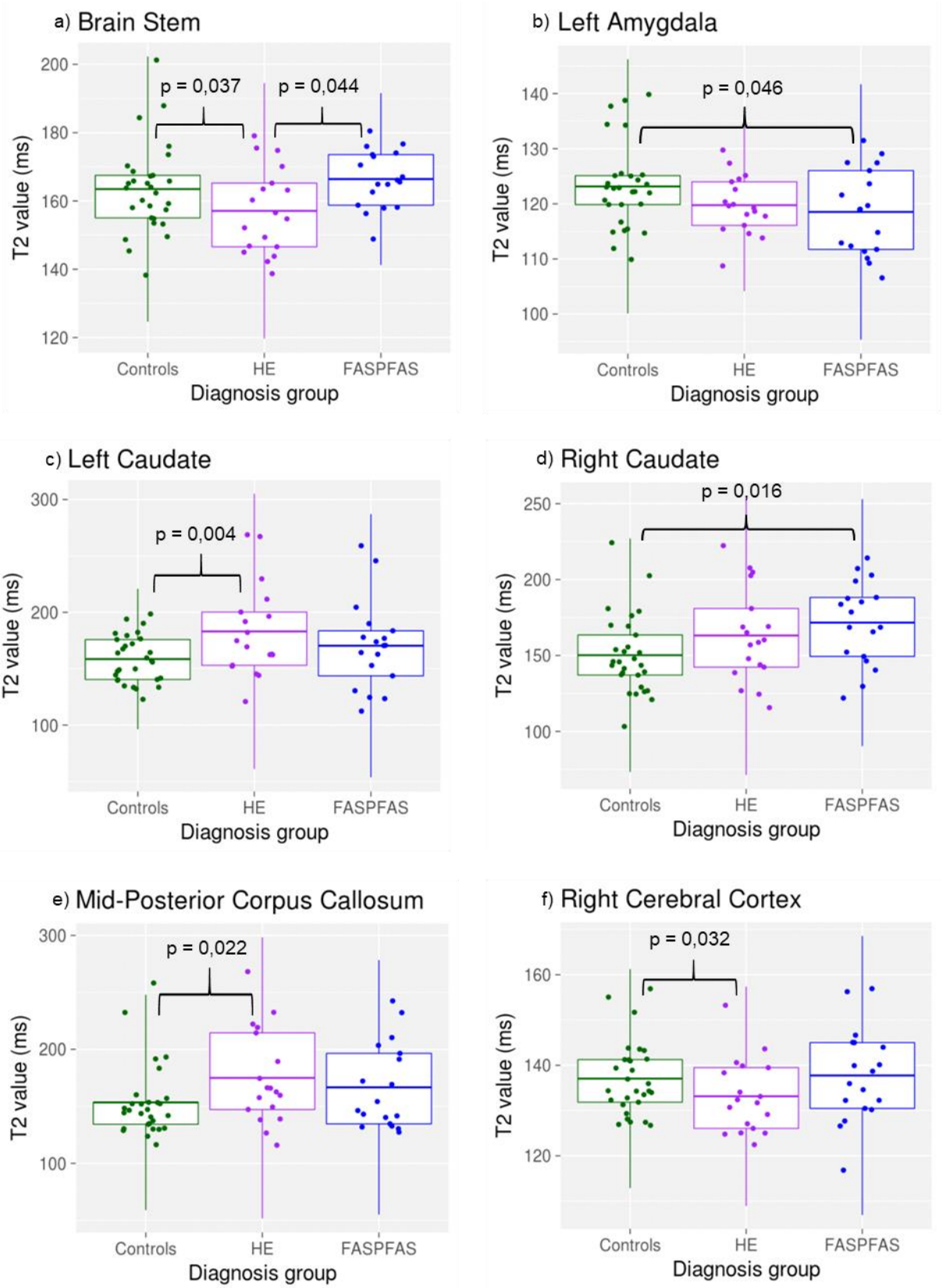
a) Brain Stem
p = 0,037
p = 0,044
T2 value (ms)
200
180
160
140
120
Controls
HE
FASPFAS
Diagnosis group
b) Left Amygdala
p = 0,046
T2 value (ms)
140
130
120
110
100
Controls
HE
FASPFAS
Diagnosis group
c) Left Caudate
p = 0,004
T2 value (ms)
300
200
100
Controls
HE
FASPFAS
Diagnosis group
d) Right Caudate
p = 0,016
T2 value (ms)
250
200
150
100
Controls
HE
FASPFAS
Diagnosis group
e) Mid-Posterior Corpus Callosum
p = 0,022
T2 value (ms)
300
200
100
Controls
HE
FASPFAS
Diagnosis group
f) Right Cerebral Cortex
p = 0,032
T2 value (ms)
160
140
120
Controls
HE
FASPFAS
Diagnosis group

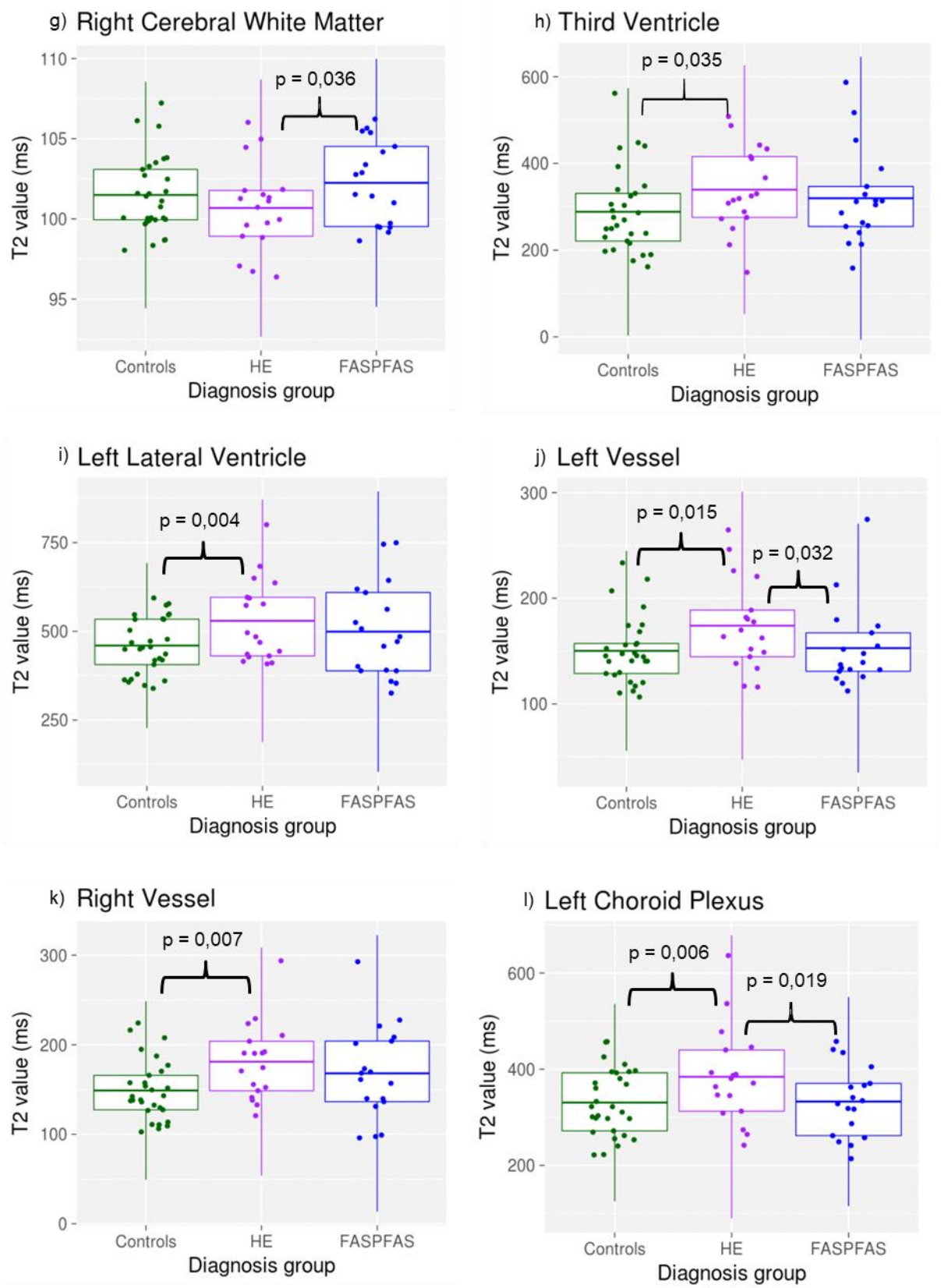

Figure 21: Box-and-whisker plots of T_2 as a function of diagnosis in regions showing significant differences between any two diagnostic groups, namely a) brain stem, b) left amygdala, c) left caudate, d) right caudate, e) mid-posterior corpus callosum, f) right cerebral cortex, g) right cerebral white matter, h) third ventricle, i) left lateral ventricle, j) left vessel, k) right vessel, l) left choroid plexus. HE, Heavily Exposed non-syndromal; FASPFAS, group comprising children with either FAS or PFAS.

Table 9: Regions where average T_2 parameter values are at least weakly associated (at $p<0.1$) with one or more of the measures describing the amount of alcohol the mother consumed across pregnancy.

	Absolute alcohol (AA) consumed per day across pregnancy (oz AA/day)		**Absolute alcohol (AA) consumed per occasion across pregnancy (oz AA/ drinking day)**		**Frequency of drinking across pregnancy (days/week)**	
Regions	**β ± Std Error (Standardised β)**	**p-value**	**β ± Std Error (Standardised β)**	**p-value**	**β ± Std Error (Standardised β)**	**p-value**
Left amygdala	-5,2 ± 2,4 (-0,3)	**0.037**	-1,1 ± 0,4 (-0,33)	**0.019**	-11,2 ± 6,4 (-0,24)	**0.087**
Left caudate	18,4 ± 10,4 (0,23)	**0.082**	4 ± 1,9 (0,27)	**0.042**	45,7 ± 27,4 (0,21)	0.101
Right caudate	24,5 ± 8,5 (0,36)	**0.006**	3,9 ± 1,6 (0,31)	**0.019**	61,9 ± 22,6 (0,34)	**0.008**
Left cerebellum cortex	-3,3 ± 2 (-0,17)	**0.096**	-0,6 ± 0,4 (-0,17)	**0.090**	-7,7 ± 5,2 (-0,15)	0.138
Central corpus callosum	-14,8 ± 11,2 (-0,17)	0.194	-2,1 ± 2,1 (-0,13)	0.313	-55 ± 29,1 (-0,24)	**0.064**
Mid-posterior corpus callosum	9,8 ± 11,5 (0,11)	0.395	3,6 ± 2,1 (0,22)	**0.088**	23,1 ± 30,1 (0,1)	0.446
Left lateral ventricle	43,3 ± 28,3 (0,17)	0.131	9 ± 5,2 (0,19)	**0.09**	109,7 ± 74,4 (0,16)	0.146
Right vessel	24,2 ± 13 (0,24)	**0.067**	6 ± 2,3 (0,31)	**0.013**	49,7 ± 34,5 (0,18)	0.155

Green shading denotes significance at $p<0.05$; gray shading denotes significance at $p<0.1$.

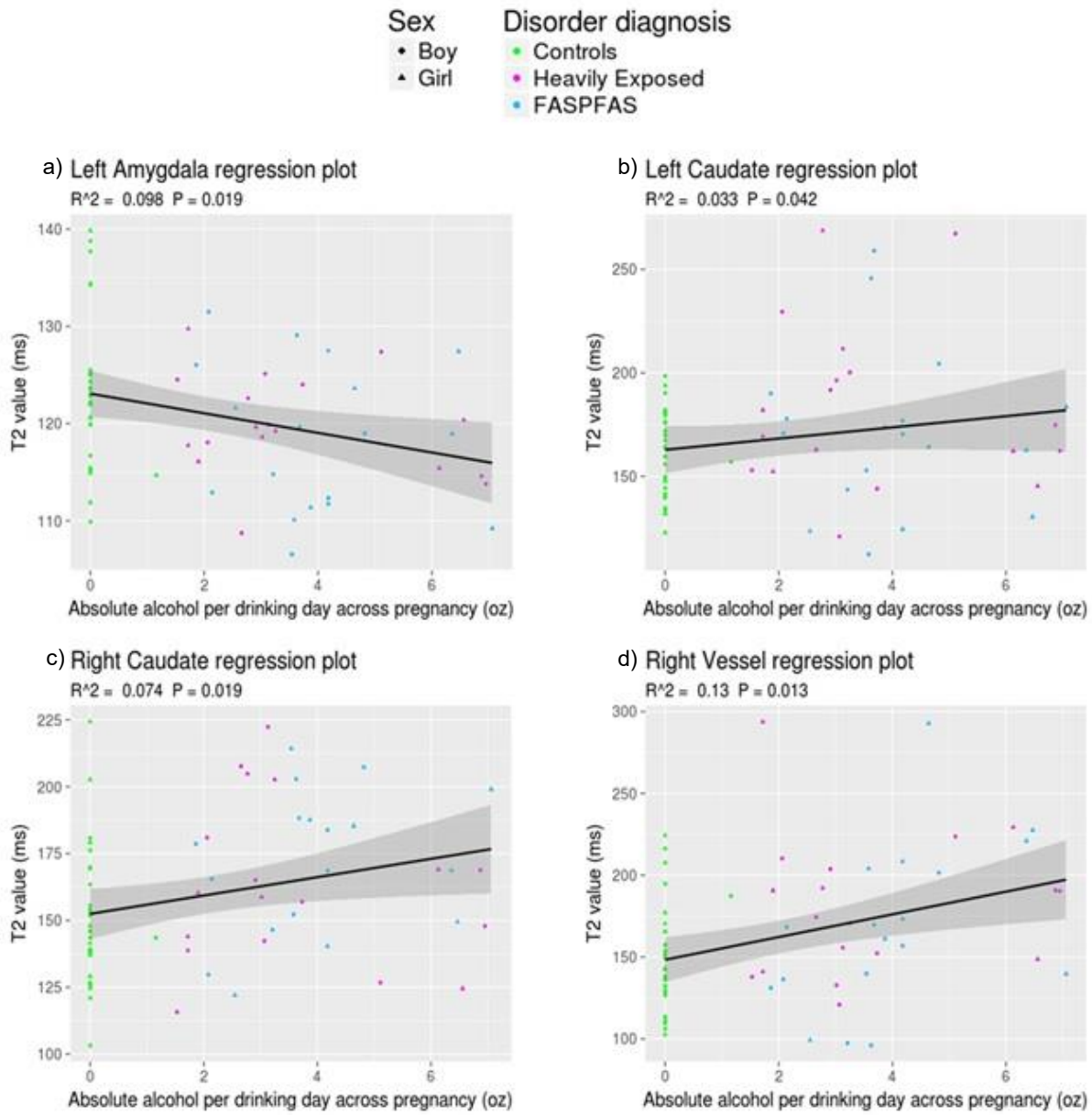

Figure 22: Plots showing T_2 parameter values as a function of the amount of alcohol the mother consumed on days when she drank during pregnancy in the a) left amygdala, b) left caudate, c) right caudate, and d) right vessel. Heavily exposed denotes children with confirmed high levels of alcohol exposure who are non-syndromal; FASPFAS denotes children with a diagnosis of either FAS or PFAS.

4.3 T_2* results

Examples of the T_2* maps and their corresponding segmentation overlays are shown for axial, coronal and sagittal orientations in Figure 23. The scalebar demonstrates the range of T_2* values measured. The colour legend of the neuroanatomical regions as segmented by Freesurfer are as in Table 4. In 5 regions, average T_2* parameter values showed differences (at $p<0.1$) between any two diagnostic groups (Table 10 and Figure 24). In the third and left lateral ventricles, increasing levels of alcohol exposure were associated with higher T_2* values, while increasing alcohol exposure was related to decreasing T_2* values in left cerebellar cortex and the optic chiasm (Table 11 and Figure 25). Regression plots were not included if $R<0.1$. None of the group differences or associations survived after FDR correction.

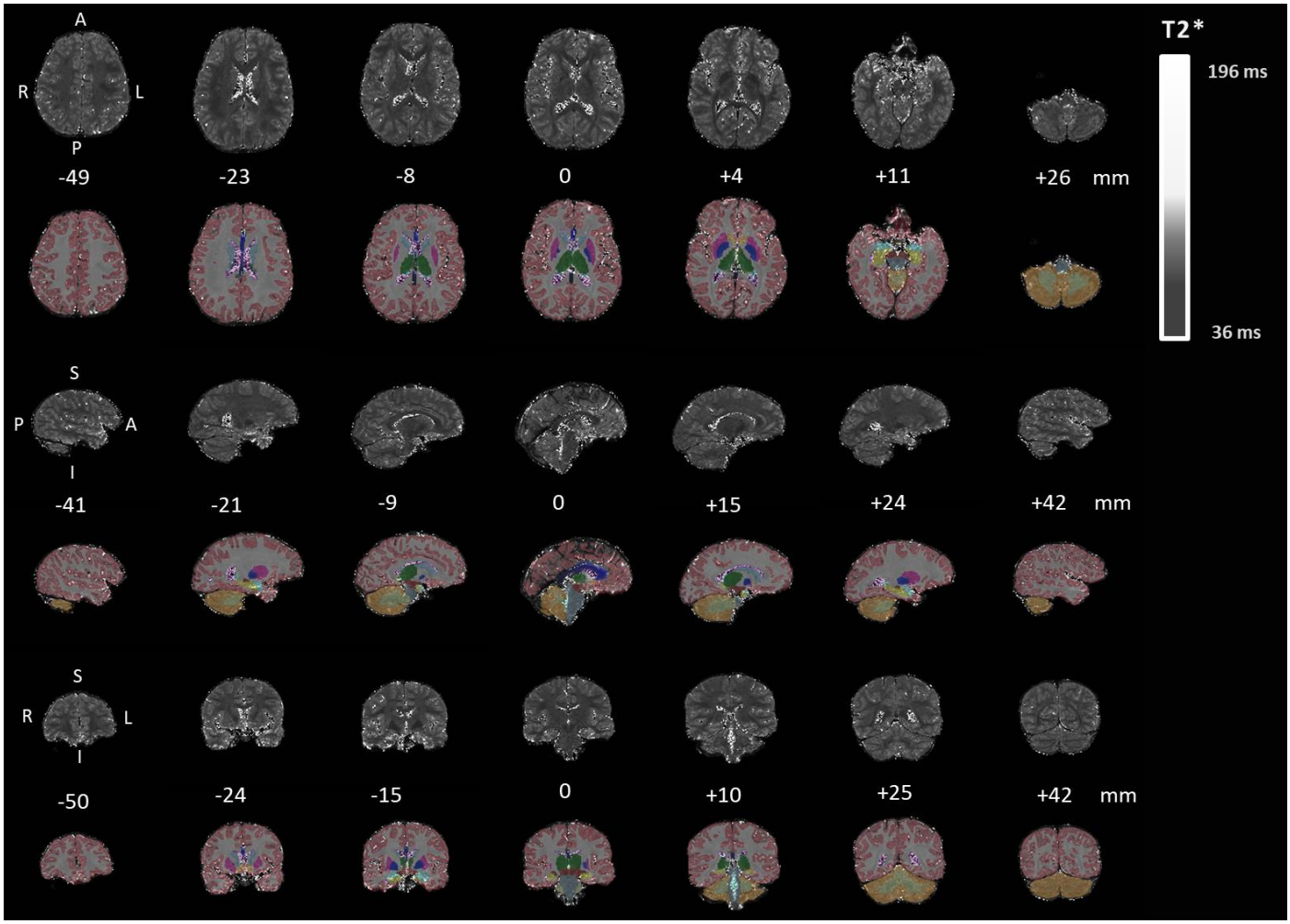

Figure 23: Example of the T_2* maps in the axial (top), sagittal (middle) and coronal (bottom) orientations. Seven slices of each orientation is illustrated in grayscale. The Freesurfer segmentation map (aseg.mgz) overlaid on the slice is illustrated below each respective slice. The middle (fourth) slice represents the approximate middle of the brain and is referenced as 0 mm. The number below each slices indicates its position (in mm) from the reference slice. For the axial view, slices start with the most superior view on the left, and end with the most inferior view on the right. For the sagittal view, slices start in the right side of the brain and progress toward the left side of the brain. For the coronal orientation, slices start in frontal cortex on the left, and move towards the back of the brain to the right. The first image for each orientation indicates the right (R), left (L), superior (S) and inferior (I) positions of the brain. Colours corresponding to different Freesurfer segmented regions are given in Table 4.

Table 10: Regions showing T_2* differences (at p<0.1) between any two diagnostic groups.

T_2* measures (ms)				Pairwise p-values		
Region	**Controls**	**HE**	**FAS/PFAS**	**Controls vs FAS/PFAS**	**Controls vs HE**	**FAS/PFAS vs HE**
Right pallidum	37 ± 4 (11)	36 ± 2 (5)	37 ± 3 (8)	0.254	0.461	**0.086**
Optic chiasm	84 ± 29 (35)	72 ± 23 (32)	70 ± 16 (23)	**0.025**	**0.08**	0.646
Third ventricle	166 ± 20 (12)	181 ± 20 (11)	179 ± 30 (17)	**0.045**	**0.05**	0.982
Left lateral ventricle	174 ± 24 (14)	196 ± 31 (16)	188 ± 36 (19)	**0.041**	**0.01**	0.589
Right inferior lateral ventricle	121 ± 23 (19)	132 ± 22 (16)	114 ± 24 (21)	**0.059**	0.264	**0.007**

Values are mean ± SD (Coefficient of Variation, %); green shading denotes significance at p<0.05; gray shading denotes significance at p<0.1.

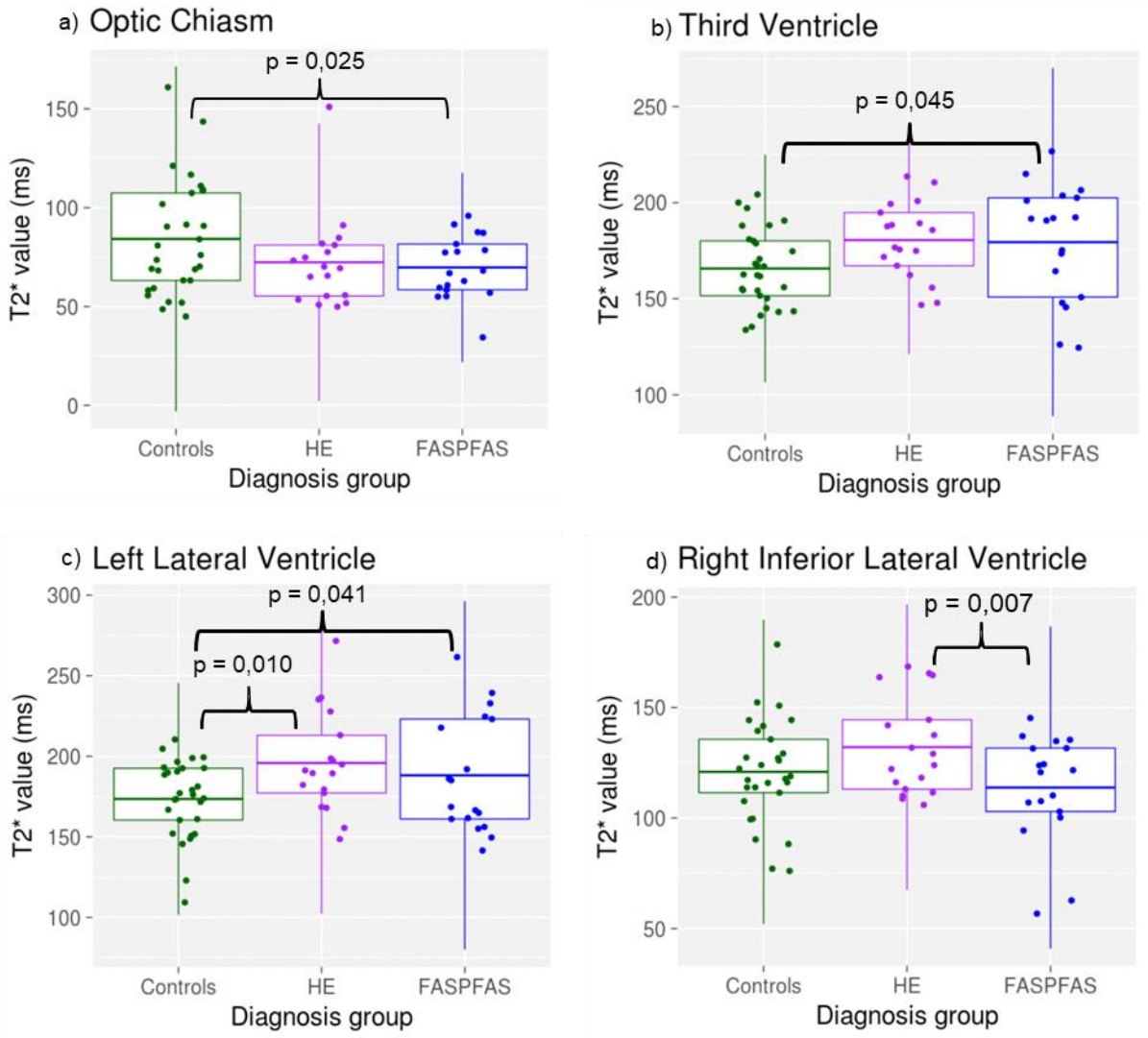

Figure 24: Box-and-whisker plots of T2* in regions showing significant differences between any two diagnostic groups, namely a) optic chiasm, b) third ventricle, c) left lateral ventricle, d) right inferior lateral ventricle. HE, Heavily Exposed non-syndromal; FASPFAS, group comprising children with either FAS or PFAS.

Table 11: Regions where average T_2* parameter values are at least weakly associated (at p<0.1) with one or more of the measures describing the amount of alcohol the mother consumed across pregnancy.

	Absolute alcohol (AA) consumed per day across pregnancy (oz AA/day)		Absolute alcohol (AA) consumed per occasion across pregnancy (oz AA/ drinking day)		Frequency of drinking across pregnancy (days/week)	
Regions	**β ± Std Error (Standardised β)**	**p-value**	**β ± Std Error (Standardised β)**	**p-value**	**β ± Std Error (Standardised β)**	**p-value**
Left cerebellar cortex	-1,6 ± 1 (-0,18)	0.102	-0,1 ± 0,2 (-0,04)	0.694	-5,6 ± 2,5 (-0,24)	**0.031**
Optic chiasm	-7,3 ± 8,6 (-0,12)	0.405	-2,8 ± 1,6 (-0,25)	**0.082**	-10,7 ± 22,8 (-0,07)	0.640
Third ventricle	10,6 ± 7,4 (0,19)	0.158	1,8 ± 1,4 (0,17)	0.193	39,7 ± 19,2 (0,26)	**0.043**
Left lateral ventricle	12 ± 9,4 (0,16)	0.205	2,9 ± 1,7 (0,21)	**0.099**	30,4 ± 24,8 (0,16)	0.224

Green shading denotes significance at p<0.05; gray shading denotes significance at p<0.1.

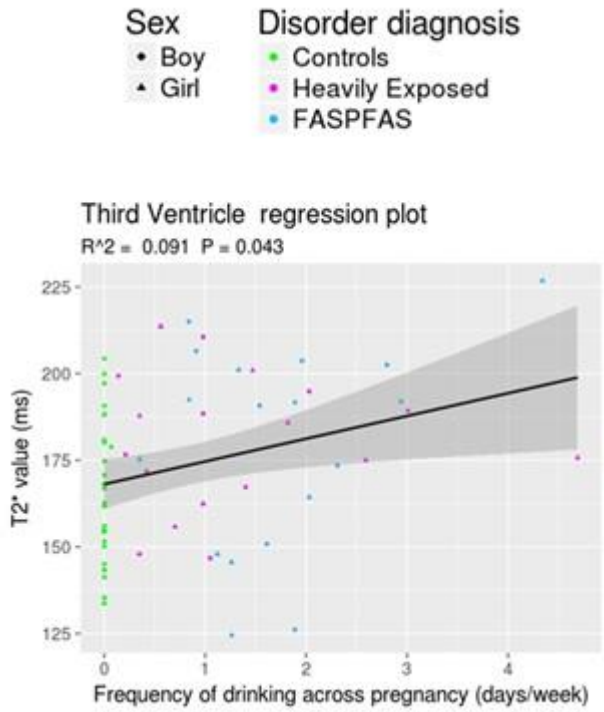

Figure 25: Plot showing T_2* parameter values in the third ventricle as a function of how frequently the mother consumed alcohol during pregnancy. Heavily exposed denotes children with confirmed high levels of alcohol exposure who are non-syndromal; FASPFAS denotes children with a diagnosis of either FAS or PFAS.

4.4 PD results

Examples of the PD maps and their corresponding segmentation overlays are shown for axial, coronal and sagittal slices in Figure 26. The scalebar demonstrates the range of PD values measured. The colour legend of the neuroanatomical regions as segmented by Freesurfer are as in Table 4. PD parameter values relative to CSF differed between diagnostic groups (at $p<0.1$) in the left hippocampus, left thalamus, left lateral ventricle and right ventral diencephalon (Table 12 and Figure 27). In 6 regions, specifically the right accumbens, right putamen, third ventricle, bilateral lateral ventricles, and right inferior lateral ventricle, increasing levels of alcohol exposure were associated (at $p<0.1$) with higher PD values (Table 13 and Figure 28). None of the group differences or associations survived after FDR correction. Regression plots were not included if $R<0.1$.

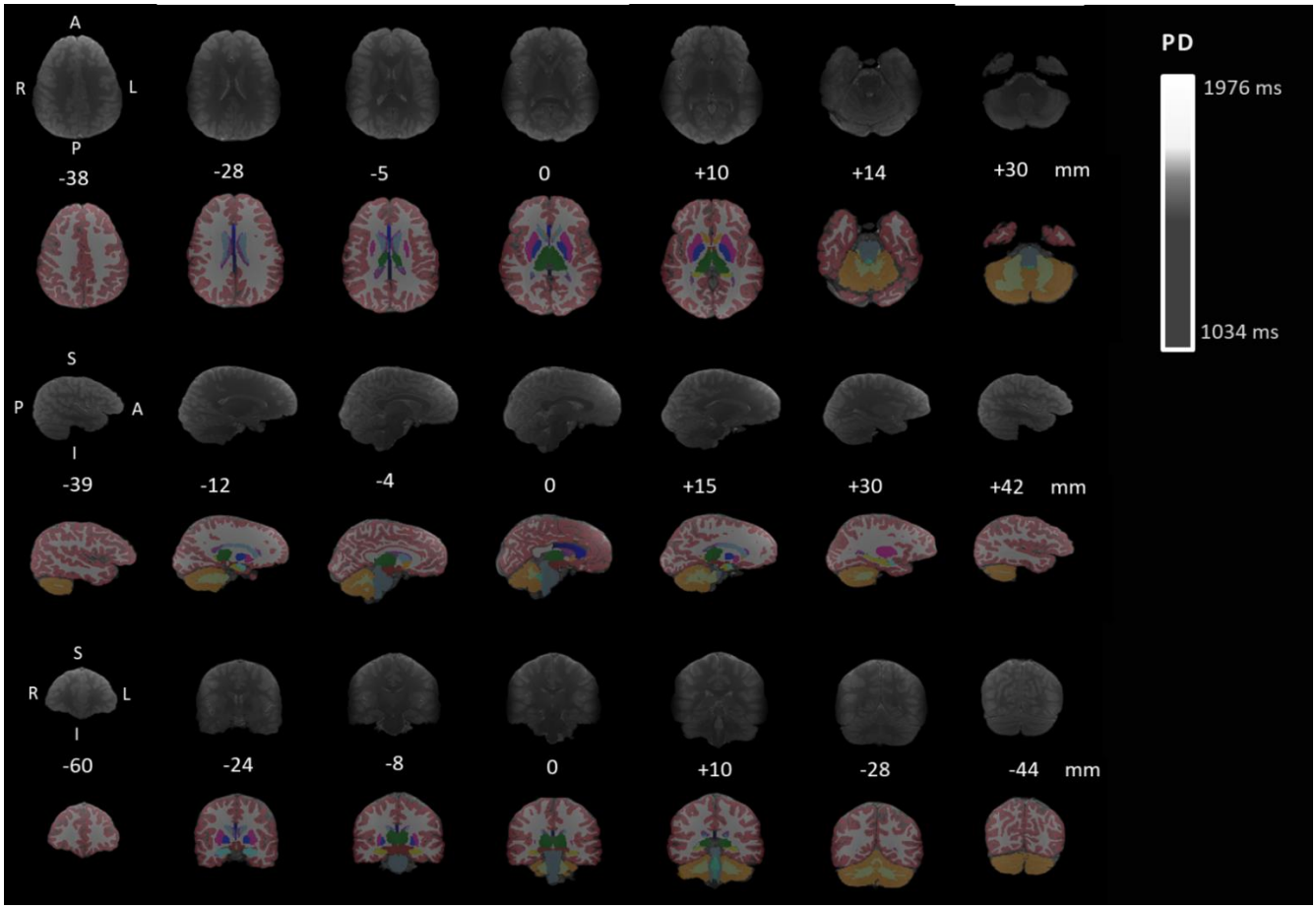

Figure 26: : Example of the PD maps in the axial (top), sagittal (middle) and coronal (bottom) orientations. Seven slices of each orientation is illustrated in grayscale. The Freesurfer segmentation map (aseg.mgz) overlaid on the slice is illustrated below each respective slice. The middle (fourth) slice represents the approximate middle of the brain and is referenced as 0 mm. The number below each slice indicates its position (in mm) from the reference slice. For the axial view, slices start with the most superior view on the left, and end with the most inferior view on the right. For the sagittal view, slices start in the right side of the brain and progress toward the left side of the brain. For the coronal orientation, slices start in frontal cortex on the left, and move towards the back of the brain to the right. The first image for each orientation indicates the right (R), left (L), superior (S) and inferior (I) positions of the brain. Colours corresponding to different Freesurfer segmented regions are as listed in Table 4.

Table 12: Regions showing PD differences (at p<0.1) between any two diagnostic groups.

PD relative to that in CSF				Pairwise p-values		
Region	**Controls**	**HE**	**FAS/PFAS**	**Controls vs FAS/PFAS**	**Controls vs HE**	**FAS/PFAS vs HE**
Left hippocampus	0.895 ± 0.059 (7)	0.883 ± 0.047 (5)	0.885 ± 0.046 (5)	0.729	**0.042**	0.117
Left thalamus	0.843 ± 0.042 (5)	0.841 ± 0.041 (5)	0.842 ± 0.034 (4)	0.248	0.383	**0.065**
Left lateral ventricle	1.179 ± 0.063 (5)	1.224 ± 0.056 (5)	1.212 ± 0.074 (6)	**0.022**	**0.030**	0.907
Right ventral DC	0.753 ± 0.042 (6)	0.749 ± 0.038 (5)	0.754 ± 0.036 (5)	0.365	0.271	**0.068**

Values are mean ± standard deviation (Coefficient of Variation, %); Green shading denotes p<0.05; Gray shading denotes 0.05<p<0.1.

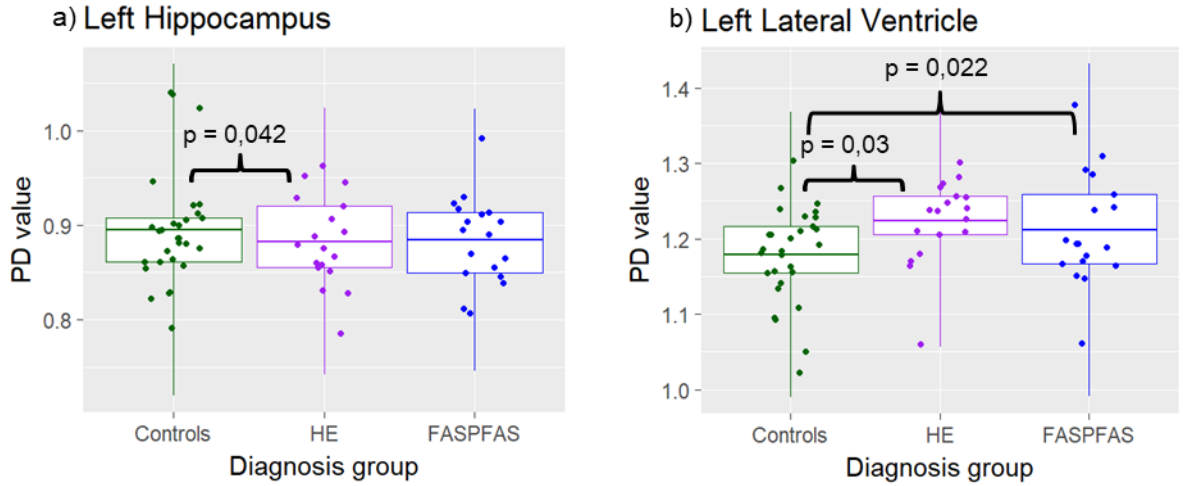

Figure 27: Box-and-whisker plots of PD (relative to CSF) in the a) left hippocampus and b) left lateral ventricle. HE, Heavily Exposed non-syndromal; FASPFAS, group comprising children with either FAS or PFAS.

Table 13: Regions where average PD values (relative to CSF) are at least weakly associated (at p<0.1) with one or more of the measures describing the amount of alcohol the mother consumed across pregnancy.

	Absolute alcohol (AA) consumed per day across pregnancy (oz AA/day)		Absolute alcohol (AA) consumed per occasion across pregnancy (oz AA/ drinking day)		Frequency of drinking across pregnancy (days/week)	
Regions	**β ± Std Error (Standardised β)**	**p-value**	**β ± Std Error (Standardised β)**	**p-value**	**β ± Std Error (Standardised β)**	**p-value**
Right accumbens area	0.016 ± 0.013 (0.15)	0.211	0.002 ± 0.002 (0.07)	0.53	0.056 ± 0.034 (0.19)	**0.1**
Right putamen	0.016 ± 0.011 (0.13)	0.161	0.002 ± 0.002 (0.07)	0.429	0.049 ± 0.029 (0.15)	**0.098**
Third ventricle	0.021 ± 0.017 (0.17)	0.23	0.001 ± 0.003 (0.06)	0.667	0.081 ± 0.045 (0.25)	**0.075**
Left lateral ventricle	0.055 ± 0.021 (0.35)	**0.01**	0.009 ± 0.004 (0.31)	**0.023**	0.144 ± 0.055 (0.34)	**0.011**
Right lateral ventricle	0.021 ± 0.017 (0.17)	0.212	0.003 ± 0.003 (0.12)	0.348	0.072 ± 0.043 (0.22)	**0.098**
Right inferior lateral ventricle	0.038 ± 0.025 (0.20)	0.136	0.006 ± 0.005 (0.18)	0.166	0.114 ± 0.065 (0.22)	**0.087**

Green shading denotes significance at p<0.05; gray shading denotes significance at p<0.1.

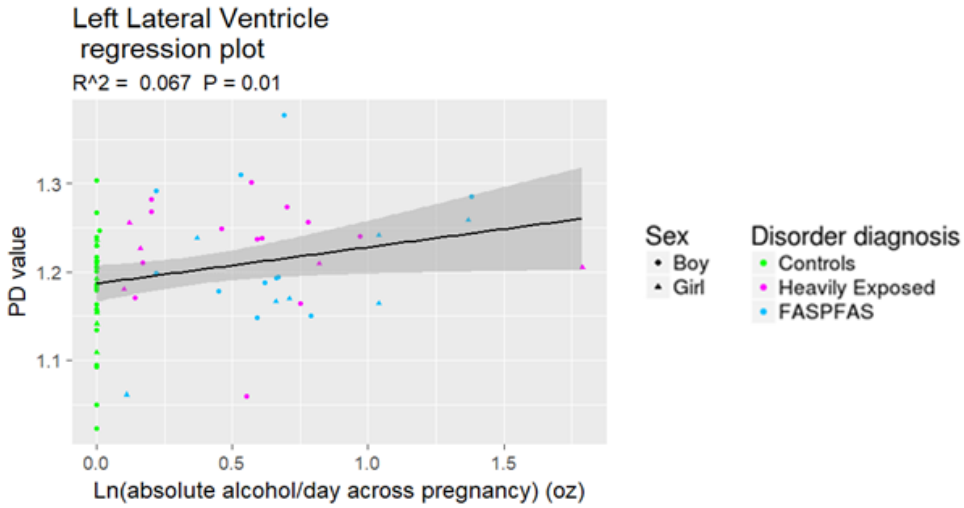

Figure 28: Plot showing PD (relative to CSF) in the left lateral ventricle as a function of ounces absolute alcohol consumed by the mother per day during pregnancy. Heavily exposed denotes children with confirmed high levels of alcohol exposure who are non-syndromal; FASPFAS denotes children with a diagnosis of either FAS or PFAS.

5. Discussion

The present study demonstrates regional PAE-related changes in T_1, T_2, T_2* and PD. Since tissue parameters are determined by tissue properties, differences observed indicate alterations in the underlying biology. Previous studies have shown, for example, that decreasing cell density (and concurrently structure) (Eickhoff *et al.*, 2005), higher water content, axonal loss, and demyelination (Van Waesberghe *et al.*, 1999; Bitsch *et al.*, 2001) are related to increasing T_1 relaxation times, while higher iron content (Ogg and Steen, 1998) reduces T_1 times. Longer T_2 values have been linked to increased free water content (i.e. fewer macromolecules), lower myelin water fractions (MWF) and lower magnetization transfer ratios (Laule *et al.* 2007; MacKay *et al.*, 2009), and shorter T_2 to increased iron content (Schenker *et al.*, 1993). Longer T_2* point to fewer macromolecules (i.e. increased free water content), increased myelin (which also contains high water content), or decreased iron content (Langkammer *et al.*, 2010). Although the presence of iron shortens T_1, T_2 and T_2* relaxation times (Bagnato, Hametner and Welch, 2013), T_2* provides the most direct information about iron content. Increasing PD mainly reflects increased free water content (Gracien *et al.*, 2019).

In our study, the most severely affected children with FAS or PFAS demonstrated shorter T_1 values than unexposed controls in right cerebellar cortex, hippocampus and ventral diencephalon, while HE children had shorter T_1 than controls only in the right cerebellar cortex, but longer T_1 in the left lateral ventricle and right vessel. Of these regions, the right cerebellar cortex and left lateral ventricle demonstrated dose dependent effects, with increasing alcohol exposure associated with shorter T_1 in the former and longer T_1 in the latter. In right accumbens, left caudate, right putamen and third ventricle, we also found association of increasing exposure with higher T_1 values.

Children with FAS/PFAS demonstrated longer T_2's than controls only in the right caudate and shorter T_2 in left amygdala. In contrast, HE children demonstrated longer T_2 in the left caudate, mid-posterior corpus callosum, third and left lateral ventricles, left and right vessel, and left choroid plexus, but shorter T_2 in the brain stem and right cerebral cortex. Notably, in the brain stem, left vessel and left choroid plexus, T_2 values in children with FAS/PFAS differed significantly from those of HE children but were similar to those of control children. Of the regions showing PAE-related differences in T_2, left and right caudate, right vessel and left amygdala demonstrated dose dependent effects, with the association being negative in the amygdala. Both FAS/PFAS and HE groups demonstrated longer T_2* values compared to controls in the third and left lateral ventricles, but shorter T_2*'s in the optic chiasm. Dose dependent effects were observed in the third ventricle and left cerebellar cortex, with the latter being negative. PD was higher in FAS/PFAS and HE groups compared to controls in the left lateral ventricle, and lower in HE children than controls in left hippocampus. Only in the left lateral ventricle did we observe association of increasing PAE with higher PD values.

Table 14: Summary of regional PAE-related changes in tissue parameters

		T_1	T_2	T_2*	PD
Cortex					
	Right cerebral cortex	-	⇓*	-	-
	Left cerebellar cortex	-	-	⇓	-
	Right cerebellar cortex	⇓	-	-	-
White matter					
	Mid-posterior corpus callosum	-	⇑*	-	-
	Optic chiasm	-	-	⇓	-
Subcortical					
	Left caudate	⇑	⇑	-	-
	Right caudate	-	⇑	-	-
	Right accumbens	⇑	-	-	-
	Right putamen	⇑	-	-	-
	Brain stem	-	⇓*	-	-
	Left hippocampus	↓#	↑#	-	⇓*
	Right hippocampus	⇓#	-	-	-
	Left amygdala	-	⇓	-	-
	Right ventral diencephalon	⇓#	-	-	-
Ventricles					
	Left lateral ventricle	⇑	⇑*	⇑	⇑
	Third ventricle	⇑	⇑*	⇑	-
	Left choroid plexus	↑	⇑*	-	-
Vessels					
	Left vessel	-	⇑*	-	-
	Right vessel	⇑*	⇑	-	-

⇑/⇓ denotes increasing or decreasing (at $p<0.05$), respectively; ↑/↓ denotes increasing or decreasing at $p<0.1$; #denotes effects observed only in children with FAS/PFAS; *denotes effects observed only in HE children; gray shading highlights regions showing PAE-related decreases in tissue parameter values.

Table 14 presents a summary of the results. In affected regions, we show findings below conventional levels of significance (i.e. at $p<0.1$) using single arrows. Effects observed only in the most severely affected children with a diagnosis of FAS/PFAS are highlighted with an octothorpe symbol (#), and those observed only in the non-syndromal HE children with an asterisk (*). Notably, mid-posterior corpus callosum, 4 of 9 subcortical regions, ventricles and vessels demonstrated PAE-related increases in tissue parameter values, while cerebellar and right cerebral cortex, optic chiasm and the remaining subcortical regions showed PAE-related decreases. Furthermore, a number of regions showed effects on multiple tissue parameters, most notably the left lateral and third ventricles, right vessel and left caudate – all of which showed PAE-related increases. Simultaneous increases in T_1 and T_2/T_2* point to increasing water content, i.e. less structure.

It is not clear why effects of PAE on T_2 are evident only in the HE group in 7 of 11 regions, while effects on T_1 in all but one region are evident in either both the FAS/PFAS and HE groups or the FAS/PFAS group only. This does not appear to be related to the degree of alcohol exposure as levels were similarly high in both groups. Mothers of children in the FAS/PFAS group consumed approximately 2.2 standard drinks per day on average, they consumed 8 standard drinks on average per drinking occasion, and they drank 1.7 days per week. Mothers of children in the HE group consumed roughly 1.8 standard drinks per day, 7.2 drinks per drinking occasion, and drank 1.3 days per week. It is possible, however, that the timing during pregnancy of the exposure differed, which may also explain, in part, why children in the HE group with similarly high exposure levels are relatively spared and do not exhibit the facial phenotype. Maternal smoking during pregnancy has been shown to affect the brain structure and function in human offspring (Bublitz and Stroud, 2012); but further research will have to be done to determine whether the fact that mothers of HE children smoked more heavily during pregnancy than mothers of the children in the FAS/PFAS group, may have contributed to these results.

Overall, T_1 and T_2* values in affected regions were related most strongly to frequency of drinking, T_2 to the amount of alcohol consumed by the mother per drinking occasion, and PD to the average amount of alcohol consumed per day. These findings broadly suggest that T_1 and T_2* values may be affected less by the amount of alcohol consumed than the frequency, while T_2 is more sensitive to the amount consumed, and further research can be done to confirm this.

In subsequent sections, we discuss our findings region-by-region.

Corpus callosum (CC):

Many studies have reported PAE-related corpus callosal damage. Structural MRI studies have shown smaller CC volume (Riley *et al.*, 1995; Biffen *et al.*, 2018), smaller CC surface area (Sowell *et al.*, 2001; Yang, Phillips, *et al.*, 2012), thinner CC splenium and anterior regions (Yang, Phillips, *et al.*, 2012), and displaced CC position (Sowell *et al.*, 2001) in children prenatally exposed to alcohol compared to unexposed controls. CC morphology has also been linked to the FASD status of the child (Suttie *et al.*, 2018). On DTI, lower FA has been reported in the body (Fryer *et al.*, 2009), mid-body (Wozniak *et al.*, 2009), genu (Ma *et al.*, 2005) and splenium (Ma *et al.*, 2005; Sowell *et al.*, 2008) of the CC, higher and lower MD values in the genu and splenium (Ma *et al*., 2005; Lebel *et al.*, 2008), and correlations between FA values and saccade reaction times (Green *et al.*, 2013) in exposed children. Spectroscopy has shown lower NAA/creatine ratios and higher absolute creatine signal intensities in the CC (Fagerlund *et al.*, 2006).

Our finding of higher T_2 in the mid-posterior CC in HE children compared to controls, points to a loss of myelin, which is consistent with previous findings of smaller CC

volume, lower FA and higher MD in exposed children. It is not clear why children in the FAS/PFAS group are not similarly affected in this region.

Caudate

The caudate has been extensively implicated in PAE, including smaller caudate volumes (Mattson *et al.*, 1996; Archibald *et al.*, 2001; Astley *et al.*, 2009; Nardelli *et al.*, 2011; Roussotte *et al.*, 2012; Treit *et al.*, 2013; Biffen *et al.*, 2018; Zhou *et al.*, 2018), shape variations (Joseph *et al.*, 2014), diminished left-right asymmetry (Suttie *et al.*, 2018), reduced activation on fMRI during response inhibition (Fryer *et al.*, 2007), lower metabolic rates on PET (Clark *et al.*, 2000), and increased levels of NAA and NAA/Cr (Cortese *et al.*, 2006). Since lower NAA typically points to neuronal dysfunction, the authors speculated that higher levels in children with FAS may indicate over compensation to make up for deficiencies elsewhere in the brain. In an fMRI study, children in the HE group recruited a sub-network in the left caudate during verbal working memory that was not observed in the control or FAS/PFAS groups (Diwadkar *et al.*, 2013).

In our study, T_2 was higher in left and right caudate, together with T_1 in left caudate. Simultaneous increases in T_1 and T_2 in this region suggest an increase in free water content and less structure. Higher T_1 and T_2 has also been detected in lesions demonstrating lower levels of NAA and higher levels of choline (Van Walderveen *et al.*, 1999; Li *et al.*, 2003). Combined, more free water and metabolic alterations provide additional evidence of caudal dysfunction.

Hippocampus

Although many studies have reported smaller hippocampal volumes in PAE-affected individuals (Willoughby *et al.*, 2008; Astley *et al.*, 2009; Coles *et al.*, 2011; Nardelli *et al.*, 2011; Roussotte *et al.*, 2012; Treit *et al.*, 2013; Biffen *et al.*, 2018), one study found the hippocampal volume to be relatively spared (Archibald *et al.*, 2001). Another study reported hippocampal shape variations compared to controls, with localized contraction associated with higher levels of alcohol exposure (Joseph *et al.*, 2014). In our study, we observed lower T_1 in the right hippocampus in children with FAS/PFAS, and lower PD in the left hippocampus in HE children. Diminished T_1 and PD point to less water content and more structure, which suggests increased cell density. This could contribute to the smaller volumes and localized contractions reported previously.

Putamen

The putamen has been shown to have smaller volume (Astley *et al.*, 2009; Nardelli *et al.*, 2011; Roussotte *et al.*, 2012; Treit *et al.*, 2013; Zhou *et al.*, 2018), lower MD (Lebel *et al.*, 2008) and lower metabolic rates (Clark *et al.*, 2000) in children with PAE compared to their control counterparts. Longer T_1 in the right putamen points to less structure, which could explain the lower MD observed by Lebel *et al*. (2008) as there would be fewer barriers to diffusion.

Cerebellum

The cerebellum of youth with FASD has less white matter (Sowell *et al.*, 1996; Archibald *et al.*, 2001) and lower total (Zhou *et al.*, 2018), vault (Mattson *et al.*, 1996) and vermal (O'Hare *et al.*, 2005) volumes. On fMRI, children with FAS/PFAS activated regions in the cerebellum during verbal working memory that were not observed in control or HE children (Diwadkar *et al.*, 2013), and demonstrated greater bilateral cerebellar and right vermal activity compared to controls during number processing (Meintjes *et al.*, 2010). DTI studies found correlations between FA values and mathematical test scores (Lebel *et al.*, 2010) as well as saccade reaction times (Green *et al.*, 2013) in clusters of the left cerebellum, and lower FA values in the left middle cerebellar peduncle (Spottiswoode *et al.*, 2011) of exposed participants. Furthermore exposed subjects have been shown to have higher myo-inositol/creatine ratios in the left cerebellum (Gonçalves *et al.*, 2009).

In our study, we find shorter T_2* in left cerebellar cortex and shorter T_1 on the right. Together, these findings point to the possibility of increased iron content in this region.

Amygdala

Children with FASD have been shown to have smaller amygdala volumes (Nardelli *et al.*, 2011; Treit *et al.*, 2013; Zhou *et al.*, 2018), and children with ARND to activate the right amygdala less during spatial working memory (Malisza *et al.*, 2012). Our finding of lower T_2 in the left amygdala suggests either lower water content or increased magnetization transfer ratios, which could contribute, in part, to dysfunction in this region.

Brain stem

During number processing, exposed subjects showed more activity in the bilateral red nuclei of the midbrain (Meintjes *et al.*, 2010), while children with ARND displayed less activation in the brain stem and left red nucleus, but more in the right red nucleus, during spatial working memory (Malisza *et al.*, 2012). DTI studies have found lower FA values in the brain stem (Sowell *et al.*, 2008) and correlations between FA values and mathematical test scores in clusters of the brain stem (Lebel *et al.*, 2010). Shorter T_2 values in this region in HE children point to less free water content, which suggests greater structure, which was not evident in children with FAS/PFAS. It is not clear how this should be interpreted in view of previous findings suggesting PAE-related decreases in structure.

Cerebrum

Subjects with PAE have been shown to have lower cerebral volumes (Mattson *et al.*, 1996; Sowell *et al.*, 1996; Archibald *et al.*, 2001; O'Hare *et al.*, 2005; Roussotte *et al.*, 2012; Treit *et al.*, 2013; Zhou *et al.*, 2018), smaller cortical surface areas (Rajaprakash *et al.*, 2014), less cortical gyrification (Hendrickson *et al.*, 2017), and both cortical thickness decreases (Zhou *et al.*, 2011, 2018) and increases (Yang, Roussotte, *et al.*, 2012). A spectroscopy study reported PAE-related reductions in NAA/creatine and NAA/choline ratios in the right parietal cortex, as well as higher levels of creatine in

the bilateral parietal cortex, choline in the bilateral parietal cortex and right frontal cortex, and NAA in the right frontal cortex (Fagerlund *et al.*, 2006).

fMRI has demonstrated functional differences between exposed subjects and controls in various areas of the cortex, including lower resting state functional connectivity in the bilateral precentral, right postcentral and right middle frontal gyri, and left crus II (Fan *et al.*, 2017); activation during memory tasks of the left dorsal prefrontal cortex instead of the left inferior frontal gyrus activated by controls (Diwadkar *et al.*, 2013); greater activity during number processing in the bilateral occipital gyri, left superior temporal gyrus, right posterior cingulate and left angular gyrus, but less activity in the right posterior horizontal intraparietal sulcus and right superior frontal and precentral sulcus (Meintjes *et al.*, 2010); activation during working memory tasks of the dorsolateral prefrontal cortical cortex but not occipital regions (Malisza *et al.*, 2012); and finally, greater activation in prefrontal cortical regions but lower activation in the right caudate during response inhibition (Fryer *et al.*, 2007).

Here we find T_2 decreases in cerebral cortex in HE children only without any accompanying changes in T_1, T_2* or PD. Since the cortex is made up of many anatomically and functionally distinct regions, it is possible that regional changes in other tissue parameters are averaged out, and as such undetectable in our analysis, which makes the interpretation of the current finding difficult. Overall though, shorter T_2 point to less free water and greater structure.

Other regions

Little is known about the remaining regions (optic chiasm, accumbens, ventral diencephalon, ventricles and vessels) in relation to PAE.

In the right accumbens we find dose dependent increases in T_1, which point to lower cell density and higher water content in this region.

The left lateral and third ventricles demonstrate both T_1 and T_2* increases, longer T_2 in only HE children and, in the left lateral ventricle, PD increases as well. The left choroid plexus, a group of cells in the ventricles that produces CSF, shows T_2 increases in HE children only. The right vessel shows T_2 increases, as well as T_1 increases in HE children only, and the left vessel T_2 increases in HE children only. Combined these findings strongly point to PAE-related increases in water content in these regions.

In contrast to the above regions, the optic chiasm and right ventral diencephalon demonstrate tissue parameter decreases in relation to PAE – in the optic chiasm T_2* is shorter and in the right ventral diencephalon T_1 is shorter in children with FAS/PFAS. Shorter T_1 in the ventral diencephalon is likely not due to increased iron content as no T_2* reductions were evident in this region. More likely, the shorter T_1 reflects reduced water content and increased cell density, which could lead to smaller volumes as observed in this region in children with FASD by Roussotte *et al.*, (2012). Unlike the

diencephalon, the optic chiasm contains large amounts of myelin and low iron concentration levels (Li *et al.*, 2012). As such, T_2* reductions in this region suggest either demyelination or the possibility of increased iron content.

6. Conclusions and Recommendations

To our knowledge, this is the first study to examine effects of prenatal alcohol exposure on tissue parameters. Overall, our findings point to regional PAE-related increases in water content and reductions in structure. Exceptions being the right cerebral cortex, brain stem, hippocampus, amygdala and ventral diencephalon where our findings point to less free water and increased cell density, and cerebellar cortex where simultaneous reductions in T_1 and T_2* suggest a possible increase in iron content.

In highly myelinated white matter structures such as the CC and optic chiasm, our results point to PAE-related demyelination, and possibly increased iron. This is consistent with animal and human findings of regional PAE-related demyelination and axonal damage (Lebel *et al.*, 2008, 2010; Sowell *et al.*, 2008; Fryer *et al.*, 2009; Wozniak *et al.*, 2009; Spottiswoode *et al.*, 2011; Green *et al.*, 2013). Since previous studies have demonstrated relationships between CC structural abnormalities and poorer neurocognitive functioning in children with FASD (Wozniak *et al.*, 2009; Biffen *et al.*, 2018), the present findings will likely also be related to functional deficits. Relationships between tissue parameter values and cognitive function were, however, not investigated in the present study.

While the present study adds to the body of work demonstrating PAE-related microstructural changes, the mechanisms underlying the observed changes could not be clearly established due to the large number of factors that affect tissue parameter values.

Future work should include examining relationships of the present findings with those from other imaging modalities. For example, calculating the magnetization transfer ratio (MTR) could provide additional information, since a substantial decrease in the MTR would indicate myelin or axonal loss, while slight or no decrease in MTR would indicate an accumulation of extracellular water (Helms, G.; 2015). It would also be interesting to investigate correlations between neurocognitive measures and brain tissue parameters, especially in white matter structures such as the CC and optic chiasm.

7. References

Abel, E. L. and Sokol, R. J. (1987) 'Incidence of fetal alcohol syndrome and economic impact of FAS-related anomalies', *Drug and Alcohol Dependence*, 19(1), pp. 51–70. doi: 10.1016/0376-8716(87)90087-1.

Abel, E. L. and Sokol, R. J. (1991) 'A Revised Conservative Estimate of the Incidence of FAS and its Economic Impact', *Alcoholism: Clinical and Experimental Research*. Blackwell Publishing Ltd, 15(3), pp. 514–524. doi: 10.1111/j.1530-0277.1991.tb00553.x.

Akber, S. F. (1987) 'Comments on "A review of ^{1}H nuclear magnetic resonance relaxation in pathology; Are T_1 and T_2 diagnostic?"', *Medical Physics*, 14(6), pp. 1090–1091. doi: 10.1118/1.595990.

Akber, S. F. (1988) 'The quagmire of relaxation times', *Medical Hypotheses*, 26(3), pp. 187–191. doi: 10.1016/0306-9877(88)90099-0.

Akber, S. F. (1989a) 'A correlation between spin lattice relaxation time and tumor growth', *European Journal of Radiology*, 9(4), pp. 198–199. Available at: http://www.ncbi.nlm.nih.gov/pubmed/2591383 (Accessed: 30 October 2019).

Akber, S. F. (1989b) 'Correlation between oxygen tension and spin-lattice relaxation rate in tumors.', *European journal of radiology*, 9(1), pp. 56–9. Available at: http://www.ncbi.nlm.nih.gov/pubmed/2731557 (Accessed: 30 October 2019).

Akber, S. F. (1990) 'Is There a Correlation between Spin-Lattice Relaxation Time and Radiation Sensitivity?', *Acta Radiologica*, 31(5), pp. 541–542. doi: 10.1080/02841859009173092.

Akber, S. F. (1992) 'A note: paramagnetic ions influence on water proton spin lattice relaxation times.', *Physiological chemistry and physics and medical NMR*, pp. 71–76. Available at: https://uct.primo.exlibrisgroup.com/discovery/fulldisplay?docid=medline1594662&context=PC&vid=27UCT_INST:27UCT&lang=en&search_scope=MyInst_and_CI&adaptor=Primo Central&tab=Everything&query=creator,contains,akber,AND&query=issn,contains,(07486642),AND&sort (Accessed: 20 October 2019).

Akber, S. F. (1993) 'Role of paramagnetic ions and water proton spin-lattice relaxation time in biological systems.', *Nuklearmedizin. Nuclear medicine*, 32(1), pp. 52–6. Available at: http://www.ncbi.nlm.nih.gov/pubmed/8385322 (Accessed: 20 October 2019).

Akber, S. F. (2008) 'Water proton relaxation times of pathological tissues.', *Physiological chemistry and physics and medical NMR*, 40, pp. 1–42. Available at: http://www.ncbi.nlm.nih.gov/pubmed/20070038 (Accessed: 13 October 2019).

Archibald, S. L. *et al.* (2001) 'Brain dysmorphology in individuals with severe prenatal alcohol exposure.', *Developmental medicine and child neurology*, 43(3), pp. 148–54. Available at: http://www.ncbi.nlm.nih.gov/pubmed/11263683 (Accessed: 20 August 2019).

Astley, S. J. *et al.* (2009) 'Magnetic resonance imaging outcomes from a comprehensive magnetic resonance study of children with fetal alcohol spectrum disorders', *Alcoholism: Clinical and Experimental Research*, 33(10), pp. 1671–1689. doi: 10.1111/j.1530-0277.2009.01004.x.

Bagnato, F. *et al.* (2011) 'Tracking iron in multiple sclerosis: A combined imaging and histopathological study at 7 Tesla', in *Brain*. Oxford University Press, pp. 3599–3612.

doi: 10.1093/brain/awr278.

Bagnato, F., Hametner, S. and Welch, E. B. (2013) 'Visualizing iron in multiple sclerosis', *Magnetic Resonance Imaging*, pp. 376–384. doi: 10.1016/j.mri.2012.11.011.

Baheza, R. A. *et al.* (2015) 'Detection of microcalcifications by characteristic magnetic susceptibility effects using MR phase image cross-correlation analysis', *Medical Physics*. AAPM - American Association of Physicists in Medicine, 42(3). doi: 10.1118/1.4908009.

Bakay, L. *et al.* (1975) 'Nuclear magnetic resonance studies in normal and edematous brain tissue', *Experimental Brain Research*. Springer-Verlag, 23(3), pp. 241–248. doi: 10.1007/BF00239737.

Bartzokis, G. and Tishler, T. A. (2000) 'MRI evaluation of basal ganglia ferritin iron and neurotoxicity in Alzheimer's and Huntingon's disease.', *Cellular and molecular biology (Noisy-le-Grand, France)*, 46(4), pp. 821–33. Available at: http://www.ncbi.nlm.nih.gov/pubmed/10875443 (Accessed: 5 October 2019).

Beall, P. T. and Hazlewood, C. F. (1983) *Distinction of the normal, preneoplastic, and neoplastic states by water proton NMR relaxation times*, *Nuclear Magnetic Resonance (NMR) Imaging*. Edited by W. Saunders. Philadelphia.

Bender, B. and Klose, U. (2010) 'The in vivo influence of white matter fiber orientation towards B 0 on T2* in the human brain', *NMR in Biomedicine*, 23(9), pp. 1071–1076. doi: 10.1002/nbm.1534.

Benjamini, Y. and Hochberg, Y. (1995) *Controlling the False Discovery Rate: A Practical and Powerful Approach to Multiple*, *Source: Journal of the Royal Statistical Society. Series B (Methodological)*. Available at: https://www.jstor.org/stable/pdf/2346101.pdf?refreqid=excelsior%3A10f65d83cb8759ba40e7dacfbe81163b (Accessed: 28 November 2018).

Berry, E. and Bulpitt, A. (2009) *Fundamentals of MRI*, *CRC Press; Boca Raton*.

Biffen, S. C. *et al.* (2018) 'Reductions in corpus callosum volume partially mediate effects of prenatal alcohol exposure on IQ', *Frontiers in Neuroanatomy*, 11. doi: 10.3389/fnana.2017.00132.

Bitsch, A. *et al.* (2001) 'A longitudinal MRI study of histopathologically defined hypointense multiple sclerosis lesions', *Annals of Neurology*, 49(6), pp. 793–796. doi: 10.1002/ana.1053.

Bizzi, A. *et al.* (1990) 'Role of iron and ferritin in MR imaging of the brain: A study in primates at different field strengths', *Radiology*, 177(1), pp. 59–65. doi: 10.1148/radiology.177.1.2399339.

Blicharska, B. *et al.* (1970) 'Investigation of protein hydration by proton spin relaxation time measurements.', *Biochimica et biophysica acta*, 207(3), pp. 381–389. doi: 10.1016/s0005-2795(70)80001-0.

Block, R. E. and Maxwell, G. P. (1974) 'Proton magnetic resonance studies of water in normal and tumor rat tissues', *Journal of Magnetic Resonance (1969)*, 14(3), pp. 329–334. doi: 10.1016/0022-2364(74)90292-3.

Bloembergen, N., Purcell, E. M. and Pound, R. V. (1948) 'Relaxation effects in nuclear magnetic resonance absorption', *Physical Review*. American Physical Society, 73(7), pp. 679–712. doi: 10.1103/PhysRev.73.679.

Boesiger, P. *et al.* (1990) 'Tissue characterization of brain tumors during and after pion radiation therapy.', *Magnetic resonance imaging*, 8(4), pp. 491–7. doi: 10.1016/0730-725x(90)90057-9.

Boisvert, D. P., Handa, Y. and Allen, P. S. (1990) ‘Proton relaxation in acute and subacute ischemic brain edema.’, *Advances in neurology*, 52, pp. 407–13. Available at: http://www.ncbi.nlm.nih.gov/pubmed/2168667 (Accessed: 30 October 2019).

Boxt, L. M. *et al.* (1993) ‘Estimation of myocardial water content using transverse relaxation time from dual spin-echo magnetic resonance imaging.’, *Magnetic resonance imaging*, 11(3), pp. 375–83. doi: 10.1016/0730-725x(93)90070-t.

Brass, S. D. *et al.* (2006) ‘Magnetic resonance imaging of iron deposition in neurological disorders’, *Topics in Magnetic Resonance Imaging*, 17(1), pp. 31–40. doi: 10.1097/01.rmr.0000245459.82782.e4.

Bratton, C. B., Hopkins, A. L. and Weinberg, J. W. (1965) ‘Nuclear magnetic resonance studies of living muscle’, *Science*, 147(3659), pp. 738–739. doi: 10.1126/science.147.3659.738.

Brown, M. F. *et al.* (1986) ‘Frequency dependence of spin-lattice relaxation times of lipid bilayers’, *The Journal of Chemical Physics*. AIP Publishing, 84(1), pp. 465–470. doi: 10.1063/1.450162.

Brown, R. W. *et al.* (2014) *Magnetic Resonance Imaging: Physical Principles and Sequence Design: Second Edition*, *Magnetic Resonance Imaging: Physical Principles and Sequence Design: Second Edition*. Edited by R. W. Brown et al. Chichester, UK: John Wiley & Sons Ltd. doi: 10.1002/9781118633953.

Bublitz, M. H. and Stroud, L. R. (2012) ‘Maternal Smoking During Pregnancy and Offspring Brain Structure and Function: Review and Agenda for Future Research’, *Nicotine & Tobacco Research*. Oxford University Press, 14(4), p. 388. doi: 10.1093/NTR/NTR191.

Cameron, I. L., Ord, V. A. and Fullerton, G. D. (1984) ‘Characterization of proton NMR relaxation times in normal and pathological tissues by correlation with other tissue parameters’, *Magnetic Resonance Imaging*, 2(2), pp. 97–106. doi: 10.1016/0730-725X(84)90063-8.

Carr, J. L., Agnihotri, S. and Keightley, M. (2010) ‘Sensory processing and adaptive behavior deficits of children across the fetal alcohol spectrum disorder continuum’, *Alcoholism: Clinical and Experimental Research*, 34(6), pp. 1022–1032. doi: 10.1111/j.1530-0277.2010.01177.x.

Castriota-Scanderbeg, A. *et al.* (2003) ‘Coefficient D(av) is more sensitive than fractional anisotropy in monitoring progression of irreversible tissue damage in focal nonactive multiple sclerosis lesions.’, *AJNR. American journal of neuroradiology*, 24(4), pp. 663–70. Available at: http://www.ncbi.nlm.nih.gov/pubmed/12695200 (Accessed: 6 November 2019).

Chu, K. C. *et al.* (1990) ‘Bulk magnetic susceptibility shifts in nmr studies of compartmentalized samples: use of paramagnetic reagents’, *Magnetic Resonance in Medicine*, 13(2), pp. 239–262. doi: 10.1002/mrm.1910130207.

Civan, M. M. and Shporer, M. (1975) ‘Pulsed nuclear magnetic resonance study of 17-O, 2-D, and 1-H of water in frog striated muscle’, *Biophysical Journal*, 15(4), pp. 299–306. doi: 10.1016/S0006-3495(75)85820-6.

Clark, C. M. *et al.* (2000) ‘Structural and functional brain integrity of fetal alcohol syndrome in nonretarded cases.’, *Pediatrics*, 105(5), pp. 1096–9. doi: 10.1542/peds.105.5.1096.

Coles, C. D. *et al.* (2011) ‘Memory and brain volume in adults prenatally exposed to alcohol.’, *Brain and cognition*, 75(1), pp. 67–77. doi: 10.1016/j.bandc.2010.08.013.

Cope, F. W. (1969) ‘Nuclear Magnetic Resonance Evidence using D2O for Structured

Water in Muscle and Brain', *Biophysical Journal*, 9(3), pp. 303–319. doi: 10.1016/S0006-3495(69)86388-5.

Cortese, B. M. *et al.* (2006) 'Magnetic resonance and spectroscopic imaging in prenatal alcohol-exposed children: Preliminary findings in the caudate nucleus', *Neurotoxicology and Teratology*, 28(5), pp. 597–606. doi: 10.1016/j.ntt.2006.08.002.

Cox, E. and Gowland, P. (2008) 'Measuring T 2 and T 2 ' in the brain at 1.5T, 3T and 7T using a hybrid gradient echo-spin echo sequence and EPI', *Proc Int Soc Magn Reson Med*, 16, p. 1411.

Croxford, J. and Viljoen, D. (1999) 'Alcohol consumption by pregnant women in the Western Cape', *South African Medical Journal*, 89(9), pp. 962–965. Available at: http://farr-sa.co.za/Reference/Alc_Consumpt_Preg_Females_WC.pdf (Accessed: 27 November 2017).

Damadian, R. (1971) 'Tumor detection by nuclear magnetic resonance', *Science*, 171(3976), pp. 1151–1153. doi: 10.1126/science.171.3976.1151.

Damadian, R. *et al.* (1973) 'Human tumors by NMR.', *Physiological chemistry and physics*, 5(5), pp. 381–402. Available at: http://www.ncbi.nlm.nih.gov/pubmed/4775587 (Accessed: 13 October 2019).

Damadian, R. *et al.* (1974) 'Human tumors detected by nuclear magnetic resonance', *Proceedings of the National Academy of Sciences of the United States of America*, 71(4), pp. 1471–1473. doi: 10.1073/pnas.71.4.1471.

Deoni, S. C. L., Peters, T. M. and Rutt, B. K. (2005) 'High-resolution T1 and T2 mapping of the brain in a clinically acceptable time with DESPOT1 and DESPOT2', *Magnetic Resonance in Medicine*, 53(1), pp. 237–241. doi: 10.1002/mrm.20314.

Dieringer, M. A. *et al.* (2014) 'Rapid parametric mapping of the longitudinal relaxation time T1 using two-dimensional variable flip angle magnetic resonance imaging at 1.5 Tesla, 3 Tesla, and 7 Tesla.', *PloS one*. Public Library of Science, 9(3), p. e91318. doi: 10.1371/journal.pone.0091318.

Diwadkar, V. A. *et al.* (2013) 'Differences in cortico-striatal-cerebellar activation during working memory in syndromal and nonsyndromal children with prenatal alcohol exposure', *Human Brain Mapping*, 34(8), pp. 1931–1945. doi: 10.1002/hbm.22042.

Drayer, B. *et al.* (1986) 'MRI of brain iron.', *AJR. American journal of roentgenology*, 147(1), pp. 103–10. doi: 10.2214/ajr.147.1.103.

Droogan, A. G. *et al.* (1999) 'Comparison of multiple sclerosis clinical subgroups using navigated spin echo diffusion-weighted imaging', *Magnetic Resonance Imaging*. Elsevier Inc., 17(5), pp. 653–661. doi: 10.1016/S0730-725X(99)00011-9.

Duyn, J. H. *et al.* (2007) 'High-field MRI of brain cortical substructure based on signal phase', *Proceedings of the National Academy of Sciences of the United States of America*, 104(28), pp. 11796–11801. doi: 10.1073/pnas.0610821104.

Eickhoff, S. *et al.* (2005) 'High-resolution MRI reflects myeloarchitecture and cytoarchitecture of human cerebral cortex', *Human Brain Mapping*. doi: 10.1002/hbm.20082.

Elster, A. (1993) 'Gradient-Echo MR Imaging: Techniques and Acronyms', *Radiology*, 186, pp. 1–8.

Escanye, J. M., Canet, D. and Robert, J. (1982) 'Frequency dependence of water proton longitudinal nuclear magnetic relaxation times in mouse tissues at 20°C', *BBA - Molecular Cell Research*, 721(3), pp. 305–311. doi: 10.1016/0167-4889(82)90083-0.

Fagerlund, Å. *et al.* (2006) 'Brain metabolic alterations in adolescents and young

adults with fetal alcohol spectrum disorders', *Alcoholism: Clinical and Experimental Research*, 30(12), pp. 2097–2104. doi: 10.1111/j.1530-0277.2006.00257.x.

Fahlvik, A. K. *et al.* (1990) 'Magnetic starch microspheres, efficacy and elimination. A new organ-specific contrast agent for magnetic resonance imaging.', *Investigative radiology*, 25(2), pp. 113–20. doi: 10.1097/00004424-199002000-00003.

Fahlvik, A. K., Holtz, E. and Klaveness, J. (1990) 'Relaxation efficacy of paramagnetic and superparamagnetic microspheres in liver and spleen', *Magnetic Resonance Imaging*, 8(4), pp. 363–369. doi: 10.1016/0730-725X(90)90043-2.

Fan, J. *et al.* (2017) 'Localized reductions in resting-state functional connectivity in children with prenatal alcohol exposure.', *Human brain mapping*. NIH Public Access, 38(10), pp. 5217–5233. doi: 10.1002/hbm.23726.

Fischl, B. *et al.* (2002) 'Whole Brain Segmentation: Automated Labeling of Neuroanatomical Structures in the Human Brain', *Neuron*. Cell Press, 33(3), pp. 341–355. doi: 10.1016/S0896-6273(02)00569-X.

Fischl, B., Salat, David H, *et al.* (2004) 'Sequence-independent segmentation of magnetic resonance images', in *NeuroImage*. doi: 10.1016/j.neuroimage.2004.07.016.

Fischl, B., Salat, David H., *et al.* (2004) 'Sequence-independent segmentation of magnetic resonance images', *NeuroImage*. Academic Press, 23, pp. S69–S84. doi: 10.1016/J.NEUROIMAGE.2004.07.016.

Fryer, S. L. *et al.* (2007) 'Prenatal alcohol exposure affects frontal-striatal BOLD response during inhibitory control', *Alcoholism: Clinical and Experimental Research*, 31(8), pp. 1415–1424. doi: 10.1111/j.1530-0277.2007.00443.x.

Fryer, S. L. *et al.* (2009) 'Characterization of white matter microstructure in fetal alcohol spectrum disorders', *Alcoholism: Clinical and Experimental Research*, 33(3), pp. 514–521. doi: 10.1111/j.1530-0277.2008.00864.x.

Fu, Y., Tanaka, K. and Nishimura, S. (1990) 'Evaluation of brain edema using magnetic resonance proton relaxation times.', *Advances in neurology*, 52, pp. 165–176. Available at: http://www.ncbi.nlm.nih.gov/pubmed/2396512 (Accessed: 30 October 2019).

Fukunaga, M. *et al.* (2010) 'Layer-specific variation of iron content in cerebral cortex as a source of MRI contrast', *Proceedings of the National Academy of Sciences of the United States of America*, 107(8), pp. 3834–3839. doi: 10.1073/pnas.0911177107.

Gatenby, R. A. *et al.* (1985) 'Oxygen tension in human tumors: In vivo mapping using CT-guided probes', *Radiology*, 156(1), pp. 211–214. doi: 10.1148/radiology.156.1.4001408.

Gatenby, R. A. *et al.* (1988) 'Oxygen distribution in squamous cell carcinoma metastases and its relationship to outcome of radiation therapy', *International Journal of Radiation Oncology, Biology, Physics*, 14(5), pp. 831–838. doi: 10.1016/0360-3016(88)90002-8.

Gelman, N. *et al.* (1999) 'MR imaging of human brain at 3.0 T: Preliminary report on transverse relaxation rates and relation to estimated iron content', *Radiology*, 210(3), pp. 759–767. doi: 10.1148/radiology.210.3.r99fe41759.

Gerberding, J. L. and Cordero, J. (2004) 'Fetal Alcohol Syndrome: Guidelines for Referral and Diagnosis National Center on Birth Defects and Developmental Disabilities Centers for Disease Control and Prevention Department of Health and Human Services in coordination with DEPARTMENT OF HEALTH AND '. Available at: https://www.cdc.gov/ncbddd/fasd/documents/fas_guidelines_accessible.pdf

(Accessed: 15 August 2017).

Go, K. G. and Edzes, H. T. (1975) 'Water in Brain Edema: Observations by the Pulsed Nuclear Magnetic Resonance Technique', *Archives of Neurology*, 32(7), pp. 462–465. doi: 10.1001/archneur.1975.00490490066006.

Gonçalves, R. D. C. F. *et al.* (2009) 'Proton magnetic resonance spectroscopy in children with fetal alcohol spectrum disorders', *Arquivos de Neuro-Psiquiatria*, 67(2 A), pp. 254–261. doi: 10.1590/S0004-282X2009000200015.

Gracien, R.-M. *et al.* (2016) 'Changes and variability of proton density and T1 relaxation times in early multiple sclerosis: MRI markers of neuronal damage in the cerebral cortex.', *European radiology*, 26(8), pp. 2578–86. doi: 10.1007/s00330-015-4072-x.

Gracien, R.-M. *et al.* (2019) 'Multimodal Quantitative MRI Reveals No Evidence for Tissue Pathology in Idiopathic Cervical Dystonia', *Frontiers in Neurology*, 10. doi: 10.3389/fneur.2019.00914.

Green, C. R. *et al.* (2013) 'Diffusion tensor imaging correlates of saccadic reaction time in children with fetal alcohol spectrum disorder', *Alcoholism: Clinical and Experimental Research*, 37(9), pp. 1499–1507. doi: 10.1111/acer.12132.

De Guio, F. *et al.* (2014) 'A study of cortical morphology in children with fetal alcohol spectrum disorders.', *Human brain mapping*, 35(5), pp. 2285–96. doi: 10.1002/hbm.22327.

Hahn, E. L. (1950) 'Spin Echoes', *Physical Review*, 80(4), pp. 580–594.

Hammer, M. (2014) *MRI Physics: Pulse Sequences*. Available at: http://xrayphysics.com/sequences.html (Accessed: 28 April 2019).

Hasgall PA *et al.* (2018) *IT'IS Database for thermal and electromagnetic parameters of biological tissues*. doi: 10.13099/VIP21000-04-0.

Hazlewood, C. F. (1979) 'A VIEW OF THE SIGNIFICANCE AND UNDERSTANDING OF THE PHYSICAL PROPERTIES OF CELL-ASSOCIATED WATER', in *Cell-Associated Water*. Elsevier, pp. 165–259. doi: 10.1016/b978-0-12-222250-4.50011-8.

Hazlewood, C. F., Nichols, B. L. and Chamberlain, N. F. (1969) 'Evidence for the existence of a minimum of two phases of ordered water in skeletal muscle', *Nature*, 222(5195), pp. 747–750. doi: 10.1038/222747a0.

He, X. and Yablonskiy, D. A. (2009) 'Biophysical mechanisms of phase contrast in gradient echo MRI', *Proceedings of the National Academy of Sciences of the United States of America*, 106(32), pp. 13558–13563. doi: 10.1073/pnas.0904899106.

Hendrickson, T. J. *et al.* (2017) 'Cortical gyrification is abnormal in children with prenatal alcohol exposure.', *NeuroImage. Clinical*. Elsevier, 15, pp. 391–400. doi: 10.1016/j.nicl.2017.05.015.

Hollingshead, A. B. (2011) 'Four Factor Index of Social Status', *Yale Journal of Sociology*, 8, pp. 21–51. doi: 10.1016/j.materresbull.2011.04.018.

Hollis, D. P. *et al.* (1973) 'Nuclear Magnetic Resonance Studies of Several Experimental and Human Malignant Tumors', *Cancer Research*, 33(9), pp. 2156–2160.

Huggert, A. and Odeblad, E. (1959) 'Proton magnetic resonance studies of some tissues and fluids of the Eye', *Acta Radiologica*, 51(5), pp. 385–392. doi: 10.3109/00016925909171110.

Iwama, T. *et al.* (1992) 'Proton nuclear magnetic resonance studies on water structure in peritumoral edematous brain tissue', *Magnetic Resonance in Medicine*, 24(1), pp. 53–63. doi: 10.1002/mrm.1910240106.

Jacobson, S. W. *et al.* (2002) 'Validity of Maternal Report of Prenatal Alcohol, Cocaine, and Smoking in Relation to Neurobehavioral Outcome', *PEDIATRICS*, 109(5), pp. 815–825. doi: 10.1542/peds.109.5.815.

Jacobson, S. W. *et al.* (2008) 'Impaired eyeblink conditioning in children with fetal alcohol syndrome', *Alcoholism: Clinical and Experimental Research*. Blackwell Publishing Ltd, 32(2), pp. 365–372. doi: 10.1111/j.1530-0277.2007.00585.x.

Jacobson, S. W. *et al.* (2011) 'Impaired Delay and Trace Eyeblink Conditioning in School-Age Children With Fetal Alcohol Syndrome', *Alcoholism: Clinical and Experimental Research*. Blackwell Publishing Ltd, 35(2), pp. 250–264. doi: 10.1111/j.1530-0277.2010.01341.x.

Jones, K. L. *et al.* (1973) 'Pattern of malformation in offspring of alcoholic mother', *Lancet*, 1(June), pp. 1267–1271. doi: 10.1097/00006254-197401000-00013.

Jones, K. and Smith, D. (1973) 'RECOGNITION OF THE FETAL ALCOHOL SYNDROME IN EARLY INFANCY', *The Lancet*, 302(7836), pp. 999–1001. doi: 10.1016/S0140-6736(73)91092-1.

Joseph, J. *et al.* (2014) 'Three-dimensional surface deformation-based shape analysis of hippocampus and caudate nucleus in children with fetal alcohol spectrum disorders', *Human Brain Mapping*, 35(2), pp. 659–672. doi: 10.1002/hbm.22209.

Kamman, R. L. *et al.* (1988) 'Nuclear magnetic resonance relaxation in experimental brain edema: Effects of water concentration, protein concentration, and temperature', *Magnetic Resonance in Medicine*, 6(3), pp. 265–274. doi: 10.1002/mrm.1910060304.

Kamman, R. L., Go, K. G. and Berendsen, H. J. (1990) 'Proton-nuclear magnetic resonance relaxation times in brain edema.', *Advances in neurology*, 52, pp. 401–405. Available at: http://www.ncbi.nlm.nih.gov/pubmed/2168666 (Accessed: 30 October 2019).

Knight, R. A. *et al.* (1994) 'Magnetic resonance imaging assessment of evolving focal cerebral ischemia: Comparison with histopathology in rats', *Stroke*, 25(6), pp. 1252–1261. doi: 10.1161/01.STR.25.6.1252.

Koenig, S. H. (1991) 'Cholesterol of myelin is the determinant of gray-white contrast in MRI of brain', *Magnetic Resonance in Medicine*, 20(2), pp. 285–291. doi: 10.1002/mrm.1910200210.

Koenig, S. H. and Brown, R. D. (1985) 'The importance of the motion of water for magnetic resonance imaging', *Investigative Radiology*, 20(3), pp. 297–305. doi: 10.1097/00004424-198505000-00013.

Kotwica, Z., Thuomas, K. A. and Persson, L. (1989) 'Magnetic resonance studies on the development of ischemic edema in an early period after occlusion of middle cerebral artery in a rat.', *Radiologia diagnostica*, 30(3), pp. 307–11. Available at: http://www.ncbi.nlm.nih.gov/pubmed/2798819 (Accessed: 30 October 2019).

Langkammer, C. *et al.* (2010) 'Quantitative MR Imaging of Brain Iron: A Postmortem Validation Study', *Radiology*. doi: 10.1148/radiol.10100495.

Laule, C. *et al.* (2007) 'Long T2 water in multiple sclerosis: what else can we learn from multi-echo T2 relaxation?', *Journal of neurology*, 254(11), pp. 1579–87. doi: 10.1007/s00415-007-0595-7.

Lebel, C. *et al.* (2008) 'Brain diffusion abnormalities in children with fetal alcohol spectrum disorder', *Alcoholism: Clinical and Experimental Research*. Blackwell Publishing Ltd, 32(10), pp. 1732–1740. doi: 10.1111/j.1530-0277.2008.00750.x.

Lebel, C. *et al.* (2010) 'Brain microstructure is related to math ability in children with fetal alcohol spectrum disorder', *Alcoholism: Clinical and Experimental Research*.

Blackwell Publishing Ltd, 34(2), pp. 354–363. doi: 10.1111/j.1530-0277.2009.01097.x.

Lee, J. *et al.* (2010) 'Sensitivity of MRI resonance frequency to the orientation of brain tissue microstructure', *Proceedings of the National Academy of Sciences of the United States of America*. National Academy of Sciences, 107(11), pp. 5130–5135. doi: 10.1073/pnas.0910222107.

Lee, J. *et al.* (2011) 'T2*-based fiber orientation mapping', *NeuroImage*, 57(1), pp. 225–234. doi: 10.1016/j.neuroimage.2011.04.026.

Lee, J. *et al.* (2012) 'The contribution of myelin to magnetic susceptibility-weighted contrasts in high-field MRI of the brain', *NeuroImage*, 59(4), pp. 3967–3975. doi: 10.1016/j.neuroimage.2011.10.076.

Lewa, C. J. and Zbytniewski, Z. (1977) 'Magnetic transverse relaxation time of the protons in transplantable melanotic and amelanotic melanoma and in some inner organs of golden hamster Mesocricetus auratus, Waterhouse.', *Bulletin du cancer*, 63(1), pp. 69–72. Available at: http://www.ncbi.nlm.nih.gov/pubmed/990511 (Accessed: 20 October 2019).

Li, B. S. Y. *et al.* (2003) 'Brain metabolite profiles of T1-hypointense lesions in relapsing-remitting multiple sclerosis.', *AJNR. American journal of neuroradiology*, 24(1), pp. 68–74. Available at: http://www.ncbi.nlm.nih.gov/pubmed/12533329 (Accessed: 6 November 2019).

Li, D. *et al.* (1996) 'Magnetic resonance imaging of the brain with gadopentetate dimeglumine-DTPA: Comparison of T1-weighted spin-echo and 3D gradient-echo sequences', *Journal of Magnetic Resonance Imaging*. John Wiley and Sons Inc., 6(3), pp. 415–424. doi: 10.1002/jmri.1880060302.

Li, T. Q. *et al.* (2009) 'Characterization of T2* heterogeneity in human brain white matter', *Magnetic Resonance in Medicine*, 62(6), pp. 1652–1657. doi: 10.1002/mrm.22156.

Li, W. *et al.* (2012) 'Magnetic susceptibility anisotropy of human brain in vivo and its molecular underpinnings', *NeuroImage*, 59(3), pp. 2088–2097. doi: 10.1016/j.neuroimage.2011.10.038.

Lin, W. *et al.* (1997) 'Quantitative regional brain water measurement with magnetic resonance imaging in a focal ischemia model', *Magnetic Resonance in Medicine*, 38(2), pp. 303–310. doi: 10.1002/mrm.1910380221.

Lindinger, N. M. *et al.* (2016) 'Theory of Mind in Children with Fetal Alcohol Spectrum Disorders', *Alcoholism: Clinical and Experimental Research*, 40(2), pp. 367–376. doi: 10.1111/acer.12961.

Ling, G. N. (1983) 'Evidence for a significant role of paramagnetic ions in the observed NMR relaxation rates of living tissues.', *Physiological chemistry and physics and medical NMR*, 15(6), pp. 505–510.

Ling, G. N. (1989) 'Further studies on the role of paramagnetic ion contents on the NMR relaxation time, T1 of normal tissues and cancer cells.', *Physiological chemistry and physics and medical NMR*, 21(1), pp. 15–18.

Ling, G. N., Kolebic, T. and Damadian, R. (1990) *Low Paramagnetic-Ion Content in Cancer Cells: Its Significance in Cancer Detection by Magnetic Resonance Imaging*, *Physiol. Chem. Phys. & Med. NMR*.

Lucas, B. R. *et al.* (2014) 'Gross motor deficits in children prenatally exposed to alcohol: a meta-analysis.', *Pediatrics*. American Academy of Pediatrics, 134(1), pp. e192-209. doi: 10.1542/peds.2013-3733.

Ma, X. *et al.* (2005) 'Evaluation of corpus callosum anisotropy in young adults with

fetal alcohol syndrome according to diffusion tensor imaging', *Alcoholism: Clinical and Experimental Research*. Blackwell Publishing Ltd, 29(7), pp. 1214–1222. doi: 10.1097/01.ALC.0000171934.22755.6D.

MacKay, A. L. *et al.* (2009) 'MR Relaxation in Multiple Sclerosis', *Neuroimaging Clinics of North America*, pp. 1–26. doi: 10.1016/j.nic.2008.09.007.

Malisza, K. L. *et al.* (2012) 'Comparison of spatial working memory in children with prenatal alcohol exposure and those diagnosed with ADHD; A functional magnetic resonance imaging study', *Journal of Neurodevelopmental Disorders*, 4(1). doi: 10.1186/1866-1955-4-12.

Manfredonia, F. *et al.* (2007) 'Normal-Appearing Brain T1 Relaxation Time Predicts Disability in Early Primary Progressive Multiple Sclerosis', *Archives of Neurology*. American Medical Association, 64(3), p. 411. doi: 10.1001/archneur.64.3.411.

Mattson, S. N. *et al.* (1996) 'A decrease in the size of the basal ganglia in children with fetal alcohol syndrome.', *Alcoholism, clinical and experimental research*, 20(6), pp. 1088–93. doi: 10.1111/j.1530-0277.1996.tb01951.x.

May, P. *et al.* (2000) 'Epidemiology of fetal alcohol syndrome in a South African community in the Western Cape Province', *American Journal of Public Health*, 90(12), pp. 1905–1912. doi: 10.2105/ajph.90.12.1905.

McRobbie, D. W. *et al.* (2006) *MRI From Picture to Proton*. 2nd edn, *2nd Edition*. 2nd edn. New York: Cambridge University Press. doi: 10.1097/00004032-200310000-00020.

Mehta, V. *et al.* (2013) 'Iron Is a Sensitive Biomarker for Inflammation in Multiple Sclerosis Lesions', *PLoS ONE*, 8(3). doi: 10.1371/journal.pone.0057573.

Meintjes, E. M. *et al.* (2010) 'An fMRI study of number processing in children with fetal alcohol syndrome', *Alcoholism: Clinical and Experimental Research*, 34(8), pp. 1450–1464. doi: 10.1111/j.1530-0277.2010.01230.x.

Miller, D. H., Thompson, A. J. and Filippi, M. (2003) 'Magnetic resonance studies of abnormalities in the normal appearing white matter and grey matter in multiple sclerosis.', *Journal of neurology*, 250(12), pp. 1407–19. doi: 10.1007/s00415-003-0243-9.

Mitchell, H. H. *et al.* (1945) 'THE CHEMICAL COMPOSITION OF THE ADULT HUMAN BODY AND ITS BEARING ON THE BIOCHEMISTRY OF GROWTH', *Journal of Biological Chemistry*, 158, pp. 625–637. Available at: http://www.jbc.org/ (Accessed: 10 January 2019).

Nardelli, A. *et al.* (2011) 'Extensive deep gray matter volume reductions in children and adolescents with fetal alcohol spectrum disorders', *Alcoholism: Clinical and Experimental Research*. Blackwell Publishing Ltd, 35(8), pp. 1404–1417. doi: 10.1111/j.1530-0277.2011.01476.x.

Naruse, S. *et al.* (1982) 'Proton nuclear magnetic resonance studies on brain edema', *Journal of Neurosurgery*, 56(6), pp. 747–752. doi: 10.3171/jns.1982.56.6.0747.

Naruse, S. *et al.* (1986) 'Significance of proton relaxation time measurement in brain edema, cerebral infarction and brain tumors', *Magnetic Resonance Imaging*, 4(4), pp. 293–304. doi: 10.1016/0730-725X(86)91039-8.

Negendank, W. *et al.* (1991) 'Evidence for a contribution of paramagnetic ions to water proton spin-lattice relaxation in normal and malignant mouse tissues.', *Magnetic resonance in medicine*, 18(2), pp. 280–93. doi: 10.1002/mrm.1910180204.

Niemi, P. T., Komu, M. E. S. and Koskinen, S. K. (1992) 'Tissue specificity of low-field-strength magnetization transfer contrast imaging', *Journal of Magnetic Resonance*

Imaging, 2(2), pp. 197–201. doi: 10.1002/jmri.1880020213.

Nusbaum, A. O., Lu, D., *et al.* (2000) 'Quantitative Diffusion Measurements in Focal Multiple Sclerosis Lesions', *American Journal of Roentgenology*, 175(3), pp. 821–825. doi: 10.2214/ajr.175.3.1750821.

Nusbaum, A. O., Tang, C. Y., *et al.* (2000) 'Whole-brain diffusion MR histograms differ between MS subtypes', *Neurology*, 54(7), pp. 1421–1426. doi: 10.1212/wnl.54.7.1421.

O'Hare, E. D. *et al.* (2005) 'Mapping cerebellar vermal morphology and cognitive correlates in prenatal alcohol exposure', *NeuroReport*, 16(12), pp. 1285–1290. doi: 10.1097/01.wnr.0000176515.11723.a2.

ODEBLAD, E. and LINDSTROM, G. (1955) 'Some preliminary observations on the proton magnetic resonance in biologic samples.', *Acta radiologica*, 43(6), pp. 469–76. doi: 10.3109/00016925509172514.

Ogg, R. J. *et al.* (1999) 'The correlation between phase shifts in gradient-echo MR images and regional brain iron concentration', *Magnetic Resonance Imaging*, 17(8), pp. 1141–1148. doi: 10.1016/S0730-725X(99)00017-X.

Ogg, R. J. and Steen, R. G. (1998) 'Age-related changes in brain T1 are correlated with iron concentration', *Magnetic Resonance in Medicine*, 40(5), pp. 749–753. doi: 10.1002/mrm.1910400516.

Peters, A. M. *et al.* (2006) 'Comparison of T2* Measurements in Human Brain at 1.5, 3 and 7 T', *Proc. Intl. Soc. Mag. Reson. Med.*, 14, p. 926.

Pitt, D. *et al.* (2010) 'Imaging cortical lesions in multiple sclerosis with ultra-high-field magnetic resonance imaging', *Archives of Neurology*, 67(7), pp. 812–818. doi: 10.1001/archneurol.2010.148.

Popova, S. *et al.* (2017) 'Estimation of national, regional, and global prevalence of alcohol use during pregnancy and fetal alcohol syndrome: a systematic review and meta-analysis', *The Lancet Global Health*, 5(3), pp. e290–e299. doi: 10.1016/S2214-109X(17)30021-9.

Rajaprakash, M. *et al.* (2014) 'Cortical morphology in children with alcohol-related neurodevelopmental disorder.', *Brain and behavior*, 4(1), pp. 41–50. doi: 10.1002/brb3.191.

Ranade, S. S., Partain, C. L. and Price, R. R. (1988) *Histopathological correlation*, *Magnetic resonance imaging.* Edited by W. Saunders. Philadelphia.

Ranade, S. S. and Shingatgeri, V. M. (1992) 'Contribution of paramagnetic trace elements of biological tissues to spin lattice relaxation times.', *Physiological chemistry and physics and medical NMR*, 24(2), pp. 165–7. Available at: http://www.ncbi.nlm.nih.gov/pubmed/1508992 (Accessed: 20 October 2019).

Rao, B. D. N. (1965) 'Relaxation effects in nuclear magnetic double resonance', *Physical Review*, 137(2A). doi: 10.1103/PhysRev.137.A467.

Renwick, J. H. and Asker, R. L. (1983) 'Ethanol-sensitive times for the human conceptus', *Early Human Development*, 8(2), pp. 99–111. doi: 10.1016/0378-3782(83)90065-8.

Riley, E. P. *et al.* (1995) 'Abnormalities of the corpus callosum in children prenatally exposed to alcohol.', *Alcoholism, clinical and experimental research*, 19(5), pp. 1198–202. Available at: http://www.ncbi.nlm.nih.gov/pubmed/8561290 (Accessed: 25 August 2019).

Rorschach, H. E. and Hazlewood, C. F. (1986) 'Protein dynamics and the NMR relaxation time T1 of water in biological systems', *Journal of Magnetic Resonance (1969)*, 70(1), pp. 79–88. doi: 10.1016/0022-2364(86)90364-1.

Roussotte, F. F. *et al.* (2012) 'Regional brain volume reductions relate to facial dysmorphology and neurocognitive function in fetal alcohol spectrum disorders', *Human Brain Mapping*, 33(4), pp. 920–937. doi: 10.1002/hbm.21260.

Sati, P. *et al.* (2012) 'In vivo quantification of T 2* anisotropy in white matter fibers in marmoset monkeys', *NeuroImage*, 59(2), pp. 979–985. doi: 10.1016/j.neuroimage.2011.08.064.

Schad, L. R. *et al.* (1989) 'Multiexponential proton spin-spin relaxation in MR imaging of human brain tumors', *Journal of Computer Assisted Tomography*, 13(4), pp. 577–587. doi: 10.1097/00004728-198907000-00005.

Schenck, J. F. (1995) 'Imaging of brain iron by magnetic resonance: T2 relaxation at different field strengths', *Journal of the Neurological Sciences*, 134(SUPPL.), pp. 10–18. doi: 10.1016/0022-510X(95)00203-E.

Schenker, C. *et al.* (1993) 'Age distribution and iron dependency of the T2 relaxation time in the globus pallidus and putamen', *Neuroradiology*. doi: 10.1007/BF00593967.

Schuhmacher, J. H. *et al.* (1985) 'Contribution of paramagnetic trace elements to the spin-lattice relaxation time in the liver.', *Investigative radiology*, 20(6), pp. 601–8. doi: 10.1097/00004424-198509000-00013.

Shah, S. S. *et al.* (1982a) 'Significance of water proton spin-lattice relaxation times in normal and malignant tissues and their subcellular fractions-II', *Magnetic Resonance Imaging*, 1(3), pp. 155–164. doi: 10.1016/0730-725X(82)90207-7.

Shah, S. S. *et al.* (1982b) 'Significance of water proton spin-lattice relaxation times in normal and malignant tissues and their subcellular fractions—I', *Magnetic Resonance Imaging*, 1(2), pp. 91–104. doi: 10.1016/0730-725X(82)90225-9.

Shioya, S. *et al.* (1990) 'A 1-year time course study of the relaxation times and histology for irradiated rat lungs', *Magnetic Resonance in Medicine*, 14(2), pp. 358–368. doi: 10.1002/mrm.1910140220.

Shmueli, K. *et al.* (2009) 'Magnetic susceptibility mapping of brain tissue in vivo using MRI phase data', *Magnetic Resonance in Medicine*, 62(6), pp. 1510–1522. doi: 10.1002/mrm.22135.

Sowell, E. R. *et al.* (1996) 'Abnormal development of the cerebellar vermis in children prenatally exposed to alcohol: Size reduction in lobules I-V', *Alcoholism: Clinical and Experimental Research*, 20(1), pp. 31–34. doi: 10.1111/j.1530-0277.1996.tb01039.x.

Sowell, E. R. *et al.* (2001) 'Mapping callosal morphology and cognitive correlates: Effects of heavy prenatal alcohol exposure', *Neurology*. Lippincott Williams and Wilkins, 57(2), pp. 235–244. doi: 10.1212/WNL.57.2.235.

Sowell, E. R. *et al.* (2008) 'Mapping white matter integrity and neurobehavioral correlates in children with fetal alcohol spectrum disorders', *Journal of Neuroscience*, 28(6), pp. 1313–1319. doi: 10.1523/JNEUROSCI.5067-07.2008.

Spottiswoode, B. S. *et al.* (2011) 'Diffusion Tensor Imaging of the Cerebellum and Eyeblink Conditioning in Fetal Alcohol Spectrum Disorder', *Alcoholism: Clinical and Experimental Research*, 35(12), pp. 2174–2183. doi: 10.1111/j.1530-0277.2011.01566.x.

Suttie, M. *et al.* (2018) 'Combined Face–Brain Morphology and Associated Neurocognitive Correlates in Fetal Alcohol Spectrum Disorders', *Alcoholism: Clinical and Experimental Research*, 42(9), pp. 1769–1782. doi: 10.1111/acer.13820.

Thomas, J. D., Warren, K. R. and Hewitt, B. G. (2010) 'Fetal alcohol spectrum disorders: from research to policy.', *Alcohol research & health : the journal of the National Institute on Alcohol Abuse and Alcoholism*, 33(1–2), pp. 118–26. Available

at: https://www.ncbi.nlm.nih.gov/pmc/articles/PMC3887502/pdf/arh-33-1_2-118.pdf (Accessed: 15 August 2017).

Tofts, P. S. (2004) 'PD: Proton Density of Tissue Water', in *Quantitative MRI of the Brain*, pp. 83–109. doi: 10.1002/0470869526.ch4.

Treit, S. *et al.* (2013) 'Longitudinal MRI reveals altered trajectory of brain development during childhood and adolescence in fetal alcohol spectrum disorders', *Journal of Neuroscience*, 33(24), pp. 10098–10109. doi: 10.1523/JNEUROSCI.5004-12.2013.

Vavasour, I. M. *et al.* (2007) 'Multi-parametric MR assessment of T 1 black holes in multiple sclerosis: Evidence that myelin loss is not greater in hypointense versus isointens T 1 lesions', *Journal of Neurology*, 254(12), pp. 1653–1659. doi: 10.1007/s00415-007-0604-x.

Van Waesberghe, J. H. T. M. *et al.* (1999) 'Axonal loss in multiple sclerosis lesions: Magnetic resonance imaging insights into substrates of disability', *Annals of Neurology*, 46(5), pp. 747–754. doi: 10.1002/1531-8249(199911)46:5<747::AID-ANA10>3.0.CO;2-4.

Van Walderveen, M. A. A. *et al.* (1999) 'Neuronal damage in T1-hypointense multiple sclerosis lesions demonstrated in vivo using proton magnetic resonance spectroscopy', *Annals of Neurology*, 46(1), pp. 79–87. doi: 10.1002/1531-8249(199907)46:1<79::AID-ANA12>3.0.CO;2-9.

Wansapura, J. P. *et al.* (1999) 'NMR Relaxation Times in the Human Brain at 3.0 Tesla', *Journal of Magnetic Resonance Imaging*, 9, pp. 531–538.

Wehrli, F. W. *et al.* (1985) 'Quantification of contrast in clinical mr brain imaging at high magnetic field', *Investigative Radiology*, 20(4), pp. 360–369. doi: 10.1097/00004424-198507000-00005.

Whittall, K. P. *et al.* (1997) 'In vivo measurement ofT2 distributions and water contents in normal human brain', *Magnetic Resonance in Medicine*, 37(1), pp. 34–43. doi: 10.1002/mrm.1910370107.

Willoughby, K. A. *et al.* (2008) 'Effects of prenatal alcohol exposure on hippocampal volume, verbal learning, and verbal and spatial recall in late childhood', in *Journal of the International Neuropsychological Society*, pp. 1022–1033. doi: 10.1017/S1355617708081368.

Woods, K. J. *et al.* (2015) 'Parietal dysfunction during number processing in children with fetal alcohol spectrum disorders', *NeuroImage: Clinical*. Elsevier B.V., 8, pp. 594–605. doi: 10.1016/j.nicl.2015.03.023.

Wozniak, J. R. *et al.* (2009) 'Microstructural corpus callosum anomalies in children with prenatal alcohol exposure: An extension of previous diffusion tensor imaging findings', *Alcoholism: Clinical and Experimental Research*, 33(10), pp. 1825–1835. doi: 10.1111/j.1530-0277.2009.01021.x.

Wright, P. J. *et al.* (2008) 'Water proton T1 measurements in brain tissue at 7, 3, and 1.5 T using IR-EPI, IR-TSE, and MPRAGE: results and optimization', *Magnetic Resonance Materials in Physics, Biology and Medicine*, 21, pp. 121–130. doi: 10.1007/s10334-008-0104-8 .

Wu, Z. *et al.* (2009) 'Identification of calcification with MRI using susceptibility-weighted imaging: A case study', *Journal of Magnetic Resonance Imaging*, 29(1), pp. 177–182. doi: 10.1002/jmri.21617.

Yang, Y., Roussotte, F., *et al.* (2012) 'Abnormal cortical thickness alterations in fetal alcohol spectrum disorders and their relationships with facial dysmorphology', *Cerebral Cortex*, 22(5), pp. 1170–1179. doi: 10.1093/cercor/bhr193.

Yang, Y., Phillips, O. R., *et al.* (2012) 'Callosal Thickness Reductions Relate to Facial Dysmorphology in Fetal Alcohol Spectrum Disorders', *Alcoholism: Clinical and Experimental Research*, 36(5), pp. 798–806. doi: 10.1111/j.1530-0277.2011.01679.x.

Yao, B. *et al.* (2009) 'Susceptibility contrast in high field MRI of human brain as a function of tissue iron content', *NeuroImage*, 44(4), pp. 1259–1266. doi: 10.1016/j.neuroimage.2008.10.029.

Yoshiharu Horikawa, M. D. *et al.* (1986) 'Proton nmr relaxation times in ischemic brain edema', *Stroke*, 17(6), pp. 1149–1152. doi: 10.1161/01.str.17.6.1149.

Zhong, K. *et al.* (2011) 'Phase contrast imaging in neonates', *NeuroImage*, 55(3), pp. 1068–1072. doi: 10.1016/j.neuroimage.2010.11.086.

Zhou, D. *et al.* (2011) 'Developmental cortical thinning in fetal alcohol spectrum disorders.', *NeuroImage*, 58(1), pp. 16–25. doi: 10.1016/j.neuroimage.2011.06.026.

Zhou, D. *et al.* (2018) 'Preserved cortical asymmetry despite thinner cortex in children and adolescents with prenatal alcohol exposure and associated conditions.', *Human brain mapping*, 39(1), pp. 72–88. doi: 10.1002/hbm.23818.